CHARACTERIZATION OF THE DEGRADATION OF SHAPE MEMORY POLYMERS

A Dissertation

by

ANDREW CHRISTOPHER WEEMS

Submitted to the Office of Graduate and Professional Studies of
Texas A&M University
in partial fulfillment of the requirements for the degree of

DOCTOR OF PHILOSOPHY

Chair of Committee,	Duncan J. Maitland
Committee Members,	Elizabeth Cosgriff-Hernandez
	Balakrishna Haridas
	Karen L. Wooley
Head of Department,	Anthony Guiseppi-Elie

May 2017

Major Subject: Biomedical Engineering

ABSTRACT

Shape memory polymer (SMP) polyurethanes have been proposed for a variety of vascular devices due to their biocompatibility, stimuli-responsiveness, and tunable properties. While this technology shows promise, a primary limitation for translation of these SMPs into the clinic is a lack of understanding of the degradation behavior and stability.

Characterization of the degradation of these SMPs revealed excellent hydrolytic stability although the presence of tertiary amines results in a rapid oxidatively-induced mass loss over time. The mechanism of degradation was found to be the scission of the tertiary amines, producing secondary amines, primary amines, aldehydes and carboxylic acids. This understanding of degradation was then used to assess the toxicity risks for SMP implants, and it was found that despite degradation these SMPs may possess minimal risks as vascular implants.

One of the goals in medical devices is biostability, or relatively minimal mass loss over time. One method of tailoring oxidative mass loss was the use of antioxidants. Bulk inclusion of antioxidants resulted in tunability of pore size, mechanical properties, shape recovery kinetics, and oxidative resistance. A limitation of this method was the retention of antioxidants in the SMP matrix after cleaning the material post-synthesis, as determined from gas-chromatography mass spectrometry (GCMS). Synthesis and incorporation of polyurethane microparticles was used to improve the retention of antioxidants, determined by gravimetric comparisons. Additionally, while the inclusion of antioxidants resulted in various property changes, SMP composites containing the particles possessed similar

scaffold pore size, shape recovery kinetics, and mechanical properties while displaying improved oxidative stability.

Further increase of the SMPs' biostability was achieved through chemical modification of the polymer structure, with glycerol and isocyanurate groups examined. Glycerol was found to improve the oxidative resistance, resulting in SMPs with lifespans of *ca* 5 years when sufficient concentrations of glycerol were used. Isocyanurate-based SMPs are predicted to have lifespans extending potentially to nearly 20 years.

The presented work demonstrates the degradation behavior, toxicity risks, and mechanism for SMPs containing tertiary amines. This work is then applied for further tuning oxidation by the biostability through chemical and physical means, including new covalently added monomers and macromers, as well as composite synthesis. This work supports the concept of SMP-based vascular occlusion materials, and it is hoped that these studies will aid in the translation of such devices into clinics in the near future.

ACKNOWLEDGEMENTS

I am exceptionally grateful to my committee chair, Dr. Duncan Maitland, for his guidance and support throughout my graduate career.

I would also like to thank my committee members, Dr. Elizabeth Cosgriff-Hernandez, Dr. Balakrishna Haridas, Dr. Karen L Wooley, and Dr. William Wustenberg for their continual support and guidance in my research and professional development.

I have been fortunate to have collaborated with many researchers across multiple disciplines, all of whom have been crucial to the work that is presented here. I would also like to expressly thank my Biomedical Device Laboratory peers that have supported me throughout the course of my research, specifically Dr. Tony Boyle, Mark Wierzbicki, Jason Szafron, Alexandra Easley and Scott Herting have provided invaluable assistance for this work. Kevin T Wacker was instrumental in numerous projects, and without his help this work would not have been completed. Without the support of my friends and colleagues at the Biomedical Device Laboratory and Texas A&M University, completion of this work would not have been possible.

Also, I would like to thank my parents. They funded and enabled my passion and curiosity. They taught me the value of hard work, patience, and perseverance.

CONTRIBUTORS AND FUNDING SOURCES

Contributors Section

I would like to acknowledge my committee chair, Dr. Duncan Maitland and committee members, Dr. Elizabeth Cosgriff-Hernandez, Dr. Balakrishna Haridas, Dr. Karen L Wooley, and Dr. William Wustenberg, and to thank them for their continual support and guidance in my research and professional development.

I would also like to thank Dr. Luz M Calle and Dr. Wenyan Li of Kennedy Space Center, NASA, who contributed to the experimental design of Chapter V, and Dr. Lawrence Dangott of the Protein Characterization Lab, TAMU, who trained me in using LCMS analysis. I am especially grateful to Dr. Jeffery Raymond and his expertise across both chemistry and engineering fields. Kevin T Wacker was instrumental in chemical analysis and experimental preparation (Chapter II, Chapter VI, Chapter VII), and without his help this work would not have been completed.

Funding Section

I would like to acknowledge the National Institute of Biomedical Imaging and Bioengineering and National Institute of Neurological Disorders and Stroke, both part of the National Institute of Health, and the NASA H Jenkins Fellowship for their support of the Biomedical Device Laboratory and my research. I would also like to acknowledge Shape Memory Medical, Inc. for their support of the laboratory and this work.

NOMENCLATURE

Accel	Accelerated
Amino	Amino-3-propanol
ATR	Attenuated total reflectance
BHT	Butylated hydoxytoluene
Bis	Bis(2-hydroxyethyl)propylamine
Boc	Boc protecting group
^{13}C	Carbon
$CaCl_2$	Calcium chloride
$CoCl_2$	Cobalt chloride
CO_2	Carbon dioxide
COOH	Carboxylic acid
$CDCl_3$	deuterated chloroform
CP	Cross polarization
DEA	Diethanolamine
DCTB	trans-2-[3-(4-tert-Butylphenyl)-2-methyl-2-propenylidene]malonoitrile
DI H_2O	Deionized water
DMA	Dynamic mechanical analysis
DMSO	Dimethyl sulfoxide
DSA	Digital subtraction angiography
DSC	Differential scanning calorimetry

DMF	Dimethylformamide
E’	Storage modulus
E’’	Loss modulus
EA	Ethanolamine
EtOH	Ethyl alcohol
ESI	Electrospray
FBS	Fetal bovine serum
FDA	Food and Drug Administration
FTIR	Fourier Transform Infrared Spectroscopy
GC	Gas chromatography
GFP	Green fluorescent protein
Gly	Glycerol
Glyco	Glycolic acid
GPC	Gel permeation chromatography
HCl	Hhydrochloric acid
HDI	Hexamethylene Diisocyanate
HDA	Hexamethylene diamine
HPED	N,N,N’,N’-Tetrakis(2-hydroxypropyl)ethylenediamine
H_2O_2	hydrogen peroxide
HP	High performance
IC_{30}	30% cell viability reduction
ID	Inner diameter

Iso	Isocyanurate Triol
IPA	Isopropyl alcohol
IPDI	Isophorone diisocyanate
KOH	Potassium hydroxide
KTFA	Potassium trifluoroacetate
Lac	Lactic acid
LC	Liquid chromatography
MALDI	Matrix assisted laser desorption/ionization
MDI	Methylene diisocyanate
Methyl	2,2’-methylenebis(6-tert-butyl-methylphenol)
MS	Mass spectrometry
NaOH	Sodium hydroxide
NCO	Isocyanate
Nile	Nile blue chloride
NMR	Nuclear magnetic resonance
NR	Natural red dye
OD	Optical density
OH	Alcohol
PBS	Phosphate buffered saline
PCL	Poly(ε-caprolactone)
PDMS	Poly(dimethylsiloxane)
PhB	Phloxine B

Piper	1,2,2,6,6-tetramethyl piperidinol
RO Water	Reverse osmosis water
r.t.	Real time
SEM	Scanning electron microscopy
SMP	Shape memory polymer
TEA	Triethanolamine
THF	Tetrahydrofuran
T_g	Glass transition temperature
TMHDI	Trimethyl hexamethylene diisocyanate
TOF	Time of flight
TriPhen	Triphenyl phosphite
Vit C	L-ascorbic acid (vitamin C)
XPS	X-ray photospectroscopy

TABLE OF CONTENTS

Page

LIST OF FIGURES

Page

LIST OF TABLES

Page

CHAPTER I

INTRODUCTION AND LITERATURE REVIEW

1.1 Polyurethane Medical Devices

Polyurethane-based medical devices have been a gold-standard of care for decades, and have been utilized in a range of products including pacemaker leads, aneurysm occlusion devices, and implant coatings.[1-5] In many commercial applications, linear polyurethanes are used due to the ease of processing, mechanical properties and excellent biocompatibility.[1,5-9] These are commonly consisting of a hard segment with urethane linkages and well-packing structures, connected by a chain extending soft segment, typically esters, ethers, or siloxanes.[1,5-8] The degradation of the carbamate and urea linkages occurs *via* hydrolysis, but this occurs over the course of years *in vivo*.[1,5-8] For this reason, polyurethanes seemed ideal for long-term implant applications.

Two well-known failures have been the cause of substantial research into toxicity risks and degradation susceptibility of these materials: pacemaker lead wire failure (non-porous polyurethanes) and the degradation of polyurethane foam coatings.[9-22] In non-porous polyurethanes, failures that have occurred include surface cracking, erosion, and chain scission.[1,5,13-15] The mechanisms of degradation in these cases are varied, with the polyester soft segments undergoing hydrolysis; proximity to the hard segment was found to impact this rate.[1,5] Polyether segments were found to be susceptible to oxidative degradation mediated by neutrophils and monocyte-derived macrophages and catalyzed by the presence of metal ions; both erosion and surface cracking have been attributed to these

factors.[1,5] The presence of stress cracking has also been attributed to the residual stresses caused in part by phase separation of the segmented polyurethanes.[13-15]

In the case of porous polyurethanes, similar failure mechanisms were reported but analysis and toxicological concerns were handled differently.[5-8,12,16-22] For polyurethanes intended to be biostable, aromatic diisocyanates were typically used during synthesis; hydrolytic by-products of methylene diisocyanates (MDI) and toluene diisocyanates, two traditionally used aromatic diisocyanates, are carcinogenic in animal models and thus would be unsuitable in biodegradable applications.[1,23-25] For the intended applications, biostability was the goal, but *in vivo* studies found that degradation was occurring, in some cases rapidly (months to years for porous polyurethanes).[18-21] Early analytical studies of this degradation reported high risks of toxic byproducts, but reviews of these studies have since indicated that many of the techniques utilized were not appropriated models of *in vivo* degradation.[18] While the authors reported that they had found these carcinogenic hydrolysis products, little focus was made to understand how the degradation that was found *in vivo* could be related to the *in vitro* data to gain an understanding the degradation process and toxicological risk.[18] In fact, the carcinogenic diamines that were found during testing were more likely present in the body as part of polyurethane chains with acid or hydroxyl end groups as a result of polyester hydrolysis, rather than are carcinogenic diamines.[18] The polyurethane chains were being cleared through the kidneys as urine, and only through post-treatment did the products become a carcinogenic risk.[18] As a result of the initial toxicity concerns, and in spite of the flaws in the research, the use of polyurethane foam coatings was dramatically decreased in the United States afterward, and

it is only recently that such materials are again considered relevant in biomedical applications.[15-17,19-20]

1.2 Shape Memory Polymers in Vascular Applications

While there were long-term toxicity concerns of polyurethane porous materials, short term performance was generally positive.[26-34] Immune response seemed to be mediated with the presence of the porous coating around implanted devices compared with the uncoated, non-porous surfaces.[34-35] First proposed by Sokolowski *et al*, aneurysm occlusion using shape memory polymer (SMPs) polyurethane foams offered a novel approach for treatment.[30,32] SMPs can be compressed into a temporary, secondary shape and stored in this shape until an external stimulus is applied, which allows for the material to recover its original geometry.[35-48] In these cases, the mechanism of recovery would be a combination of thermal and solvent actuation.[28-30,39-42] The use of SMPs allowed for minimally invasive devices to be employed for the occlusion of large void spaces, a procedure which had previously required the packing of coils into the aneurysm space in the hopes of occluding it without rupturing or having a recanalization post-procedure.[30,32,49] However, SMPs are not just limited to neurovascular aneurysm occlusion devices.[28-30,39-42] Other occlusion devices could be improved through the incorporation of SMPs, such as venous occlusions.

Previous studies on the biocompatibility and thrombus formation of these SMPs indicates that within an hour of implantation in the aneurysm space, a stable blood clot will form.[33-34] Compared with bare metal coils which may never fully develop a complete thrombus or fully heal, these materials hold substantial promise in terms of performance.[33-34] In regards to biocompatibility, initial studies demonstrated that both the thermoplastic and

thermoset versions of SMPs synthesized from aromatic diisocyanates (MDI and carbodiimide modified MDI) as well as aliphatic diisocyanates (hexamethylene diisocyanate (HDI)) possessed good biocompatibility.[26-27] Over the course of 90 days in porcine aneurysms, the porous SMPs allowed for transition from fibrin to order collagen connective tissue throughout the aneurysm. Inflammatory scoring of the aneurysm was performed by counting the presence of macrophages and leukocytes in the aneurysm; SMPs had reduced local inflammatory cells compared with the suturing materials, as well as neovascular buds present, indicating that these SMPs are promising for long-term *in vivo* applicaitons.[33]

1.3 Characterizing the Degradation of Shape Memory Polymers

While the SMPs present with good biocompatibility out to 90 days in a porcine aneurysm, it is unknown how the long-term degradation behavior of these materials will occur. Wilson *et al* presumed that these SMPs would be biodurable, with degradation occurring at the carbamate linkage due to hydrolysis; the use of aliphatic diisocyanates was intended to improve the biocompatibility of the hydrolysis products.[36] Regardless of theory, however, translation of a medical device into the clinic requires extensive testing of degradation and toxic risk associated with it, with materials unknown to the Food and Drug Administration (FDA) often requiring more extensive testing.[50]

Degradation studies of polyurethanes, as mentioned previously, have identified a variety of failure mechanisms.[1,5] Primarily, these mechanisms can be related to oxidative or hydrolytic chain scission, although enzymatic degradation may occur.[1,5-8,50] Hydrolytic conditions that are appropriate for testing medical devices are phosphate buffered saline (PBS, pH=7.4) and 0.1 M sodium hydroxide (NaOH), and oxidative conditions are usually

3% H_2O_2 (real time) and 20% H_2O_2 catalyzed by 0.1 M $CoCl_2$.[1,5-11,50] While accelerated testing through elevated temperatures is suggested by some, including the International Starndards Organization (ISO) standard 10993-13, it appears that there are discrepancies between *in vivo* and *in vitro* results.[1,5-11,50] It has been suggested that while the Arrhenius equation may be used to predict acceleration, the role of the glass transition temperature (T_g) is not taken into account in this way.[9] Due to this, testing performed with more aggressive (but still reasonable) environmental conditions at body temperature may provide more accurate modeling of long-term behavior.[9]

While the degradation rates are more readily available using *in vitro* testing, the mechanism by which degradation occurs is less easily attainable in some cases. Predictions of the degradation pathway are usually accomplished using surface characterization (FTIR), along with scanning electron microscopy (SEM), thermal characterizations such as differential scanning calorimetry (DSC) or dynamic mechanical analysis (DMA), and examinations of the polymer chains using mechanical testing, gel permeation chromatography (GPC) or light scattering to examine chain length, and possible nuclear magnetic resonance (NMR) to examine changes in the chemical groups present. [1,5-11,50] However, in thermoset materials, analysis is hindered by the lack of solubility and the crosslinked nature of the polymer. Many conventional techniques recommended by ISO are not appropriate to perform on the bulk material, or will not produce the complete understanding of the degradation pathway. In this case, it is necessary to more closely examine the components individually, using model compounds, to determine their

susceptibility to the degradation environment if preliminary bulk testing reveals concerning behavior.[50]

While determining the mechanism of degradation is necessary, the other component of long-term risk assessment for medical devices is determining the toxicity of the degradation products.[23-25,51-56] Toxicological studies may be referenced for many starting materials, depending on their industrial uses, but degradation products may be more difficult to assess with accuracy.[55-60] In the case of SMPs, the fully degraded started material can be used to determine the risks of the bulk material through cell exposed to varying dilutions of the products. While this does not give detail on the individual products, it does allow for understanding overall toxicity levels that are tolerable, and for examining any synergistic effects of the products. Synthesis of select products may be used to gain further understanding of toxicity risks and be used for predicting limitations on the use of the biomaterial (maximum device size, etc).

The long-term degradation behavior and toxicity risks of the SMP foams has not yet been fully understood. Therefore, this research is aimed at investigating the degradation of polyurethane SMPs intended for vascular applications. The degradation mechanisms, rates, and toxicity risks will be studied to provide an understanding of the long-term utility and safety of these materials in endovascular devices, although the presented process is applicable for many implantable polymer systems.

1.4 Rationale for Increasing the Biostability of Shape Memory Polymers

Even with the cytotoxicity testing, degradation mechanism understanding, and the toxicological risk assessment that will accompany FDA submissions, reducing the rate of degradation (and thus the rate of degradation product formation) may be a useful tactic to assuage concerns of toxic risk associated with a device. A device that is considered biostable will be subjected to different regulatory considerations than one that is degradable.[50]

The desire to decrease the rate of oxidation in the SMPs was counterpoint to maintaining the biocompatibility and functionality of the current SMP formulations. Tuning the composition while maintaining the polyurethane linkages, high crosslinks, aliphatic monomers, and tertiary amines still offers avenues for increasing the biodurability. Previous work into reducing oxidation has indicated that the presence of antioxidants in the polymer bulk will reduce the mass loss rate.[7,73] EM Christenson incorporated Santowhite® into poly(ether urethane) and poly(carbonate urethane) films, which were shown to inhibit *in vivo* degradation in subcutaneous implants over a year.[7] Many other medical implants also utilize antioxidants to reduce oxidation of materials, with butylated hydroxy toluene (BHT) and its derivatives being common choices.[74-93] BHT and similar derivatives, as well as a hindered amine light stabilizer, vitamin C, and triphenyl phosphite were examined for their utility in reducing the oxidative mass loss of porous SMPs.

A limitation of this approach was the retention of antioxidants in the SMP throughout both the cleaning process as well as the time that the material is implanted. Unlike films, porous SMPs possess very high surface area, which increased the diffusion of physically incorporated antioxidants out of the bulk; covalently bound antioxidants may have altered

performance or may impact the properties of the polymer. The use of microparticles was investigated as an alternative to direct incorporation of the antioxidants.

While the incorporation of antioxidants may allow reduction in the rate of oxidation and mass loss due to tertiary amine fragmentation, a more stable chemistry could be useful for long-term stability. Glycerol, as well as isocyanurate triol, were examined as alternative starting materials to the amino alcohols, as these monomers may be less susceptible to oxidative fragmentation compared with the tertiary amines.

The characterization of degradation and assessment of toxicity risk of SMP is discussed in Chapter 2 and 3, respectively. Chapter 4 discusses the use of antioxidants for increasing biostability, and Chapter 5 expands upon this through the use of antioxidant-containing microparticles. Chapter 6 discusses the use of glycerol for producing more biostable SMPs, and Chapter 7 examines isocyanurate triols.

CHAPTER II

CHARACTERIZATION OF THE DEGRADATION BEHAVIOR OF SHAPE MEMORY POLY(AMINO URETHANE UREAS) INTENDED FOR VASCULAR OCCLUSION APPLICATIONS

2.1 Introduction

Polyurethanes have been in use for over fifty years as medical materials.[1-5,12,11-13] During this time, several widespread failures of these materials have been reported in both literature and the clinic, with two of the most notable being polyurethane coatings for pacemaker wire leads, and porous polyurethane coatings. [1-5,12,11-13,17-20,114] A recent 2016 study found that for pacemaker/defibrillator lead damage within the first year of device implantation has resulted in *ca* $1.1 billion costs, with damage to the leads occurring 0.47% to 1.94% of implanted devices, depending on specific application.[14] In a smaller case study, 27 pacemaker leads were returned to the manufacturer and analyzed, with 8 of the devices having undergone material failure that lead to 4 high voltage failures and one death, with an average implantation time of *ca* of 25.5 months. [15] Based upon the study being performed and the device selected for analysis, these failure rates may range from 0.19 %/year to 2.71 %/year or higher.[14-15] Failures for commercially available medical devices result in patient morbidity and mortality, and a major cause of these failures is the lack of analysis performed prior to implantation of the devices, which ultimately results in decreased understanding of the *in vivo* behavior.[1-5,12-15,113] Correlations between the *in vivo* and *in vitro* responses for the selected materials must be performed to not only characterize the rates of degradation, but also to determine the possible mechanisms, products, and associated patient risks.

Some of the analysis performed on the porous polyurethane systems has led to contradictory results; lab methodology used for testing was not supported by *in vivo* data.[17-20,114] The urethane coatings were reported to undergo hydrolysis in the body, resulting in the presence of aromatic amines formed during hydrolysis of the carbamate, but the amine formation was a result of testing conditions that did not align with what the material would have experienced *in vivo*, ultimately resulting in data that does not accurately predict stability, and therefore toxicity risks, overtime.[5-8,18-22,38] Additional long term studies of these polyurethane foams have further indicated a reduced rate of tumorogenesis, no association with cancer and the use of the aromatic diisocyanates, and no long term risk of cancer in studies ranging from animal to human studies, although a few studies still point to possible risks within the first few years after implantation.[17-21,114] These conflicting outcomes present the need for better analyses of degradation and toxicity. [1,37]

For many polyurethane systems, oxidation is also known to occur in addition to hydrolysis, but is typically limited to the chain extenders in the soft segment, such as ether linkages.[1,4,5-8] Despite these degradation concerns, tissue engineered scaffolds, drug delivery therapeutics, and devices continue to utilize poly(urethane urea) chemistries due to the versatility of the compositions and the ease with which traditional polymerization yields the final products.[1-3,113] However, there are still a lack of studies that provide adequate correlations between *in vivo* and *in vitro* behaviors as well as degradation mechanisms and toxicity assessments.

In fact, polyurethanes have gained even greater interest as medical materials due to inherent shape memory properties.[26-27,36-37,71,115] Ideal vascular materials will incorporate

stimuli-responsive polymers (for minimally invasive procedures) with a controlled biostability that do not suffer from the limitations of thermoplastic systems.[36] An example of a series of stimuli-responsive polyurethanes intended for minimally-invasive medical devices was initially developed by Wilson *et al*., with the intent to overcome toxicity limitations while also improving on the shape-responsiveness of the polymers.[36] The developed shape memory polymers (SMPs) are amorphous, highly crosslinked, and have ultra-low density.[26-27,36-37,71] These SMPs were derived from monomers that are symmetric, multi-functional, and aliphatic, based upon the use of polyaddition reactions between diisocyanates and amino tri- or tetra-ols.[36] This approach was used to produce highly crosslinked networks that possess high-strain-low-stress shape recovery, T_gs tunable around body temperature, and excellent biocompatibility, confirmed using both *in vitro* cellular studies as well as histological analysis of implants.[26-27,36-37,71] However, given that the alcohols used in the synthesis of these SMPs are also polyamines, it was important to consider their ultimate fate, and to conduct material degradation studies. Similar amino alcohol species have also found use in carbon dioxide remediation, where fragmentation is common, although environmental conditions are varied; other applications of polyamines include gene and drug delivery.[115-123]

Here we present the comparison of *in vivo* and *in vitro* degraded SMP samples. We utilize commonly available laboratory techniques to demonstrate methodology for determining rates of degradation based upon morphology, composition, and thermal properties in thermosets. The mechanism of degradation and the rate of specific degradation product formation are also determined through the use of model compound studies and

analytical techniques. The relationship between the benchtop studies and the *in vivo* materials were further characterized using spectroscopic and morphological techniques, allowing for the determination of conditions to accurately model the degradation of the materials. The determination of the concentration of hydrogen peroxide (H_2O_2), the main oxidative source for degradation, as well as the degradation products, was used to determine the toxicological risk associated with treating the largest plausible aneurysm.

2.2 Materials and Methods

N,N,N',N'-Tetrakis(2-hydroxypropyl)ethylenediamine (HPED, 99%, Sigma Aldrich), triethanolamine (TEA, 98%, Sigma Aldrich), hexamethylene diisocyanate (HDI, TCI America, >98%), 2,2,4-trimethyl hexamethylene diisocyanate (TMHDI, TCI America, a mixture of 2,2,4 and 2,4,4 monomers, > 97%), isophorone diisocyanate (IPDI, Sigma Aldrich, 98%) were the monomers used in the synthesis of bulk SMPs. Hexyl isocyanate (TCI America, >98%) was used without purification. H_2O_2 (50%), sodium hydroxide (NaOH pellets, Sigma, >97%), phosphate buffered saline (PBS, Sigma, pH=7.4), cobalt chloride ($CoCl_2$, anhydrous, Alfa Aesar, 98%) were used for degradation solutions, in reverse osmosis (RO) water. Ethanol (EtOH, 195 proof, Sigma), isopropyl alcohol (99%, IPA, Sigma Aldrich), acetone (99%, Sigma) were used for cleaning. Phloxine B (PhB, 99%, Sigma) was used for confocal microscopy.

Bis(2-hydroxypropyl)amine (>98%), 3-amino-1-propanol (>99%), ethanolamine (>99%), diethanolamine (>99%), oxalic acid (>99%), glycolic acid (99%), glyoxal (40% in H_2O), and allyl alcohol (>99%) were purchased from Sigma Aldrich, and were used without further modification. Di-tert-butyl dicarbonate (99%), molecular iodine (99.99%, trace

metals basis), sodium thiosulfate (99%), and hydrogen chloride solution (4 M in dioxane) were obtained from Sigma Aldrich, as well.

Acetonitrile (99.93%, HPLC grade, Sigma), methanol (50% in H_20 with 0.1% v/v formic acid, LCMS grade, Sigma), methanol (99.9%, LCMS grade, Sigma), and water solution (0.5 % v/v formic acid, HPLC grade, Sigma) were used with liquid chromatography. Pancreatin, collagenase, and trypsin were purchased from Sigma, and used without modification.

Porous SMP foams were synthesized using a two-step method, composed of an isocyanate premix and an alcohol premix. The isocyanate premix was made by dissolving stoichiometric amounts of alcohols in diisocyanates, and curing the premix. The stoichiometry is the isocyanate index (NCO index, ratio of [NCO]:[OH]); the NCO index of the premix is 2.5-3.0, adjusted to achieve a variety of pore sizes and densities. The premix was heated in a 36-hour cycle to 50 °C (room temperature for 6 hours, 20 °C/hr to 50 °C, isothermal for 18 hrs) before returning to room temperature. The alcohol premix was made prior to the foaming process, and contained the remaining alcohol moieties (HPED and TEA), surfactants (Siloxanes, industrially named DC 5943 and DC 198), catalysts (tin (II) 2-ethylhexanoate and triethylamine), and blowing agents (Enovate) to achieve a final NCO index of 1.05. The two components are mixed in a high speed speedmixer before being placed in a 90°C oven for 20 minutes, followed by an overnight cold cure in the fume hood. Figure 1 shows the final product in bulk, and SEM images of pores.

Non-porous SMP films were synthesized using the same polyaddition, with stoichiometric amounts of diisocyanates added to an alcohol mixture of HPED and TEA.

Alcohol ratios were varied, as were diisocyanate species. The NCO index was *ca* 1.05 for films. The polymer mixture was heated to 120 °C at 30 °C/hr, isothermal at 120 °C for 2 hrs, and then allowed to cool to room temperature.

Samples were cleaned using water and IPA rinses at 35 °C (2x water for 15 minutes under sonication, followed by 2x IPA for 15 minutes under sonication, with tumbling steps in between sonication, followed by 4x water for 15 minutes with sonication and 30 second tumbling in between) and dried at 50 °C under vacuum overnight.

Samples were characterized using differential scanning calorimetry (DSC) and dynamic mechanical analysis (DMA). For DSC (Q-200 DSC, TA Instruments, Inc., New Castle, DE), *ca* 5 mg samples were examined from -40°C to 120°C at a rate of 10°C/min, with the glass transition temperature (T_g) determined from the third heating cycle. For DMA, a Q800 TA DMA (TA Instruments, New Castle, DE) was used for a single temperature sweep from 0°C to 100°C at 2°C/min was used, with the peak tan δ value being taken as the T_g.

SMP foam cell structure and film surfaces were examined using scanning electron microscopy (SEM). Foams and films for SEM imaging were sputter-coated prior to imaging at 10 kV with 11x and 110x magnifications.

Degradation solutions were made on a 1 L scale. Phosphate buffered saline(PBS, pH=7.4) was made by adding RO water to packets of PBS solution, mixed well, and stored at 4 °C. 0.1 M NaOH solutions were made by adding 12 g of NaOH to 3 L of RO water, mixed well, and stored at 4 °C. 3% H_2O_2 solution was made by diluting 180 mL of 50% H_2O_2 with 2820 mL of RO water, mixed well, and stored at 4 °C. 20% H_2O_2 with $CoCl_2$ was

made by first weighing 7.77 g of $CoCl_2$ into a beaker, which was dissolved in 400 mL of RO water. 400 mL of 50% H_2O_2 was diluted with 200 mL of RO water, which was then poured into the $CoCl_2$ solution. The H_2O_2 solution was kept cold prior to dilution and addition. It sat for 10 min to warm to room temperature prior to use. The 20% H_2O_2 (accelerated) solution and 3% H_2O_2 (real time) were used for oxidative solutions. PBS was the real time hydrolytic and NaOH solution was the accelerated hydrolytic condition.

Sample cubes were then cut (2 cm x 2 cm x 2 cm) from the dried blocks using a hot wire cutter. Sections were taken from the center of the blocks to ensure that minimal changes to the foam pores had occurred due to cleaning. Masses were then recorded for each cube, and each cube was placed in a labeled, sealed vial.

SMP cubes were submerged in 30 mL of solution in a sealed vial. The vials were placed in a 37 °C oven (± 0.1 °C, measured with a thermocouple over 3 days). Samples were incubated for 3 days before replenishing the solution, checked daily to monitor solution levels, and were weighed every week for real time testing, and every 3 days for accelerated testing. Samples were then removed, rinsed thoroughly in ethanol, blotted with a Kim Wipe and placed on a second Kim Wipe in a 50 °C oven. Vacuum was pulled overnight, at 30 mm Hg. After removal from the oven, samples were weighed and returned to the vials, with freshly replenished solution. Sample analysis is detailed below. Films were tested using the same protocol, but were cut into DMA bars with thicknesses of ~3 mm.

The mass was converted to remaining mass percentage, and the average change and standard deviation was recorded and plotted.

Attenuated total reflectance Fourier transform infrared spectroscopy (ATR-FTIR) spectroscopy was used to determine any spectroscopic changes to the bulk material, although no significant changes were expected. ATR-FTIR spectra were taken using a Bruker ALPHA infrared spectrometer (Bruker, Billerica, MA) using 32 scans per spectra for both background and samples. Spectra data was collected in absorption mode with a resolution of 4 cm^{-1}. OPUS software was used to examine spectra, identify peaks, and perform baseline and atmospheric corrections. Examinations were performed in triplicate to confirm results.

Solution state nuclear magnetic resonance (^{13}C 125 MHz and ^{1}H 500 MHz) was performed on an INOVA 500 spectrometer and spectra were referenced to solvent, $CDCl_3$ or DMSO-d_6 . Solid state CP (cross-polarization) MAS NMR (^{13}C 100 MHz) was performed using a 4.0 mm ^{13}C probe on an Avance-400 Solids spectrometer (Bruker). A frequency of 123.63 MHz was used, with a spin speed of 5 kHz and 90° pulse lengths of 4.5 µs. A recycle delay of 5 s and a contact time of 1.6 ms were the used measurement parameters. Edited CP MAS NMR experiments were performed as well, to observe positively-phased signals for C and CH carbons, negatively-phased CH_2, and zero-intensity signals for CH carbons to assist in peak assignments, with an external TMS standard.

X-ray photoelectron spectroscopy (XPS) was performed on dry samples using an Omicron XPS/UPS system with Argus detector. A magnesium x-ray source, a 124 mm electrostatic hemisphere dispersive energy analyzer and a 128 channel micro-channel plate Argus detector with 0.8 eV resolution. A CN10 charge neutralizer was used to reduce surface charging. Experimental parameters were a X-ray emission current of 5 mA and an anode voltage of 15 kV, and 10 µA with a beam energy of 5 eV for the CN10 neutralizer; a

rectangular aperture (0.311 mm x 3.22 mm was used. Survey scans from 1100 eV to -10 eV were performed with a step of 1 eV and a dwell time of 0.05 s. High resolution scans for C1S (305-282 eV), N1S (408-396 eV) and O1 (516-503 eV) peaks were selected, with steps of 0.05 eV, a CAE of 20 and dwell time of 0.1 s.

Stoichiometric amounts of TEA and HPED were added to respective, and sealed, 20 mL round bottom flasks equipped with stir bars. The flasks were charged with a slight excess of hexyl isocyanate, and nitrogen was purged into the flask. The reactions were allowed to continue overnight at 50°C. TEA-hexyl produced a waxy solid, and HPED-hexyl produced a viscous liquid. Both products were purified using silica column chromatography.

Standards were synthesized to confirm degradation products and species. Bis(2-hydroxypropyl) amine, 3-amino-1-propanol, ethanolamine, diethanolamine, oxalic acid, glycolic acid, glyoxal, and allyl alcohol were found to be representative end groups of the main degradation products. Di-tert-butyl dicarbonate was added in stoichiometric amounts to each solution of amines (10 mmol) in a 10 mL round bottom flask with a stir bar, along with 1 mmol molecular iodine, as a catalyst, and was allowed to react over night at 50 °C. Stoichiometric amounts of hexyl isocyanate were then added to the solution and allowed to react for 24 hours, under nitrogen at 50 °C. Characterization confirmed the presence of carbamates, and deprotection was performed using 4 M HCl in dioxane for 3 hours. LCMS standards were washed with sodium thiosulfate (aq.) to remove iodine, and then the organic phase was collected and dried at 50 °C under vacuum (30 in Hg). Samples were diluted to 0.1 mg/mL, and then diluted by 50x 6 additional times to produce 6 calibration standards.

Samples were dissolved in 50% methanol with 0.5% formic acid, the same solvent used for LCMS characterization.

Samples were incubated at 37 °C with 50% hydrogen peroxide (uncatalyzed). Aliquots were separated, filtered through activated carbon, and characterized; the remainder of the sample was left in solution. Degradation rates and products were characterized using NMR (^{1}H, ^{13}C), LC-MS, and FTIR characterization.

LCMS was performed using a ThermoFisher Orbitrap with a Hewlett Packard LC attachment, and a C18 normal phase silica gel column. The chromatography profile was 23 minutes long, altering from 95% methanol to 90% acetonitrile over 18 minutes with a linear gradient, with the remaining time at 95% acetonitrile to remove contaminants.[123] A blank of 50% methanol with 0.5% formic acid was used to clean the column.

Green fluorescent protein (GFP)-expressing fibroblasts (NIH3T3/GFP, Cell Biolabs Inc., USA) were expanded then seeded onto control (unmodified) and degraded films at a density of 20,000 cells/film in normal growth media, which contained high glucose Dulbecco's Modified Eagle Medium (DMEM, GE Biosciences, USA) with 10% fetal bovine serum (FBS) (Atlanta Biologicals, USA), and 1% penicillin/streptomycin (100 U/µg/mL, Invitrogen, USA). For foam studies, foams were soaked overnight in cell-binding media, which contained normal growth media with 1% dissolved gelatin, prior to cell seeding. After initial cell seeding, films and foams were transferred to new well-plates to ensure cell growth was limited to the polymeric biomaterial.

To investigate cell proliferation, an Alamar Blue assay (Thermo Fisher, USA) was utilized per the manufacturer's instructions to calculate percent reduction of reszurin (blue)

to resorufin (pink). Proliferation within foam samples was normalized to accessible surface area via considerations of foam volume and percent porosity. At the respective time points (Day 0, Day 1, Day 3, and Day 7), cell morphology was evaluated using fluorescence microscopy with an excitation of 488 nm (Nikon Ti-U Inverted Microscope, USA); for Day 0 time point, cells were allowed to adhere for three hours prior to imaging. Representative images were selected over the course of imaging three replicates for each film or foam.

2.3 Results and Discussion

Porosity of the SMPs can be controlled through a combination of NCO index, premix viscosity, catalyst concentrations, and concentration of physical blowing agents that are used. By removing the catalysts and blowing agents, non-porous films were produced; decreasing premix visocisty and NCO indexed results in larger pore sizes and reduced densities of the SMPs.

The reactions of the alcohols with the diisocyanates produces the urethane linkage that dominates throughout the bulk material, although other linkages will be present in small concentrations. Urea will from as a result of water reacting with an isocyanate to produce a primary amine, which then may react to form a urea linkage; the primary amine may also be a chain end. It is known that allophanate and biuret linkages may form (tri-branching urethane and urea, respectively) due to catalyst presence. Substitution of the diisocyanates or alcohols does not affect gel fraction of the materials (all greater than 99%), or the physical attributes of the material. The end result is a highly crosslinked, amorphous polymer with controllable pore size, density, and composition.

By increasing TEA concentration, the T_g of the material decreases, and increasing HPED results in increased T_g. The increasing HPED also results in greater crosslink density, higher elastic modulus, and greater hydrophobicity. As the diisocyanate is substituted from HDI to THMDI to IPDI, modulus, thermal transition, and hydrophobicity will increase as well.

For porous SMPs incubated in accelerated hydrolytic solution, no changes in the pore structure were found (no strut erosion, membrane rupture, pore collapse) after 36 weeks. This result contrasted with the behavior in real time oxidation: pore collapse and membrane rupture/erosion were found to occur within 4-6 weeks (**Figure 2.1**). For non-porous materials, surface erosion appeared as pitting and the formation of surface rippling, culminating in total material collapse. This behavior was found, qualitatively, to be dependent on both pore size and T_g.

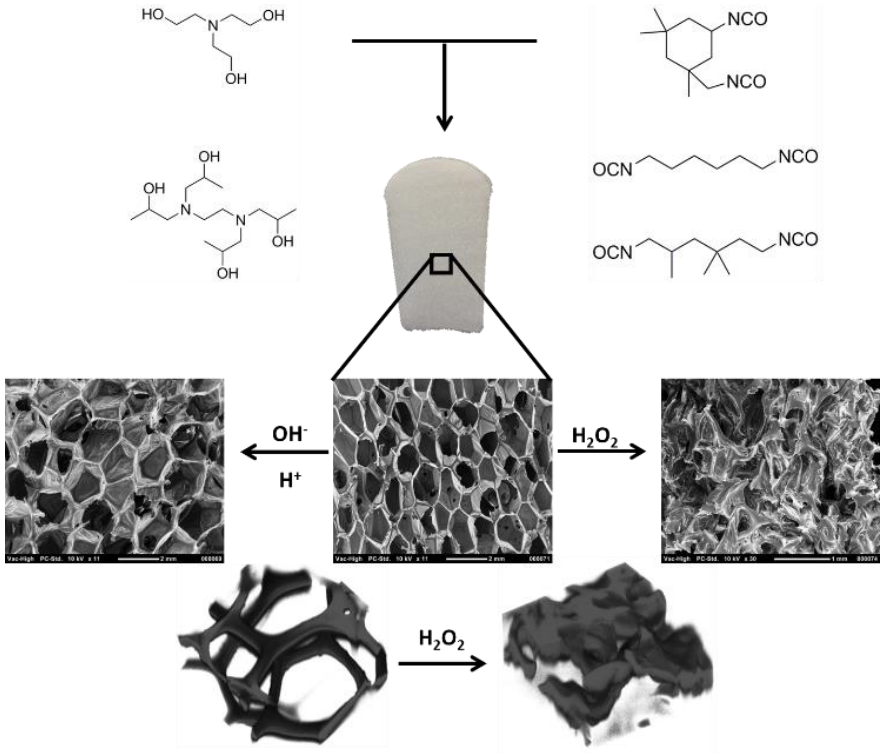

Figure 2.1. Starting materials used for the synthesis of SMPs and a representative porous scaffold (top), along with representative SEM images for the original pores, after 250 days in accelerated base solution, and 45 days in real time oxidative solution. 3-D pore structures demonstrating the material collapse are displayed (bottom).

SEM of non-porous SMP displayed no significant changes for hydrolytically degraded films. For oxidative films, the hydrophobicity (and thermal transition) had distinct differences on the degradation and the topology of the film after incubation. For higher

thermal transitions/more hydrophobic samples, films displayed more significant surface cracking and surface rippling over time. Cracking did not occur across the entire surface, and while presenting rapidly (within a few days of incubation) did not dominate the surface over the testing period. Surface rippling occurred across the majority of the surfaces, after significant time passed, and was more predominantly seen in real time oxidative solutions. Conversely, the more hydrophilic/lower T_g films displayed significantly greater surface pitting and bubbling. This occurred for both accelerated and real time oxidative testing.

The surface area for the porous scaffolds was determined microscopically, and comparisons between the rates of degradation between the porous and non-porous materials was performed. The larger pores (lower surface area) result in a slower mass loss rate compared with smaller pores. The non-porous films have lower T_gs, but slower degradation rates. This behavior may be due to the presence of membranes in the porous materials, which allows for the formation of concentration gradients prior to the membrane perforation and removal as well as providing increased surface area. Simultaneously, the hydroxyl radicals are also degrading the struts, which eventually results in the complete material collapse as well as surface pitting and cracking.

A lack of mass loss over the examined period of 250 days in accelerated hydrolytic solution was observed, in agreement with SEM results. Accelerated oxidative testing (20% H_2O_2, 0.1 M $CoCl_2$) resulted in rapid oxidation and total mass loss within days for materials with T_gs ranging from 20 °C to 130 °C; degradation rate was T_g dependent, as well as concentration and surface-area dependent (**Figure 2.2**). SMPs in accelerated oxidative solution underwent complete mass loss in less than 30 days, with HDI degrading in 9 days,

TMHDI in 20 days, and 50% IPDI/50% TMHDI in *ca* 28 days. These results are supported by gravimetric analysis in 3% H_2O_2 solution. Porous SMPs incubated in this solution displayed similar trends based on T_g and diisocyanate species. The time to 50% mass loss of the porous SMPs in 3% H_2O_2 is *ca* 100 days for HDI, and 150 days for TMHDI using extrapolation.

Gravimetric analysis of the non-porous SMPs revealed rapid mass loss over the course of the study when incubated in oxidative solutions. With the TMHDI non-porous SMPs, the rate of degradation was distinctly dependent on the T_g, as the HPED: TEA 0:100 (TEA as the alcohol monomer) films degraded significantly faster compared to the HPED:TEA 100:0 (HPED as the alcohol monomer). This dependence on T_g is demonstrated by the substitution of the diisocyanate species in films containing only HPED as the alcohol monomer. In these gravimetric studies using 3% H_2O_2, HDI films degraded more rapidly, and IPDI films were found to be extremely oxidatively resistant. These behaviors agree with examinations of the porous SMPs, such as with the delay in the onset of mass loss found in real time oxidative testing.

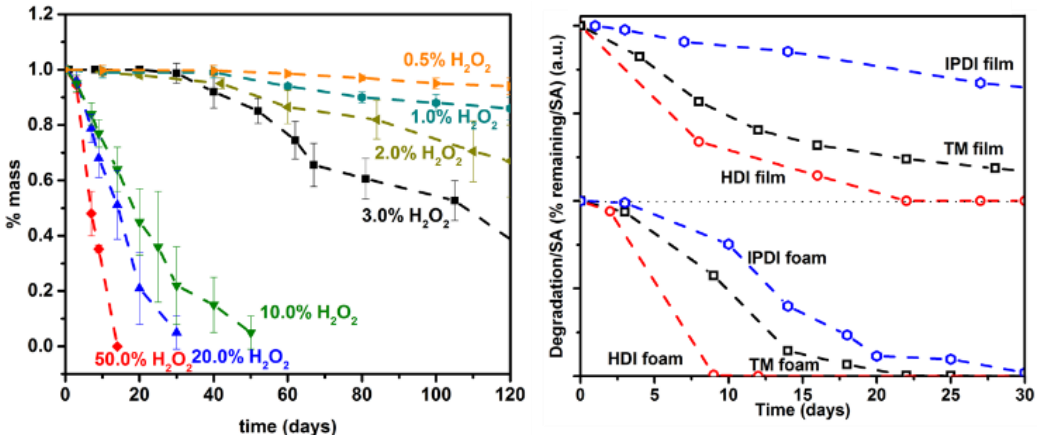

Figure 2.2. Gravimetric results for SMPs displaying the effect of varied hydrogen peroxide concentration (left) on mass loss rate and the effect of porosity (right). H_2O_2 concentration dependency is demonstrated for HDI based porous SMPs (TEA: HPED 40: 60), and the porosity dependency displays results for the three diisocyanates used with alcohol ratios of TEA:HPED 40:60. All experiments were conducted at 37°C.

Figure 2.3 indicates the major amine degradation products observed by LCMS. Both alcohols will oxidize to form the respective amine oxides (N-oxides) or aminium radical cations (**Figure 2.4** and **2.5**).[29,30,36,38] The tetra-ol (HPED, starting material 7) will have steps analogous to the triol TEA to form N-oxide(s) or radical cation(s) (product 8), prior to any fragmentation occurring. One of the N-oxides fragments by C-N cleavage to form an aldehyde (eventually a carboxylic acid) and a secondary amine, which may further fragment to form a primary amine endgroup (product 10). Further fragmentation at this amine (C-N), could produce either an aldehyde and subsequent acid end group after concomitant release

of ammonia (product 13). Alternatively, the N-oxide (product 9) may fragment to form another secondary amine (product 14). Internal C-N fragmentation (product 13→18 or 17→19) would result in the formation of small molecule aldehydes (glyoxal), glycolic acid, and carboxylic acids (oxalic acid) from cleavage of the ethylene chain linking the amine groups. These small molecules will form through a glyoxylic acid intermediate (product 15) before formation of oxalic acid (product 16). Oxalic acid formation appears more likely than dialdehyde (glyoxal) due to consumption of aldehyde in the highly oxidative environment.

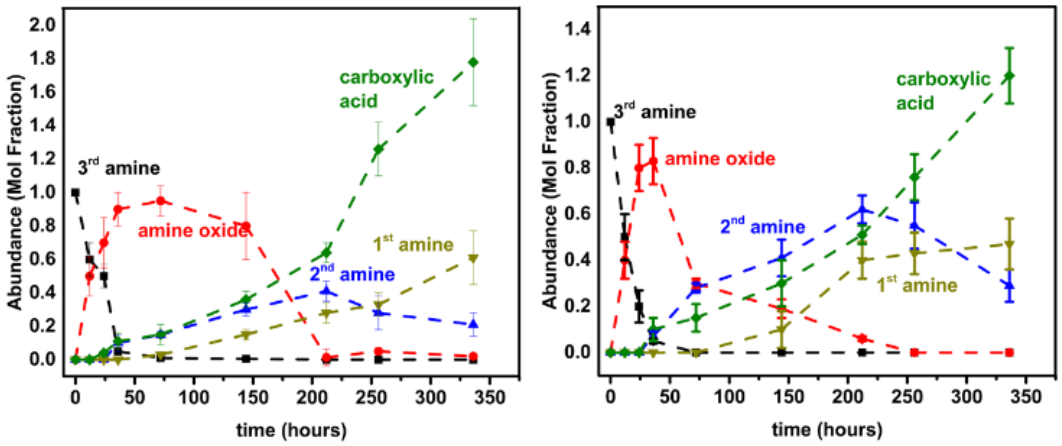

Figure 2.3. Abundances of major degradation products for the model study, determined from LCMS, displaying abundance of degradation products for HPED-hexyl (left) and TEA-hexyl (right). All experiments were conducted at 37°C.

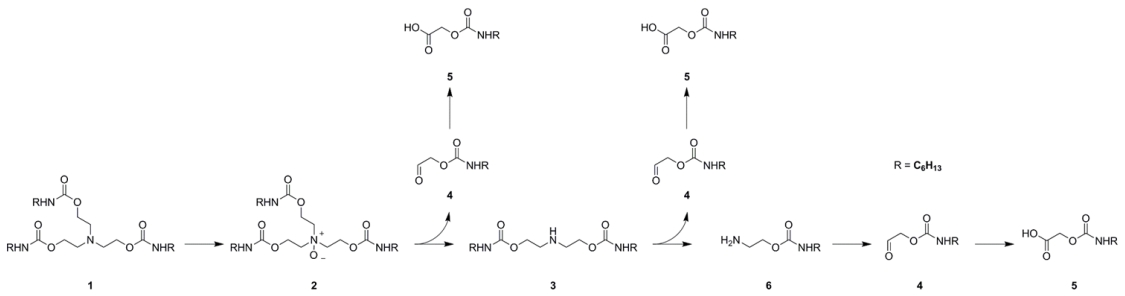

Figure 2.4. Proposed degradation pathway for TEA in an oxidative environment. The observed species are the TEA-hexyl starting material (1), which oxidizes to the N-oxide (amine oxide, 2). Fragmentation combined with oxidation and reduction will lead to the formation of the secondary amine (3), and an aldehyde (4), which further oxidizes to a carboxylic acid (5). The secondary amine fragments to form the primary amine (6), which will also lead to carboxylic acid (5); the byproduct of the primary amine fragmentation is ammonia.

Spectroscopic analysis of *in vivo* samples indicates that oxidation occurs, but at a slower rate than what is indicated as real time by previous (*in vitro)* studies.[1,5,12,13] Surface analysis was performed using FTIR, X-ray photoelectron spectroscopy (XPS) and SEM (**Figure 2.6**).[1,5] SEM images reveal that the material underwent collapse similar to what is found for *in vitro* samples: membranes are completely destroyed by 90 days, with some fragments still seen at 30 days. Surface pitting is also greater over time. Spectroscopic comparison indicates similar changes in peak location and relative height compared with *in vitro* testing, albeit at a slower rate. This is supported by C1s analysis via XPS, confirming oxidation of the material surface. Based upon the relationship between the mass loss and the

gel fraction and the determined mechanisms, a release rate of degradation products was determined. (**Figure 2.7**). The size of products was determined by MS and used to further characterize the types of products that would accumulate over time, with the smallest, most soluble products being the most prominent. The carbamic acid products, which are a result of the long term oxidation of the urethanes, were found to have the lowest concentration over time, with little change in the generation of carbamic acids over the course of the study. Low molecular weight products containing acid and aldehyde end groups were the most common products, followed by low molecular products with amine end groups.

The variation in T_g associated with moisture is due to the plasticization of the urethane bonds *via* interruption of the hydrogen bonding by water molecules. Without a solvent, sufficient temperature is required for movement of the polymer backbone, which allows for shape change associated with the return the entropic maximum that determines the primary shape of the material. In the presence of a solvent that can interrupt the hydrogen bonding, such as water or ethanol, the required temperature for the shape to change to occur is dramatically reduced, and shape recovery can be achieved at lower temperatures through the use of solvent as opposed to a purely thermally-driven recovery mechanism.[132-133]

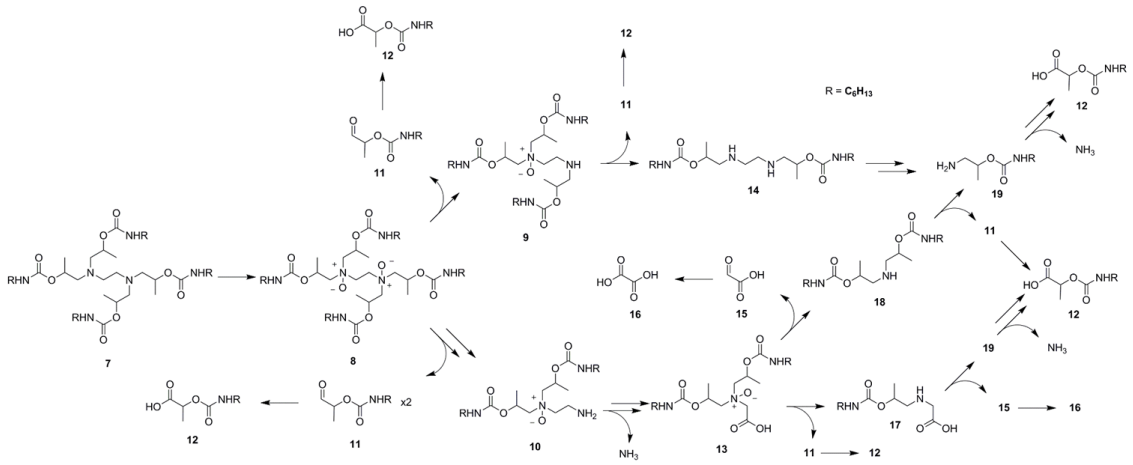

Figure 2.5. Proposed degradation pathway for HPED in an oxidative environment. The starting compound (7) can oxidize to the N-oxide (8). Fragmentation will lead to a secondary amine (9), or an N-oxide and a primary amine (10) which will further degrade to a single N-oxide (13). The formation of (9) also yields an aldehyde (11), which further oxidizes to a common final degradation product, (12). The degradation of (13) with competing asymmetric C-N fragmentation pathways is governed by sterics and electronics *e.g.* product (17) versus (18) from (13). Degradation to form (18) will yield a small molecule glyoxylic acid (15) that oxidizes to oxalic acid (16). Analagous competitive cleavage is also possible with other degradation intermediates such as (9). The byproduct of the primary amine (19) degradation is ammonia.

Surface area calculations revealed a relationship with pore size: with increasing pore size, surface area decreases. Pore size is defined as the average diameter of the pore. As this diameter decreases, and porosity of the material increases, surface area increases. For non-porous materials, however, the surface area is smaller, and this relates to a slower rate of degradation. The behaviors of the pores and the degradation were determined *via* confocal

microscopy, allowing for 3D representation of the pore. As mentioned previously, during oxidation the pores of the material are eroded away rapidly. This is followed by a reduction in strut diameter. The membrane removal occurs over the initial three days (accelerated oxidative solution, 20% H_2O_2 with 0.1 M $CoCl_2$), confirmed by SEM. Towards the end of the process, the struts begin to erode and reduce in diameter.

Gravimetric analysis was related to the morphological changes and the network behavior through examination of spectroscopic changes (Fourier transform infrared spectroscopic analysis (FTIR), solid state ^{13}C nuclear magnetic resonance (^{13}C NMR). The scission of the C-N bond in the tertiary amine was indicated through both the shift in the urethane peak (1688 cm^{-1} to 1702 cm^{-1}) relative to the urea peak (at 1640 cm^{-1}) in FTIR, as well as the formation of new peaks in the ^{13}C NMR spectra within the amine region (60 ppm and 67 ppm converging into a single peak at 65 ppm that shifts to 68 ppm) indicative of primary amine formation. Solid state ^{13}C NMR showed no change in the urethane peak resonance (155 ppm); and any potential formation of an aldehyde may be obscured by a spinning side band. Neither FTIR nor solid state ^{13}C NMR spectroscopic signals indicated distinct change during the more mild hydrolytic testing, under both real time and accelerated conditions.

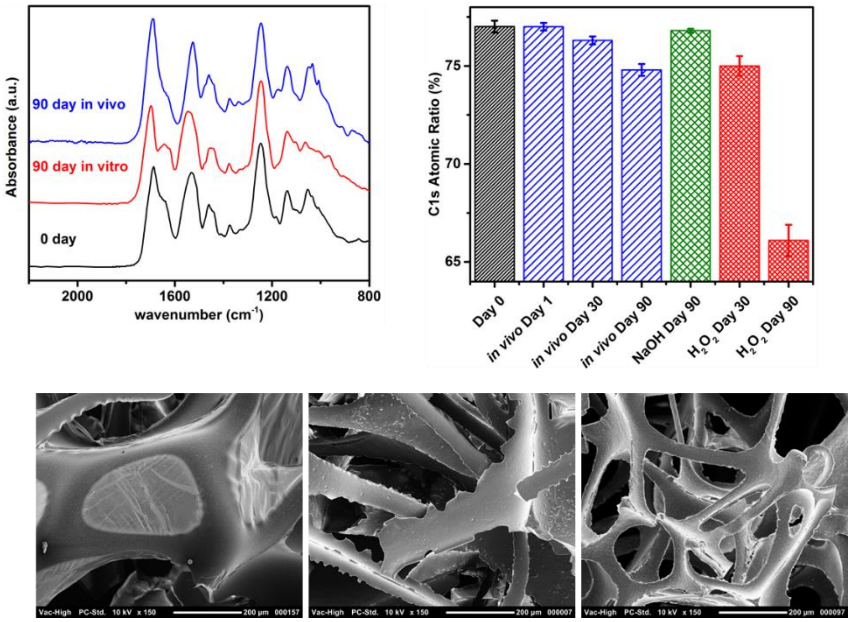

Figure 2.6. Spectroscopic analysis of implanted, porous, HDI SMPs (HDI with an alcohol composition of 60% HPED and 40% TEA). (A) displays FTIR comparison (between 2200 and 800 cm^{-1}) for an untreated sample (day 0), a sample degraded in 3% H_2O_2 for 90 days (90 day *in vitro*), and a sample explanted from the porcine sidewall aneurysm after 90 days (90 day implant). (B) displays the C1s peak XPS comparison of the same samples, as well as a 1 day implant (Day 1 implant), a 30 day implant (Day 30 implant), a sample degraded in 0.1 M NaOH for 90 days (Day 90 NaOH). SEM images of day 0 (C), day 30 (D), and day 90 (E) are presented as well. Using SEM, it is apparent that the membranes are degraded over the course of the implantation, with residual membranes shown in (D) compared with (C) (complete membranes are present) and (E) (no membranes remain). Further, the struts are more pitted and marked in (E) (90 day implant), compared with day 0 and day 30 implant surfaces.

Table 2.1. The calculated degradation times relative to the *in vivo* samples.

Species	FTIR (days)	XPS (days)	Strut thickness (days)
In vivo Day 30	30	30	30
In vivo Day 90	90	90	90
H_2O_2 (30 day)	20 ± 1	14 ± 1	16 ± 3
H_2O_2 (90 day)	48 ± 2	42 ± 1	46 ± 4

Due to the observations of material breakdown macroscopically and gravimetrically, yet the limited solid-state FTIR and ^{13}C NMR evidence for the chemistry occurring during degradation of the thermosets, model studies were undertaken. Although the harsh conditions of the oxidatively-degraded samples showed distinct spectroscopic changes to the amine (C-N bond), indicating the scission of the tertiary amine, limitations in the detailed analysis of the thermoset networks (limited analysis *via* NMR, mass spectrometry, *etc*., as a result of insolubility), required the examination of degradation products using small molecule analogs and LC-MS.[29] The small molecule structures include urethane and amino linkages to simulate the chemical moieties in the SMP thermosets.

As demonstrated by the solution NMR spectra, carboxylic acids are formed rapidly during the degradation process in 50% H_2O_2. ^{1}H NMR indicates the formation of carboxylic acid with significant presence of aldehyde (relative to the carboxylic acid peak). ^{13}C also confirms presence of aldehyde and acid resonances at *ca.* δ 207 and 173 ppm. LCMS also

quantified the degradation products**.** The NMR spectra support the degradation products as presented in **Figure 2.4** and **2.5** (aldehyde and carboxylic acid formation). At any time during the degradation of the bulk material, sufficiently small network fragments may be solubilized and interact directly with or be taken up by cells present at the material interface. Other products are indicated by literature and were found, but accounted for less than 0.05% (by mass) of the total. It is important to note that in the degradation of small molecule urethanes, ethyl carbamate, which is a known mutagen, is a product of concern to the Food and Drug Administration (FDA). However, this product, which would require the deoxygenation of the carboxylic acid endgroup followed by oxidative fragmentation of the hydrocarbon backbone at the beta position to the urethane. This would need to occur preferential to the more favored decarboxylation and occur either in sequence or simultaneously to the hydrocarbon oxidation, all of which are unlikely as singular events.

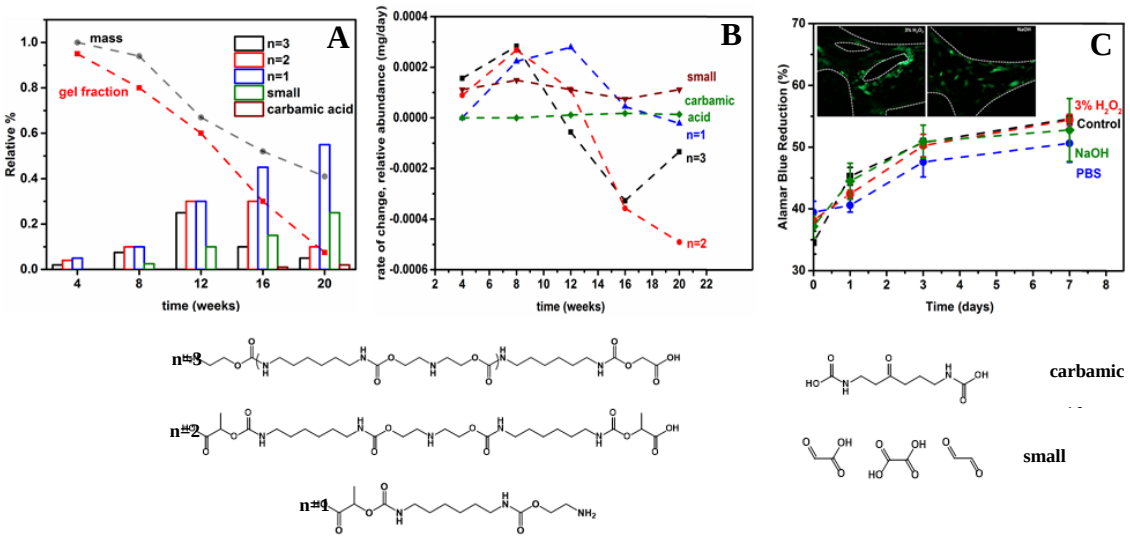

Figure 2.7. (A)The relationship between mass loss over this same time and the gel fraction is overlayed on the theoretical accumulation degradation products based upon relative size, and the rate of change of product accumulation (B). The cytocompatibility of films incubated in degradation solutions is presented, displaying no changes between the original and materials degraded for 12 weeks (C). Selected molecular species are displayed, demonstrating the relative sizes of the degradation products.

The rate of mass loss at 50% H_2O_2 is the equivalent of the 20% H_2O_2 catalyzed by $CoCl_2$ (Figure 3). This indicates that mass loss of the polymer, which occurs by 2 weeks at these conditions, happens after the consumption of the tertiary amines and the initial formations of the secondary and primary amines, respectively. Additionally, the delay in mass loss found over the initial few days and concomitant mass increase is most likely due to the formation of amine oxides from the available amines. Only after remaining amines

have been oxidized will significant chain scission begin to occur, and subsequent mass loss observed. The oxidized SMP will not crystallize at any point in the degradation product, further indicating that the majority of the oxidation results in the generation of small molecule degradation products (primary amine end groups rather than longer chains containing repeating secondary amines).

Surface analysis indicates that the time implanted at the aneurysm site differs from the literature standard 3% H_2O_2 solution as a real-time approximation. This difference is such that 45 ± 3 days *in vitro* is the equivalent of 90 days *in vivo*. The urethane peak shift in FTIR (1689 to 1694 cm^{-1}) and change in the percentage of C1s determined by XPS indicated a surface aged to the equivalent of 48 ± 2 days and 42 ± 1 days, respectively (**Table 2.1**). This suggests that a 1% or 2% H_2O_2 solution would be a more appropriate solution for modeling degradation for these highly porous SMP scaffolds when they are used in endovascular applications, with the comparison between the H_2O_2 concentration-dependent rates displayed in **Figure 2.2**; the lower-than-anticipated degradation rate is most likely due to the combination of surface chemistry, high surface area, and the porosity.[5.32,33] As compared to the silk and polypropylene present at the aneurysm sites, these SMPs display reduced inflammatory response and higher neovascularization, resulting in lower numbers of macrophages and neutrophils at the implant site, which in turn results in lower levels of peroxides and superoxides, and will ultimately decrease the oxidation rate at the material surface.[119-121]

Comparison of the *in vivo* and *in vitro* surfaces indicates, again, the loss of membranes over the course of degradation. Additionally, the struts of the SMP are thinner,

with surface pits forming and residue being clearly visible. The initial SMPs do not contain these issues. Cytocompatibility of the degraded SMPs was confirmed *via* examination of cellular proliferation. The change in cytocompatibility between the original SMPs and those incubated in degradation solutions was examined using direct contact studies, with no differences between surfaces found. Cell morphology and proliferation were found to be equivalent across the control, oxidative, and hydrolytically treated surfaces.

Analysis of the degradation products and interpolation of the concentration vs degradation rate allowed for determination of the concentration and species of degradation products (**Figure 2.6**) based upon the now determined rate of material degradation (**Figure 2.2**). This analysis allows for the identification of molecular species that are known to be toxic, carcinogenic, or have other risks associated with them, as well as to determine the formation rate of these products. Through this analysis, it is possible to further understand the long-term behavior of these implants and the toxicological risks associated with potential exposure to degradation products. While a complete toxicological risk assessment is ultimately necessary prior to commercialization, the most immediately concerning products of SMP fragmentation are glycolic acid and oxalic acid, which could limit the maximum mass of implanted materials if the daily dose rate exceeded the human safe exposure limit of 0.54 mg/kg body weight/day, determined from reproductive effects in animal studies; for an average 70 kg human this threshold is 37.8 mg/day for oxalic acid, which has a lower threshold compared with glycolic acid.[130-131] The analysis of SMP degradation indicates that the levels of exposure for a SMP foam that has a total mass of *ca* 400 mg (*ca* 32.0 to 36.6 mg total dose of oxalic acid, a daily dose of 0.7 to 0.8 mg/day, which is 1.1µg/kg/day) are

well below what would be considered a patient protective safe exposure limit per day. [130-131] An actual SMP device may be up to 100 mg, but most devices will in fact be less massive than this.

These degradation products may not completely oxidize, as well. The roles of primary amines and aldehydes in the adhesion of biomaterials with tissue has been the subject of recent study, with aldehydes in particular being of interest; increasing concentration of aldehydes increased the adhesion of the biomaterial to the tissue.[132-133] In the case of the presented SMPs, oxidation of the material produces aldehydes along with lower amines. This increased adhesion, in addition to the high porosity of the SMP, may explain previous results that demonstrate excellent biocompatibility of the SMP out to 90 days.[33,127-129,132-133]

While these results indicate the promise of such materials for use in vascular occlusion applications, further work is needed to definitively conclude that there are minimal cytotoxic concerns from degradation products. Based upon the mechanism and relative sizes of degradation products presented here, cytotoxicity testing of individual degradation product species is needed to determine the concentration thresholds and relationship with the rates of exposure. These experiments should also include mutagenicity testing, to determine that no adverse events will occur as a result of long term exposure over the life of the biomaterial.

2.4 Conclusions

In conclusion, we have demonstrated the degradation analysis of porous and non-porous SMPs intended for implantable vascular medical devices, and correlated the *in vivo* and *in vitro* behaviors. The use of amino-alcohols allows for degradation of the SMPs *via* an oxidative mechanism that results in the formation of lower amines and aldehydes, determined through model compound studies and analytical characterization. The degraded materials still possess excellent cytocompatibility, indicating their utility for long-term usage. Characterization of *in vivo* SMP samples was used to determine the rate of degradation and the relationship of the macrophage presence to the oxidation that is displayed. The *in vitro* degradation was used to confirm the mechanism of degradation in the bulk SMP, as well as to assess the rate of degradation product formation and examine the potential toxic risk these products pose to the host.

It is our belief that while many applications propose the use of amine-containing materials and similar structures, there is insufficient information currently available to accurately and appropriately assess the risks associated with using such materials for medical applications. The presented work provides results that support the use of these SMPs for vascular device, specifically for cerebrovascular aneurysm occlusions, and introduces the methodology required for accurate assessment of long-term stability and safety. Wide-spread use of such methods will allow for more accurate, safer modeling of implantable biomaterials and increase the translation of more reliable devices with fewer patient risks.

CHAPTER III

CYTOCOMPATIBILITY OF DEGRADATION PRODUCTS PRODUCED BY AMINO-ALCOHOL BASED ALIPHATIC, THERMOSET SHAPE MEMORY POLYURETHANES INTENDED FOR VASCULAR TISSUE ENGINEERING

3.1 Introduction

Shape memory polymers (SMPs) have been proposed for a variety of minimally-invasive medical devices due to the material's ability to change its geometry from one shape to another upon the application of a stimulus.[28,31,49] Medical devices that made from SMPs would be responsive to an external thermal or thermal-solvent stimuli, allowing for delivery of small device volumes before they recover their expanded, original form to be utilized in a variety of applications, such as for void-space filling applications.[29,40] An example of this is cerebral aneurysm occlusion, originally proposed by Sokolowski *et al* as a possible application for highly porous, polyurethane SMPs.[30,32] Material limitations of the SMPs used by Sokolowski led to the development of alternative porous, polyurethane-based SMPs with varied molecular architecture, such as the highly crosslinked aliphatic SMPs developed by Wilson *et al*.[27,36]

Polyurethanes were selected for these and other blood contacting applications due to their typically good bio- and cytocompatibility.[51-53] However, previous studies have indicated possibilities of toxicity and carcinogenicity as a result of urethane hydrolysis and by-products of the starting materials.[18] While this is typically associated with aromatic polyurethanes and diisocyanates, stability and toxicity risks are of concern for all biomaterials designed intended for long-term *in vivo* applications.[1,9-11,18] For this reason,

studies that characterize the degradation behavior, the degradation products, the rates of product formation, and the compatibility of such products are crucial before the translation of biomaterials from the lab into the clinic.

Previous studies have indicated that the symmetric, aliphatic, thermoset polyurethane SMPs developed by Wilson *et al* and utilized by Boyle *et al* and others, undergo mass loss as a result of an oxidatively-induced polymer scission mechanism (**Figure 3.1**).[36,39-40,134] This degradation is the result of tertiary amine oxidation to a N-oxide, followed by oxidation-reduction reactions that ultimately form secondary and primary amines, as well as aldehydes, carboxylic acids and possibly ammonia.[134] Further studies also revealed only minimal oxidation of the urethane linkage (carbamate) and the backbone of the diisocyanate starting monomers, indicating that the mass loss is primarily occurring due to tertiary amine fragmentation.[134]

HDI-TEA unit HDI-HPED unit

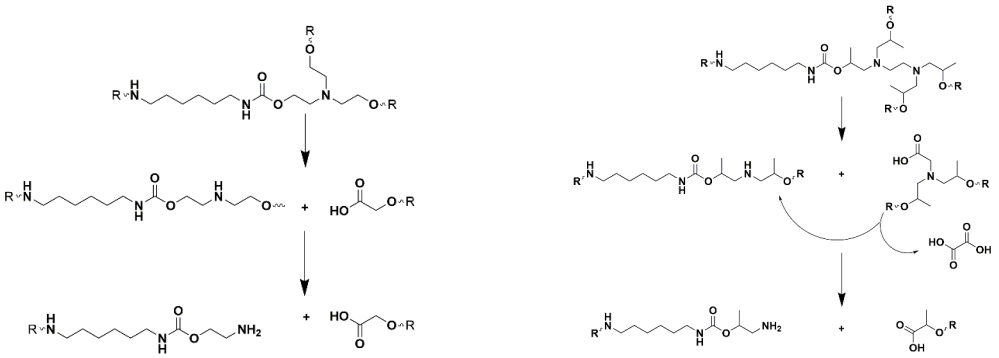

Figure 3.1. Proposed general pathways of oxidation of shape memory polymers containing amino alcohols triethanolamine (TEA) and hydroxypropyl ethylenediamine (HPED), where R denotes a proton or the continuation of the chain.

There are a number of concerns about toxic side effects from the degradation products produced by these SMPs; polymeric amines as well as acidic by products have been linked to cytotoxic effects.[55-56] Carboxylic acids may result in increased local pH, which ultimately can damage host tissues or the device, and some aldehydes are also known to be toxic.[55-56] Metabolism of amines and polyamines is known to result in a variety of outcomes, with some products being extremely toxic and others simply acting as antioxidants.[55] This indicates that there are many biocompatibility considerations for *in vivo* applications of materials, not just the initial bulk compatibility but the degradation products and leachable components, as well.[23-27,54-56,123]

These thermoset SMPs are synthesized from polyaddition reactions of aliphatic diisocyanates such as hexamethylene diisocyanate (HDI), trimethyl hexamethylene diisocyanate (TMHDI), or isophorone diisocyanate (IPDI), with poly functional amino alcohols such as triethanolamine (TEA) and hydroxypropyl ethylenediamine (HPED).[36,49,134] Hexamethylene diamine (HDA), which may occur as a synthesis by-product (hydrolysis of residual diisocyanate) or hydrolysis of the urethane bond, has been demonstrated to have cytocompatibility, resulting in improved cellular proliferation and adhesion when tested as a surface treatment.[59] In the body, HDI may be hydrolyzed to the diamine, react with tissue prior to hydrolysis to yield a diamine product, form a diacetylated product or a derivative containing an amine and an acetyl group.[23] The product is then excreted, although this is assuming it can enter the body from the material, but as a result of both the synthesis and cleaning processes for implantable biomaterials, the concentration of HDI should be negligent, although there is a possibility of HDA present.[23-25] It is expected that the behavior of IPDI and TMHDI is similar to that of HDI.[23-25] TEA is known to be cleared from the body rapidly, with *ca* 50-90% cleared in the first hour and the majority of the remainder in the following ten hours following intravenous injections.[57-58] Degradation products include those identified by previous studies, such as diethanolamine, monoethanolamine, and the corresponding aldehydes and carboxylic acids.[134] HPED is not known to be cytotoxic, but the *in vivo* behavior is expected to be excreted similarly to the TEA, but more slowly, and metal-diamine complexes have been proposed for antithrombogenic applications.[59] The HPED that is not passively excreted through the kidneys may chelate with metals present in

the body and/or oxidize to N-oxides followed by excretion or fragmentation during cellular metabolism.[60]

While a review of literature indicates that the leachable compounds are cytocompatible in sufficiently low concentrations, the toxicities of degradation products are not known and are difficult to accurately assess accurately. In this study, we characterized the size of degradation products from porous HDI-based SMPs, and synthesized selected products for cytocompatibility testing. These synthesized products were tested for cytocompatibility, and were then compared to the cytocompatibility of SMPs that had been exposed to degradation environments, as well as those that had been completely degraded in order to confirm our results and examine any synergistic effects of the products. The toxic levels were used to determine parameters for dosing of degradation products and maximum implantable material mass. These levels and parameters were finally compared to *in vivo* behavior, to access toxicity risks for these SMPs in vascular applications.

3.2 Methods and Materials

N,N,N',N'-Tetrakis(2-hydroxypropyl)ethylenediamine (HPED, 99%, Sigma Aldrich), triethanolamine (TEA, 98%, Sigma Aldrich), hexamethylene diisocyanate (HDI, TCI America, >98) were the monomers used in the synthesis of bulk SMPs. Hexyl isocyanate (TCI America, >98%) was used without purification. Hydrogen peroxide (50%, H_2O_2), sodium hydroxide (NaOH pellets, Sigma, >97%), phosphate buffered saline (PBS, Sigma, pH=7.4), cobalt chloride ($CoCl_2$, anhydrous, Alfa Aesar, 98%) were used for degradation solutions, in reverse osmosis (RO) water. Ethanol (EtOH, 195 proof, Sigma), isopropyl alcohol (99%, IPA, Sigma Aldrich), acetone (99%, Sigma) were used for cleaning.

Catalase (from bovine liver, 2000 to 5000 units/mg, suitable for cell culture) was obtained from Sigma Aldrich.

Bis(2-hydroxypropyl) amine (>98%), 1-amino-2-propanol (>93%), ethanolamine (>99%), diethanolamine (>99%), oxalic acid (>99%), glycolic acid (99%), lactic acid (80% in H_2O) were purchased from Sigma Aldrich, and were used without further modification. Glyoxal (40% in H_2O) was purchased from Sigma Aldrich and recrystallized prior to use. Di-tert-butyl dicarbonate (99%), dimethyl sulfoxide (99%), tetrahydrofuran (99%, THF). and hydrogen chloride solution (4 M in dioxane) were obtained from Sigma Aldrich, as well.

Acetonitrile (99.93%, LCMS grade, Sigma), methanol (50% in H_20 with 0.1% v/v formic acid, LCMS grade, Sigma), methanol (99.99%, LCMS grade, Sigma), and water solution (0.5 % v/v formic acid, LCMS grade, Sigma) were with mass spectrometry (MS).

MS was performed using a ThermoFisher Orbitrap in positive mode, with injection and column temperatures at 50°C. A blank of 50% methanol with 0.5% formic acid was used between samples to clean the column. MALDI mass spec with a 4800 Plus MALDI/ TOF/TOF Analyzer (Applied Biosystems, MSD Sciex, ThermoFischer Scientific) was used to examine bulk SMP degradation. Solution state nuclear magnetic resonance (^{13}C 75.4 MHz and ^{1}H 300 MHz) was performed on a Mercury 300 spectrometer and spectra were referenced to solvent, $CDCl_3$ or d_6-DMSO. Fourier Transform Infrared Spectroscopy (FTIR) attenuated total reflectance (ATR) was performed using a Bruker ALPHA FTIR-ATR (Bruker, Billerica, MA). An Omicron XPS system (Mg/Al x-ray source) with an Argus detector was used for elemental analysis of the final SMPs prior to degradation.

Typical procedures for the protection of amino alcohols is described for 1-amino-2-propanol. A slight excess of glacial tert-butyl carbonate (3 g, 0.014 moles) was added 1 g amino-2-propanol in 20 mL vials (0.013 moles) with 1 mL of THF. The reaction was allowed to take place at room temperature while stirring. After one hour, the vial was heated to 50 °C for 24 hours and held under vacuum for an additional 12 hours, yielding a viscous clear liquid (yield 98%, Boc-Amino).[135-136]

^{1}HNMR (*d*$_6$-DMSO): δ 3.5 (p, 1H, OHC**H**CH$_3$CH$_2$NH-), 3.5 (d, 2H, OHCHCH$_3$C**H$_2$**NH-), 1.4 (s, 9H, -NHCOOC(C**H$_3$**)$_3$), 1.1 (d, 3H, OHCHC**H$_3$**CH$_2$NH-). ^{13}CNMR (*d*$_6$-DMSO): δ 156.3, 77.9, 67.4 (THF), 65.9, 48.2, 28.6, 28.6, 21.4 (THF). MS theory: 175.1209, MS experimental: 176.1246 (m+H$^+$). The protected forms of ethanolamine (Boc-Ea), diethanolamine (Boc-DEA), and bis (2-hydroxypropyl) amine (Boc-Bis) were synthesized in the manner described above.

HDI (0.85 g, 0.005 moles) in DMSO (2 mL) was added dropwise to the Boc-Amino (1.84 g, 0.011 moles) over the course of five minutes at room temperature. The reaction was allowed to proceed overnight while stirring in a sealed flask at 50 °C, followed by another 12 hours at 60 °C. 4M HCl in dioxane (4 mL) was added to the product, and allowed to react overnight, and the same volume of 4M NaOH (4 mL) was used to wash the product, followed by two washed with DI H$_2$O. The aqueous layer was discarded and the organic layer was characterized (yield 76%). ^{1}HNMR (*d*$_6$-DMSO): δ 4.8 (h, 1H, NH$_2$CH$_2$C**H**CH$_3$O-), 3.2 (t, 2H, NH$_2$C**H$_2$**CHCH$_3$O-), 2.8 (d, 2H, NH$_2$C**H$_2$**CHCH$_3$O-), 1.6 (q, 2H, -OCONHCH$_2$**CH$_2$**CH$_2$), 1.4 (d, 3H, NH$_2$CH$_2$CHC**H$_3$**O-), 1.3(q, 2H, -OCONHCH$_2$CH$_2$C**H$_2$**-

). ^{13}CNMR (d_6-DMSO): δ 156.4, 67.8, 46.5, 40.9, 30.1, 27.1, 18.6. Theoretical mass: 318.2267. Experimental mass: 319.2301 (m+H^+).

Synthesis of HDI-ethanolamine (HDI EA), HDI-lactic acid (HDI Lac), and HDI-glycolic acid (HDI Gly) were performed in the same manner described above.

A typical procedure for the synthesis of amino alcohol carbamates containing secondary amines is described for HDI diethanolamine 1-amino-2-propanol (HDI DEA Amino) (**Figure 3.2**). HDI (0.89g, 0.005 mol) was added to a reaction flask containing Boc-DEA (0.75g, 0.004 mol) and DMSO (2 mL), and was allowed to react for 10 minutes at room temperature. Boc-amino-2-propanol (0.6g, 0.003 mol) was added dropwise over 5 minutes to the solution before sealing the vial, purging with nitrogen, and allowing the reaction to proceed over the course of 24 hours at room temperature, followed by 8 hrs at 50°C while stirring. The crude product was deprotected in 4M HCl (4 mL) for 12 hours while stirring, followed by 4M NaOH (4 mL) for an additional 4 hours. The product was washed twice in DI H_2O, and the organic layer collected. Yield (54%). ^{1}HNMR (d_6-DMSO): 4.9 (s, 1H, $NH_2CH_2C\mathbf{H}CH_3O$-), 4.3 (t, 2H, -$NHCH_2C\mathbf{H_2}OCONH$-), 3.3 (t, 2H, $NHC\mathbf{H}_2CH_2CH_2$-), 2.9 (t, 2H, -$NHC\mathbf{H_2}CH_2OCONH$-) 2.8 (d, 2H, $NH_2C\mathbf{H_2}CHCH_3O$-), 1.6 (5, 2H, -$NHCH_2C\mathbf{H_2}CH_2$-), 1.5 (d, 3H, $NH_2CH_2CHC\mathbf{H_3}O$-), 1.4 (t, 2H, -$NHCH_2CH_2C\mathbf{H_2}$-). ^{13}CNMR (d_6-DMSO): 157.1, 156.3, 68.3, 63.4, 48.9, 41.2, 30.3, 27.3, 18.8. Characterization of the product using MS revealed 74% HDI DEA amino propanol (Theoretical MS: 591.3956, 864.5664. Experimental MS: 592.4003 (m+H), 296.6995 (M/2+2H)), and 26% with two HDI-DEA repeat units (Theoretical MS: 864.5664 (311.1780, M/3 +3Na). Experimental MS: 311.1709 (M/3+3Na)).

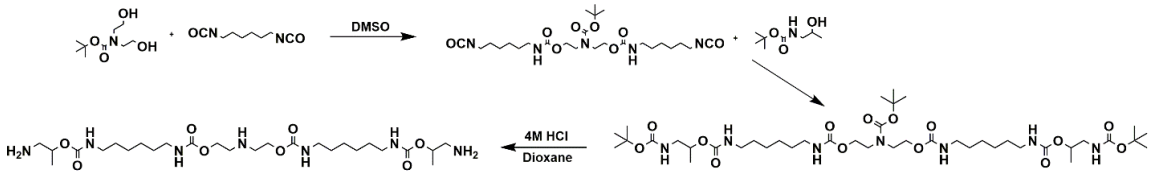

Figure 3.2. Synthetic scheme of HDI diethanolamine 1-amino-2-propanol (HDI DEA Amino).

The products HDI diethanolamine ethanolamine (HDI DEA EA), HDI bis(hydroxypropyl)amine ethanolamine (HDI Bis EA), HDI bis(hydroxypropyl)amine 1-amino-2-propanol (HDI Bis Amino), HDI diethanolamine lactic acid (HDI DEA Lac), HDI diethanolamine glycolic acid (HDI DEA Gly), HDI bis(hydroxypropyl)amine lactic acid (HDI Bis Lac), HDI bis(hydroxypropyl)amine glycolic acid (HDI Bis Gly) were synthesized in the same manner.

Porous SMP foams were synthesized using a two-step method, composed of an isocyanate premix and an alcohol premix, described in detail elsewhere.[20,35] The isocyanate premix was made by dissolving stoichiometric amounts of alcohol moieties (TEA, HPED) in diisocyanates (HDI). The stoichiometry is described by the isocyanate index (NCO index, ratio of [NCO]:[OH]); the NCO index of the premix is 0.35, and the remaining alcohols were mixed into the alcohol premix to produce a NCO index for the SMP of 1.05. The premix was heated in a 36-hour cycle to 50 °C (room temperature for 6 hours, 20 °C/hr to 50 °C,

isothermal for 18 hrs) before returning to room temperature. The alcohol premix was made prior to the foaming process, and contained the remaining alcohols (HPED and TEA), surfactants (Siloxanes industrially named DC 5943 and DC 198), catalysts (tin (II) 2-ethylhexanoate and triethylamine, industrially named T131 and BL-22, respectively), and blowing agents (Enovate, Honeywell Products, Inc).[20,35] The two components were mixed in a high speed speedmixer before being placed in a 90°C oven for 20 minutes, followed by an overnight cold cure in the fume hood. Compositions were with alcohol compositions of 80% HPED and 20% TEA (HH80) and 20% HPED with 80% TEA (HH20) were degraded for testing. The percentages denote the ratio of the alcohol composition. SMPs were cleaned using alternating washed of IPA and RO H2O while sonicating (three times each) at 50°C.

Characterization of the SMP foam was performed using XPS and FTIR, as well as confirming shape memory using volume recovery in RO H_2O and SEM analysis of pores (**Figure 3**). Theoretical elemental composition: C: 57.52%, O: 27.35%, N: 15.13%.[36] Experimental elemental composition: 57.25%, O: 27.92%, N:14.38%, Sn: 0.45% (Si was present as well, due to the surfactants used. Compositions were adjusted to exclude surfactant components).

Degradation product structures were determined in previous studies, where the end groups were identified and quantified over time, and related to the *in vivo* rate of oxidation.[134] This rate was then correlated to the mass loss found *in vitro,* and further used to determine the *in vivo* concentration of H_2O_2.[50,134] This allowed for extrapolation of the rate of degradation product formation *in vivo*. SMPs were degraded using similar protocols, with

3% H_2O_2 solution, and solutions were analyzed using MALDI MS to determine product size distribution over the course of degradation.[134]

Synthesized degradation products were dissolved in cell culture media composed of Dulbecco's Modified Eagle Medium (DMEM; VWR, Radnor, PA), 10% newborn calf serum (NBCS; Sigma-Aldrich, St. Louis, MO), 1% penicillin/streptomycin (P/S; VWR, Radnor, PA), and 0.1% fungizone (VWR, Radnor, PA). Cytotoxicity assays were performed using dilutions of products in order to calculate the concentrations at which a 30% reduction in cell viability would be observed (IC_{30} threshold) for each product.

50% H_2O_2 was allowed to sit for 10 minutes prior to use, and was then added to vials.[20] 1 g of SMP was placed into a vial with 50 mL of H_2O_2 solution. The vials were incubated at 37°C until the samples were completely degraded (no solid mass was visible). The resulting solutions were diluted 50X with DI water and 100 µg/mL catalase was added to quench residual H_2O_2. A final H_2O_2 concentration less than 1 ppm was confirmed for each sample using a ferric thiocyanate kit (CHEMetrics, Midland, VA). A sample of fresh 50% H_2O_2 and a sample of DI water, respectively, were diluted and treated with catalase to serve as controls for the cytotoxicity assay.

Media samples for cell exposure were made using 10X DMEM diluted to 1X with each sample solution. These media samples were also supplemented with 10% NBCS, 1% P/S, 0.1% fungizone, 3.5 mg/mL glucose, 3.7 mg/mL sodium bicarbonate, 4 µg/mL folic acid, and 20 µL/mL L-glutamine solution to afford a final media composition similar to the cell media described in the previous section.

For each assay, 3T3 Fibroblasts (ATCC, Manassas, Virginia) were seeded in 96-well tissue culture plates at a concentration of 5,000 cells/well and incubated in a humidified incubator at 37°C with 5% CO_2 for 24 hours. Cell morphology was observed in all wells using a Nikon Eclipse TE2000-S inverted microscope (Nikon, Melville, NY) and even cell distribution was confirmed before treatment. Cell culture media was aspirated and cells were incubated with degradation product samples to determine cytocompatibility. Varied concentrations of the products were prepared by adding fresh cell culture media of the appropriate volume. An untreated control (fresh cell culture media) was included in each assay to provide a reference for 100% cell viability. For degraded foam samples, fresh cell culture media controls were made from 10X DMEM, using sterile DI water as the diluent instead of a degraded foam solution. Cells were incubated with treatments for 48 hours at 37°C with 5% CO_2.

Following incubation, cell morphology was observed to evaluate changes induced by addition of the product solutions. The solutions were removed and a Neutral Red (NR) Uptake Assay Kit (Sigma-Aldrich, St. Louis, MO) was utilized to quantify cell viability. After incubation with NR for 2.5 hours the cells were quickly fixed with the NR assay fixative solution containing 0.1% $CaCl_2$ in 0.5% formaldehyde. The dye was solubilized in the NR assay solubilizing solution containing 1% acetic acid in 50% ethanol for measurement. The amount of dye in each well was quantified by measuring the optical density (OD) at 540 nm using a Tecan Infinite M200 Pro plate reader (Tecan, Morrisville, NC). Cell viability is expressed as a percentage using equation 1 (Eq 1).

$$Cell\ Viability\ (X) = \frac{OD_{540}(X) - OD_{540}(Blank)}{OD_{540}(Untreated\ Control) - OD_{540}(Blank)} \quad \text{Eq. 1}$$

X is any treatment group, blank is a well with no cells, and the untreated control is used as a standard that equals 100% viability.

Gravimetric analysis results were used to determine a worst-case scenario for degradation product accumulation, as well as models for more accurate predictions of product accumulation or release from the bulk. Rates of mass loss were examined to determine the most appropriate method for assessing toxic risk using 3% H_2O_2.

3.3 Results and Discussion

SMPs were found to possess high porosity, good shape recovery at *in vivo* conditions, and spectroscopically were found to agree with previous studies (**Figure 3.3**).[27,36-37,49,134] Material characterizations of these SMPs is reported elsewhere in greater detail, but T_gs range from 0 to 80°C, depending on the diisocyanate species used, the ratio of TEA to HPED, and method of analysis.[27,36-37,49,134] In general, increasing HPED results in higher thermo-mechanical properties. Shape recovery was not altered by composition, but recovery rate and strain fixity is dependent on T_g and the effect of plastization.[27] Morphology of the SMPs is controlled through both the chemical and physical blowing reactions.[27] While the use of a low-boiling point solvent or non-reactive molecule is useful for achieving greater porosity and lower density, this is also tunable through alteration of catalysts (both amine and metal) used during synthesis of the alcohol premix.

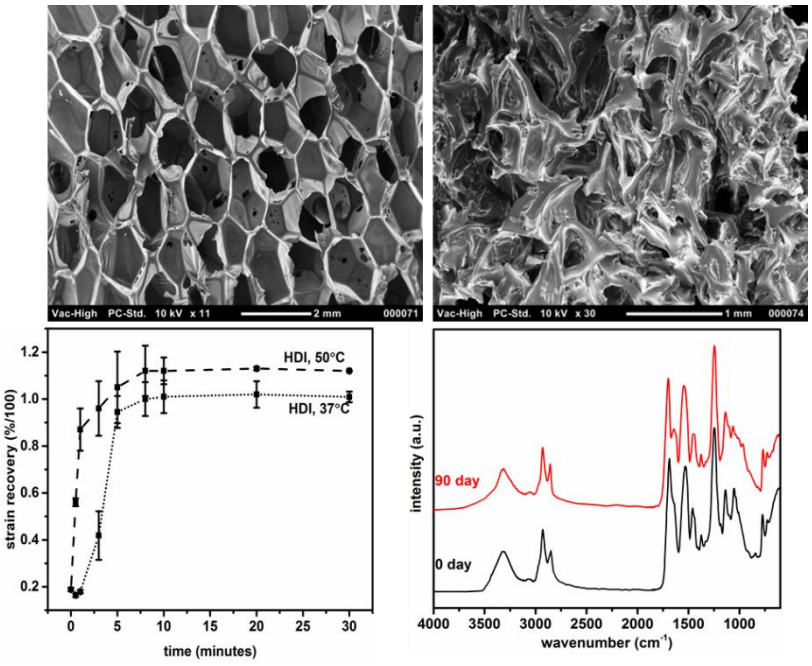

Figure 3.3. Basic characterization of porous SMPs. SEM images before (A) and after (B) 90 days of real time oxidation (3% H_2O_2 at 37°C), shape recovery testing of the original materials at two relevant *in vivo* temperatures (37°C and 50°C) (C), and FTIR spectra of the before and after oxidized materials.

Using FTIR, the carbonyl peak was found at *ca* 1689 cm^{-1}, indicating the formation of a carbamate with strong hydrogen bonding.[27] Further, FTIR indicates the formation of urea (1635 cm^{-1}) and tertiary amine peak at *ca* 1030 cm^{-1}. The tertiary amine was found to decrease upon oxidation of the material and a slight shoulder was found at 860 cm^{-1}, both of which are expected with amine oxidation.[134] The degradation of the amino alcohols occurs as the tertiary amine oxidizes, initially forming N-oxides, after which it may fragment to

form secondary amines and aldehydes.[134] The aldehydes may further oxidize to form carboxylic acids, and the secondary amines may further fragment to primary amines.[134] This is displayed for idealized sections of the SMP in Figure 1, where general overviews of the fragmentations are presented for both TEA and HPED, individually.

Over the course of real-time degradation testing, samples were taken and analyzed using MALDI-MS. Sample analysis indicates that the soluble components of the SMP are primarily fragments below 1 kDa, with most fragments occurring between 200 and 700 Da. This was found to be consistent over the course of *in vitro* oxidation, indicating that while larger products may be formed, they are at least not soluble in the *in vitro* test media. For the purposes of this analysis, it was assumed that these larger products will only have limited exposure upon implantation and were not considered further.

Mass loss of the SMPs is dependent on the concentration of H_2O_2, and while many literature standards indicate that 3% H_2O_2 is appropriate for real time testing, previous studies indicate that 1% to 2% H_2O_2 is more appropriate in some applications for these SMPs.[134] However, 3% H_2O_2 was selected as the rate of degradation for risk assessment to provide a safety factor (safety factor of 6, determined by calculated times to total SMP mass loss). To determine the rate used for the analysis, linear fitting was performed, with both the average fit across the mass loss profile as well as the greatest rate of change of mass determined from both the mass loss studies and gel fraction studies. The average rate of mass loss is 1.01 %/day, with an upper limit of 1.25 %/day and lower limit of 0.68% per day, all of which assume a constant mass loss and no change in degradation behavior as the material collapses and surface area changes.

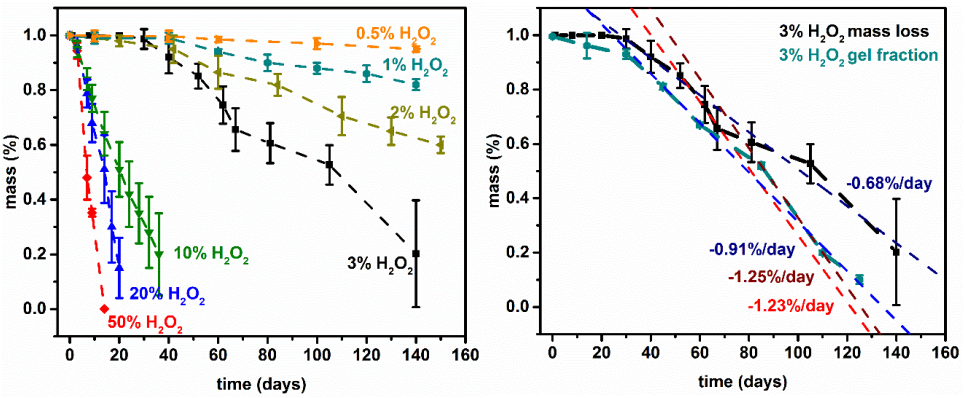

Figure 3.4. Mass loss profiles based upon the concentration of H_2O_2 (left), and fitted linear approximations of degradation displaying the maximum rate of change and the fitted rate of change for both mass loss and gel fraction measurements of SMPs degraded in 3% H_2O_2 (right). All experiments were conducted at 37°C.

The cytotoxicity thresholds (IC_{30}) were determined from cell viabilities using dilutions of degradation products (**Table 3.1**, **Figure 3.5**), as well as those for the fully degraded SMP bulk. Thresholds ranged from 2.04 mg/mL (HDI lactic acid) to 0.031 mg/mL (glyoxal). The majority of the products had similar thresholds between 0.1 mg/mL to 0.4 mg/mL.

While there may be residual H_2O_2 in the bulk SMP degraded foam solutions, it appears that the addition of the catalase reduces its toxicity to marginal levels for this analysis. Additionally, the catalase in fresh cell culture media does not appear to alter cell viability at the examined concentrations.

For the examined products, IC_{30} values were established along with morphological changes to the fibroblasts after exposure (**Figure 3.5**, **Figure 3.6**). With an IC_{30} threshold of 0.115 mg/mL, HDI DEA Gly was exposed to cells at 0.05 mg/mL without changes in viability of morphology, relative to the controls. However, at concentrations of 0.15 mg/mL, viability had decreased to 52.9% and a far greater number of cells are spherical, rather than extended.

Table 3.1. Cytotoxicity threshold established for degradation products and degraded bulk material.

Product	IC30 (mg/mL)
HDI Bis Amino	0.276
HDI Bis EA	0.219
HDI DEA EA	0.488
HDI DEA Amino	0.333
HDI DEA Lac	0.626
HDI Bis Gly	0.283
HDI Bis Lac	0.103
HDI DEA Gly	0.115
HDI Amino	0.125
HDI EA	0.355
HDI Gly	0.292
HDI Lac	2.04
Oxalic acid	0.047
Glyoxal	0.031
HH20 Foam	0.30
HH80 Foam	0.20

Despite the excellent healing and reduced inflammation of these SMPs when examined to 90 days in porcine aneurysms, there are still long-term risks associated with implanted materials that slowly degrade.[33-34] In the case of SMP foams, examining the worst-case scenario of 1.25 %/day is used for assessing toxicity risks over the SMP lifespan. A limitation of this experimentation is determining the distribution of products that will be produced and soluble *in vivo*. However, if it is assumed that only the smallest products are soluble and taken up by cells, or that only the small products are tested for toxicity, it is possible to establish theoretical thresholds based upon assumptions that include no deviation from the predicted degradation pathway, such as due to metabolism or excretion, and no toxicity changes due to interactions of the degradation products between themselves. Based upon this, calculations were made that established the product production per day (per kg body mass) for comparison to cytotoxic levels.

The two products with the lowest IC_{30} thresholds were glyoxal and oxalic acid. Glyoxal has been found to be present in patient blood plasma levels up to 0.3 µmol/L (*ca* 0.1 mg assuming 70 kg patient), which would constitute nearly 20% of the levels produced by 1 g of SMP, in the case of the HH20 composition.[138]

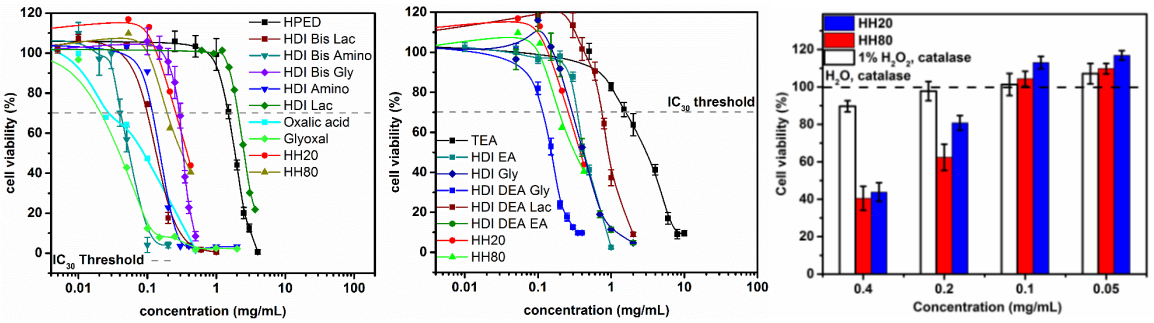

Figure 3.5. Cell viability curves for HPED degradation products (top left), TEA degradation products (top right), and bulk SMP foam (bottom) after complete degradation. All experiments were conducted at 37°C.

More concerning are the oxalic acid levels, which could limit the maximum mass of implanted materials if the daily dose rate exceeded the human safe exposure limit of 0.54 mg/kg body weight/day, determined from reproductive effects in animal studies; for an average 70 kg human this threshold is 37.8 mg/day for oxalic acid.[139-140] The analysis of SMP degradation indicates that the levels of exposure for 1 g at 1.25 %/day (*ca* 63.8 mg total as a maximum possible dose) are well below what would be considered a patient protective safe exposure limit. [139-140]

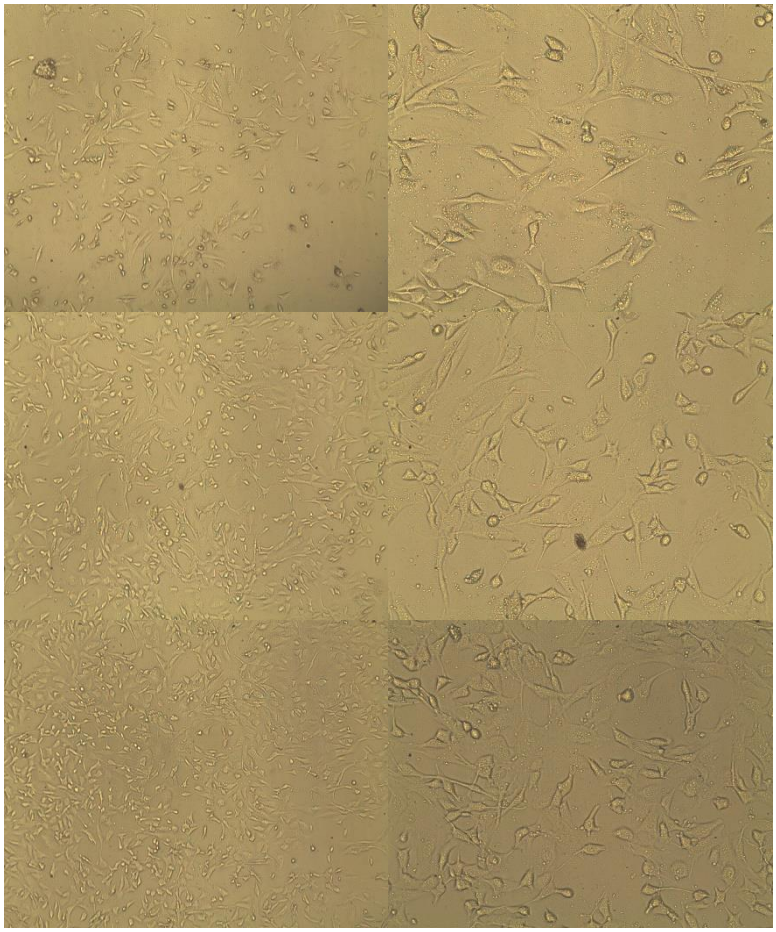

Figure 3.6. Brightfield microscopy images of cells exposed to HDI DEA Gly with concentrations at 0.15 mg/mL (top), 0.1 mg/mL (middle), and 0.05 mg/mL (bottom), displaying an increasing compatibility trend that increases from top to bottom.

For the other products, it appears that the HDI Bis Amino product may be concerning if it is released in large enough concentrations, most likely due to its structural similarity to polyamines.[141] However, it does appear that the HPED will be the limiting starting material based upon the examined degradation behaviors, based upon the IC_{30} thresholds for both the starting materials and the degradation products.

The 1.25 %/day mass loss rate determined from gravimetric analysis was used to approximate theoretical accumulation of degradation products, assuming 1 g of SMP foam (typical masses for peripheral occlusion applications will be *ca* 100 mg, while neurovascular applications will be *ca* 20 mg), a perfectly homogenous material, constant mass loss upon implantation or exposure, and that only the smallest fragments would be produced during degradation. These assumptions provide a total factor of safety of 60 (**Table 3.2**).

Table 2.2. Factors of Safety use in analysis of toxicity risks for SMP degradation.

	Assumed	*In vivo*	Factor of Safety
Device Mass	1.0 g	<0.1 g	10
Rate of Mass Loss	1.25 %/day (80 days)	~0.2 %/day (500 days)	6
Patient mass	70 kg	70 kg	1
Total			**60**

This theoretical model was used to determine product accumulation for a 70-kg patient (average adult size) over the course of degradation, levels which were then compared to the IC_{30} values. The composition of the SMPs will alter both the production of products (due to changes in stoichiometric ratios of TEA to HPED) as well as the IC_{30} threshold value, although all examined compositions were found to below its respective limit using this analysis. As presented in **Table 3.3** for the SMP compositions studied by Rodriguez *et al* and Horn *et al*, noted as HH60 (HDI-based SMPs containing 60:40 HPED to TEA as the alcohol moiety ratio), the product daily production rates (doses) are below the toxicity thresholds, a trend found for all of the examined SMP formulations.[33-34] Furthermore, while the levels that are predicted for the products are below IC_{30}, this model is limited by examining only the smallest products. Developing a more complex model would decrease these specific product values due to the lower doses of the smaller products, although these larger products might possess different synergistic effects as well as different IC_{30} thresholds. Such analysis would also require a greater understanding of the solubility and material-cell interactions over the course of SMP degradation. This limitation is partially addressed through the use of fully degraded SMPs, and previously examined SMPs that had undergone incubation in degradation solutions, all of which confirm cytocompatibility for the SMPs in the examined forms or at device-relevant degradation product dosages.[134]

Table 3.3. Cytocompatibility thresholds and approximated rates of production for select degradation products. A theoretical calculation is denoted by *.

Product (HH60)	IC_{30} (mg/mL)	1 g (1.25 %/day) (mg/kg body weight/day)
HDI Amino	0.125	0.0807
HDI EA	0.355	0.0327
HDI Gly	0.292	0.0721
HDI Lac	2.04	0.0883
Oxalic acid	0.047	0.0114
Glyoxal	0.031	0.0073
HH60*	0.221	0.1332

These results, combined the with utilized safety factors of accelerated mass loss based upon 3% H_2O_2 and maximum rate of change for determining material lifespan, indicate that these SMPs pose minimal risk for use in adult patients in vascular applications. Further work is needed to examine the roles of the aldehyde end group-containing degradation products, which were neglected here. Recent studies of aldehyde-containing biomaterials have indicated that polymers with aldehyde end groups increase tissue-adhesiveness, even in diseased tissue.[132-133] While it is unknown what function the aldehydes will have for these SMPs in vascular applications, it is possible that some of the reduced inflammation found with these SMPs is due to superior tissue adhesion.[33-34,132-133] It is also expected that while the amine degradation products may be taken up by cells and further metabolized, it is also possible that these products will be excreted due to both their size and potential charge Previous work with polyamines and cationic amines have demonstrated that

these molecules, if sufficiently small, will be readily cleared *via* the renal system, which is the main method of clearance for cationic metabolites in healthy patients.[142-144] In lieu of *in vivo* data to provide an understanding of degradation product excretion, metabolism, and migration, the use of toxicity risk assessment is useful for continuing to justify translation of the SMPs into vascular occlusion devices.

3.4 Conclusions

Despite the large number of medical devices available on the market for use in humans, there are many that are not well understood as material properties relate to degradation. Here we have demonstrated methods for further predicting the toxicological risk associated with the long-term implantation of polymeric materials. While the degradation mechanism was previously examined, here it is utilized to develop a series of degradation products for testing of the compatibility of the SMP material over long implantation times. For conformation of the method, bulk SMP was degraded, tested, and compared to theoretical levels. Theoretical calculations of degradation products were developed to reflect the worst-case levels of product formation for 1 g of material, indicating that even with these factors of safety and excessive amounts of material present the SMPs pose a minimal long term risk for patients. Most importantly, the methods of testing presented here may be tailored to any implantable material system for validating the cytotoxicity risk posed over the lifespan of an implant.

It is important to note that this study was performed to assess toxicity risk, but it does not fully confirm a lack of toxicity. True confirmation is only achieved through *in vivo* studies in the region of interest in appropriate animal models or human subjects. This testing,

however, provides important insight into the toxicity risks that may occur. Such information can be useful in developing such studies as well as for guiding the translation of these SMP biomaterials into certain device applications. However, despite some of the limitations of this approach, the use of several methods for assessing cytocompatibility limitations and toxicity risks (synthesized degradation products, partially degraded SMPs, fully degraded SMPs) does indicate that these SMPs, when used as vascular occlusion devices, will pose minimal risk for patients.

CHAPTER IV

OXIDATION-RESISTANT SHAPE MEMORY POLYURETHANES CONTAINING ANTIOXIDANTS

4.1 Introduction

Polyurethanes have been known to undergo degradation for decades, with notable failures including breast implants and pacemaker wires.[1,5-8,16-17,22,114] While this has raised concerns about the long-term stability of these materials for *in vivo* applications, polyurethanes are still widely used in blood contacting applications due to their excellent biocompatibility.[1,5-8,16-17,22] When porous, polyurethane-based shape memory polymers (SMPs) were first developed, one application suggested for these materials was aneurysm occlusion.[26-30] Due to the SMP's ability to undergo shape change from a compressed shape to the original shape when exposed to a stimulus, these SMPs are ideally suited for minimally invasive medical devices.[26-30,36]

Failures of polyurethanes have had notable impact on devices in both polyurethane breast implants and pacemake wire coatings.[1,5-7,16-17,114] The breast implant coatings demonstrated variable failures, with many patients never experiencing failure, pain, or adverse effects from long term implantation.[6,17,114] However, *in vitro* analysis indicated that hydrolysis of the urethane bond, as well as from the reaction of residual diisocyanate starting materials with water, produced aromatic diamines.[1,5,7] These degradation products are known to be carcinogenic, and so the failure of these systems posed some risk to patients if urethane hydrolysis was occurring.[1,5-7,16-17,114]

Due to the limitations of aromatic, thermoplastic polyurethanes, a new series of polyurethanes was needed for long-term implantable medical devices. Wilson *et al* developed a series of thermoset polyurethane SMPs from symmetric, aliphatic monomers in an effort to produce more stable polyurethanes that possess high strain recoveries and improved biocompatible if hydrolysis were to occur.[36] While the hydrolytic stability of these SMPs was found to be improved, the use of amino alcohols results in a rapid oxidation mechanism in these materials.[116,134,117-121] The tertiary amine oxidizes to a N-oxide (amine oxide) in the presence of a hydroxyl radical, followed by the eventual formation of a secondary amine and corresponding aldehyde; further oxidation-reduction fragmentations results in the formation of a primary amine, a second aldehyde, and a carboxylic acid as a result of aldehyde oxidation.[116,134,117-121] The primary amine may oxidize to form ammonia, as an eventual end product.[116,135,117-121] The diisocyanate and urethane linkage were also examined in oxidative solution, revealing minimal changes to both.[134] The tetra functional alcohol used in the SMPs, N,N,N',N' tetrakis (2-hydroxypropyl) ethylenediamine (HPED), may also produce oxalic acid as an eventual fragment, which has been linked to the necrosis of renal tubule cells and the formation of oxalate crystals.[131,134,182] Prevention of N-oxide formation will reduce the onset of fragmentation and mass loss of the bulk SMP, ultimately reducing the rate of formation of oxalic acid and other potentially harmful oxidation products. A radical scavenger included in the polymer offers an avenue to reduce the rate of oxidation, and eventual mass loss, and potentially could be translated into other systems that have oxidatively-induced degradation.[74,213]

Numerous antioxidant systems have been studied in polymer systems. Hindered amine light scavengers (HALS) antioxidants have found success in polyurethanes for coatings applications.[75-81] HALS systems are successful due to their scavenging efficiency as well as the ability to reform the antioxidant after scavenging.[75-81] Phenol and phenol-derived antioxidants have also been used with varying degrees of success, as well as phosphite antioxidants.[82-83] Butylated hydroxytoluene (BHT) has been used successfully in other polymer systems, with specific applications in medicine and medical materials.[84-87] BHT and its derivatives has high scavenging efficiencies and good solubility, unlike other efficient scavengers such as tannic acid.[84-85] While many other methods exist for incorporating or utilizing antioxidants in polymer systems, directly incorporating the antioxidant into the polymer chain and physical addition of the antioxidant as small molecular weight additives are used frequently, and so the use of physical additives and chemically bound small molecules was selected.[88-93] It is expected that these antioxidants will scavenge radicals preferentially to the tertiary amines, in order to reduce mass loss of the SMP without compromising the bulk integrity of the polymer, as is the case when synthesizing composite SMPs, and without requiring the initial polymer chain degradation that is utilized by in-chain antioxidants or antioxidant degradation products.[90-93]

SMPs can undergo shape change when exposed to a variety of stimuli, including thermal, electric and magnetic fields, solvent, and light.[36] Many SMPs slated for medical applications use thermal, solvent, or a combination of the two.[36,40] The mechanism for shape recovery is controlled by the entropy of the molecule, with the SMP assuming a maximum entropic-configuration during synthesis.[29] The secondary, or temporary, shape of the

polymer is set by raising the temperature of the polymer above the transition temperature (glass transition temperature T_g in the case of amorphous polymers) and mechanically deforming it until has cooled into the new configuration (which has reduced entropy relative to the original configuration).[29,36] Application of the heat again drives the recovery of the original shape, as the polymer again assumes the original, maximum entropy configuration. [29,36] The shape fixation may be temporary as the polymer relaxes, but polymers with strong intramolecular interactions such as hydrogen bonding may have improved fixity, and not undergo spontaneous shape recovery with a stimulus being applied. [29,36] For thermally-drive actuations, the T_g is the point at polymer chain mobility is sufficient to allow it to return to the configuration of maximum entropy.[29] Solvent-actuations are similar, but the solvent interrupts the intramolecular interactions, allowing for shape recovery to occur at lower temperatures, also known as a wet T_g.[40] Polyurethanes, polyamides, polyesters, among others, possess both a dry and wet T_g. For medical applications, this change in T_g (plasticization of the bonds) allows for the shape recovery of an implanted SMP when it reaches ambient moisture and temperature of the body, rather than an elevated temperature that may damage native tissue or proteins.[211-212]

However, for SMPs that utilize a thermal actuation mechanism for shape recovery, the use of chemical methods for changing the oxidative degradation profile may compromise functionality of the biomaterial. Examination of chemical crosslinked (covalently bound) and physically added/absorbed antioxidants in porous SMP scaffolds (foams) were performed to determine the effects on thermal, mechanical, and shape memory properties. The utility of antioxidants for controlling degradation was then examined using accelerated

oxidative degradation testing and extraction testing in the form of cleaning the SMPs. Degradation products analysis was to access the risk of the SMPs overall for use in vascular occlusion applications.

4.2 Methods and Materials

All chemicals were purchased from Sigma Aldrich and used without modification or cleaning, unless otherwise stated. HPED (99%), triethanolamine (TEA, 98%, Alfa Aesar), hexamethylene diisocyanate (HDI, TCI America) and trimethyl hexamethylene diisocyanate (TMHDI, TCI America, a mixture of 2,2,4 and 2,4,4 monomers) were used as monomers. BHT, triphenyl phosphite (Triphen), 1,2,2,6,6 tetramethyl piperidinol (Piper), didodcyl 3, 3 thiodipropionate (Thio), L-ascorbic (Vit C), and 2,2'-methylenebis(6-tert-butyl-methylphenol) (Methyl) were chosen as antioxidants. Antioxidant structures are displayed in **Figure 4.1**.

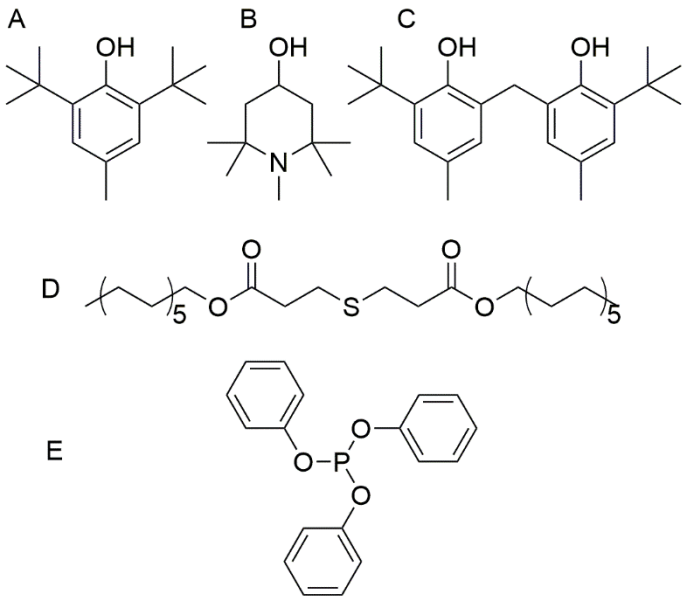

Figure 4.1. Antioxidant structures used to produce oxidatively stable porous SMPs. (A) butylated hydroxytoluene, (B) 1,2,2,6,6 tetramethyl piperidinol, (C) 2,2'-methylenebis(6-tert-butyl-methylphenol), (D) didodecyl 3,3 thiodipropionate, (E) triphenyl phosphite.

Deuterated dimethyl sulfoxide (DMSO, 99.99%, Sigma Aldrich), ethanol (97%, Sigma Aldrich), and isopropyl alcohol (99.5%, Sigma Aldrich) were used as solvents. Ethyl isocyanate (98%, Sigma Aldrich) was used without purification. Cobalt chloride ($CoCl_2$), hydrogen peroxide (H_2O_2, 50%, Sigma Aldrich), acetone (99%, Sigma) were used for degradation solutions.

Acetonitrile (99.93%, HPLC grade, Sigma), methanol (50% in H_20 with 0.1% v/v formic acid, LCMS grade, Sigma), methanol (99.9%, LCMS grade, Sigma), and water solution (0.5 % v/v formic acid, HPLC grade, Sigma) were used with liquid chromatography.

Porous SMP scaffolds were synthesized using a traditional two-step polyurethane foam synthesis process.[20,35] First, an isocyanate premix was made by adding 35-40% of the desired alcohol moieties (molar %, with percentage varied to control premix viscosity and thus scaffold pore size) to the full measure of diisocyanates. This premix was cured over 36 hours at 50°C to achieve the desired viscosity. The second step was the production of the alcohol premix, consisting of the remaining alcohols, antioxidants (added at 5 % and 10 % by wt), surfactants and catalysts.[20,35] The premix was homogenously mixed using high shear mixing, which also dissolved the antioxidants into the solution, and was then mixed to the isocyanate premix using a high speed shear mixer, followed by the addition of a physical blowing agent. The scaffold was cured at 90°C for 20 minutes, followed by cold curing over night at ambient conditions.[27,37,71]

Foam cell structure was determined by cutting axial and transverse samples that were examined using scanning electron microscopy (SEM). Samples were mounted onto a stage and sputter coated with gold using a Cressington Sputter Coater (Ted Pella, Inc., Redding, CA) for 60 seconds at 20 mA. Samples were then examined using a Joel NeoScope JCM-5000 SEM (Nikon Instruments Inc., Melville, NY) at 11X magnification and 15 kV under high vacuum.

Attenuated total reflectance Fourier transform infrared spectroscopy (ATR-FTIR) spectroscopy was used to determine any spectroscopic changes to the bulk material. ATR-

FTIR spectra were taken using a Bruker ALPHA infrared spectrometer (Bruker, Billerica, MA) using 48 scans per spectra for both background and samples. Spectra data was collected in absorption mode with a resolution of 4 cm^{-1}. OPUS software was used to examine spectra, identify peaks, and perform baseline and atmospheric corrections. ^{1}H and ^{13}C NMR were performed using a Mercury 300 MHz NMR in deuterated d_6-DMSO.

Extractions were performed using isopropyl alcohol at 50°C for 1 hour, extracted with sonication. 4 g of SMP were used for the extractions, and the final mass and concentration of the extracted antioxidants was determined for the entire 16 g of starting SMP. Gas chromatography mass spectrometry (GCMS, positive mode) was used to determine the extracted concentration using a Thermo Scientific DSQ II Series Single Quadrupole GCMS (ThermoFisher Scientific, Waltham, MA), as well as the degradation products from the model compounds. A 10 uL sample volume was injected, with a dwell time of 4 seconds. The initial temperature was 50°C, heated to 320°C at a rate of 20°C/min. The flow rate was 50 mL/min with a surge pressure of 0.44 psi using methanol.

Product determination was confirmed using liquid chromatography mass spectrometry (LCMS). Samples were diluted 100-fold in a 50% methanol (49.95% water, 0.05% formic acid) solution, and injected into a normal phase C18 silica column. The injection volume was 10µL, and the mass flow rate was varied from 0% acetonitrile to 95% acetonitrile over a 6-minute gradient. An Exactive Plus OrbiTrap Mass Spectrometer (ThermoFisher Scientific, Waltham, MA) was used to perform MS. The capillary temperature was 100 °C. Spectral data was collected over a 30 second integration, and Xactive software (ThermoFisher Scientific, Waltham, MA) was used for analysis.

Degradation products of select antioxidants were determined using model compound studies and literature reviews. The behavior of TMHDI and HPED in the urethane network was examined by Weems *et al*, and is not repeated here.[134] Model studies of antioxidant behavior were performed using unmodified antioxidants in 50% H_2O_2, heated to 60°C to aid in reactivity and solubility, and analyzed using both GCMS and LCMS. Additionally, model reactions of ethyl isocyanate with antioxidants were performed to examine urethane formation. 5 mmol of reagents were added (NCO:OH ratio), after which they were heated to 50°C in a sealed vial overnight. The solution was then heated at 80°C under vacuum. Unreacted ethyl isocyanate would be removed from the solution, leaving primarily urethane, antioxidants, and ureas. The products were characterized for relative abundance using LCMS.

Differential scanning calorimetry (DSC) was also used to measure both wet and dry T_g using a Q-200 DSC (TA Instruments, Inc., New Castle, DE). Samples of *ca* 5.0 mg ± 1.0 mg were sealed in TZero aluminium pans and placed in the heating cell. The sample was cooled to equilibration at -40°C, heated to 120°C at 10°C/min, cooled 10°C/min to -40°C and heated to 120°C at 10°C/min. The half-height transition of the final heating cycle was the reported T_g. Wet samples were weighed and sealed in the same manner, and were then heated from -40°C to 80°C at 10°C/min.

Thermogravimetric analysis (TGA) was used to assess any changes in thermal degradation temperatures. A TA Q50 TGA (TA Instruments, New Castle, DE) was used to heat samples to 500°C at 10°C/min under a mixed atmosphere of oxygen and nitrogen

(60mL/min to 40 mL/min respectively). Samples were examined for the onset of degradation temperature and major transitions in the mass loss profiles.

Shape recovery of cylindrical foam samples (6 mm diameter, 10 mm length, six samples per series) crimped over a wire was examined at 50°C in RO water to determine the volume recovery behavior (strain recovery).[214-215] Samples were crimped to a minimal diameter (*ca* 1.0 mm using a SC150-42 Stent Crimper (Machine Solutions, Flagstaff, AZ) by first being equilibrated at 100°C for ten minutes, and then radially compressed and cooled to room temperature. Samples relaxed for 12 hours and were tested over the course of 30 minutes in 37°C H_2O. Image J was used for analysis of the change in diameters over time.

Uniaxial tensile testing was performed on ASTM d638 IV samples using an Instron Tensile Tester with 500 N load cell. The extension rate was set to 5 mm/min at room temperature, and seven samples were tested for each species. Elastic modulus, strain to failure, ultimate tensile strength calculated.

For analysis of degradation rates, cleaned samples were completely immersed in respective solutions of 20% H_2O_2 with 0.1M $CoCl_2$ at 37°C. Sample solutions were changed every 3 days to ensure a relatively stable ion concentration, and once per week samples were removed, cleaned in EtOH, and dried in at 50°C under vacuum (30 in Hg), after which sample mass was recorded and samples returned to fresh solution.[135]

4.3 Results

NMR confirmed the formation of urethane linkages for Methyl and Piper antioxidants only; other examined species contained original structures and small

concentrations of urea linkages. Proposed structures and mass spec are displayed in **Figure 4.2**.

The spectra of the SMP foams displayed the characteristic hydroxyl bands at *ca* 3250-3500 cm^{-1}, the methyl band at 2800-3000 cm^{-1}, the carbonyl band at 1688 cm^{-1} that denotes the urethane bond and the corresponding should for the urea bond at *ca* 1640 cm^{-1}, and the skeletal carbon peak at 1252 cm^{-1}. The Methyl and Thio SMPs display shoulders on the carbonyl at *ca* 1710-1730 cm^{-1} that correspond to the ester bonds in the antioxidants (Thio) or the formation of a new urethane linkage (Methyl). The increase in the relative height of the urethane carbonyl of the Piper SMP compared with the control indicates the formation of the urethane linkage.

Table 4.1 displays thermal analysis of the bulk SMPs. T_g for these materials was found to be *ca* 55C for the control, as well as for Piper. Methyl and BHT both displayed increased T_g (61.5°C and 57.2°C respectively). These same two antioxidants also resulted in increased onset of thermal degradation temperatures (control at *ca* 273°C, BHT at 303°C and Methyl at 299°C). All antioxidant SMPs, except for the Thio, displayed an increased onset of thermal degradation.

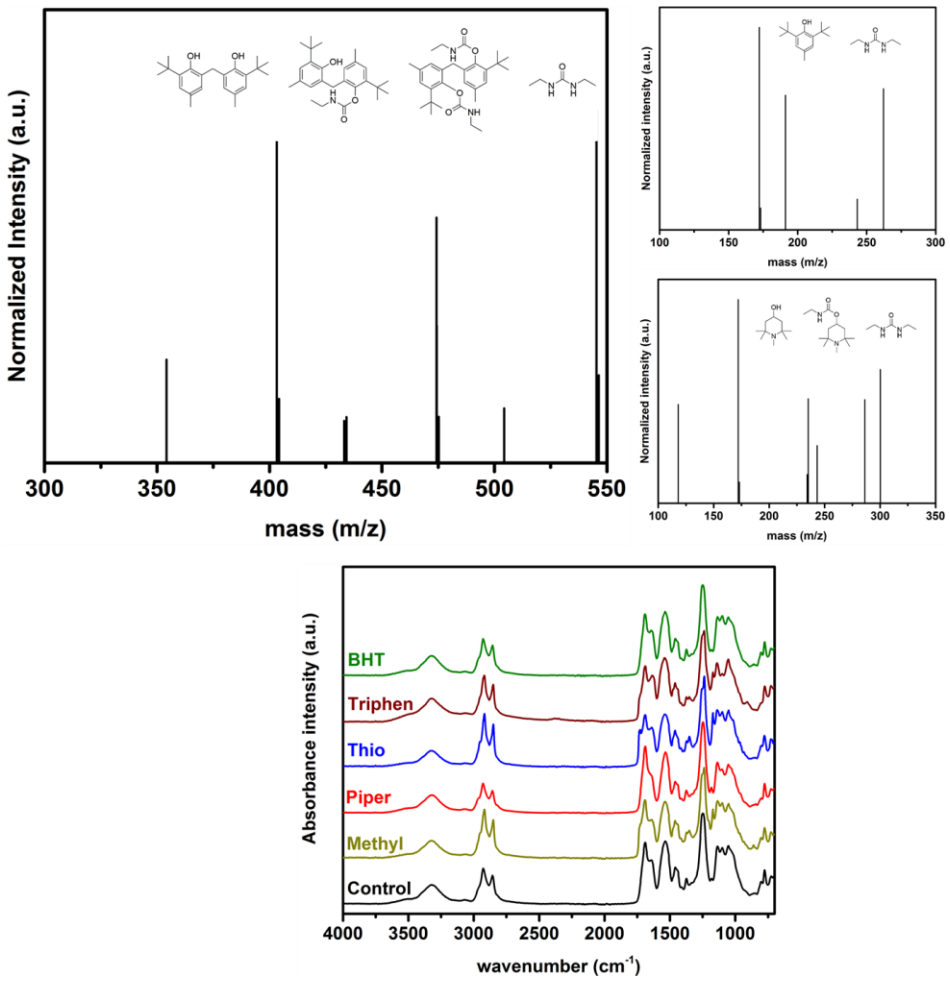

Figure 4.2. Spectroscopic analysis of the antioxidant reactions with isocyanates using model compounds BHT, Methyl and Piper, and FTIR-ATR of the antioxidant-containing SMPs.

Table 4.1. Thermal characterizations of antioxidant SMPs.

Species	T_g (°C)	Wet T_g (°C)	T_d (onset temp) (°C)	T_d (derivative peak) (°C)
Control	55.3 ± 0.3	10.4 ± 1.0	239 ± 2	273 ± 3
Piper	55.0 ± 0.3	11.5 ± 1.1	250 ± 1	279 ± 1
Methyl	61.5 ± 0.2	14.2 ± 1.4	260 ± 3	299 ± 4
BHT	57.2 ± 0.8	10.2 ± 1.9	261 ± 1	303 ± 2
Thio	41.0 ± 3.0	5.2 ± 0.5	236 ± 1	267 ± 1
Triphen	38.9 ± 0.3	12.3 ± 1.3	247 ± 3	279 ± 4

Mechanically, the Methyl again displayed enhanced properties relative to the control and the other examined species (**Figure 4.3, Table 4.2**). The elastic modulus of the control was 0.25 MPa, while Methyl displayed a 2.32 MPa; strain to failure for the control was 165% while Methyl's was 128%, indicating that this increase in elastic modulus did not compromise the mechanical integrity of the material severely. Of the other examined antioxidants, Piper displayed slight increases in elastic modulus (0.28 MPa), and all species displayed increased strain to failure and tensile strength, except for Triphen. The Triphen SMP displayed nearly twice the strain to failure (283 %), while also possessing reduced tensile strength (0.35 MPa compared to 0.41 MPa for the control) and a lower elastic modulus (0.11 MPa).

Unfortunately, the Methyl SMPs displayed little shape recovery(*ca* 35% recoverable strain) (**Figure 4.3**). This may be due to the increased rigidity of the polymer. The other covalently bound antioxidant, Piper, also had slightly reduced shape memory (*ca* 90%

recoverable strain. The other SMP species did not have significantly altered shape memory properties.

Extractions of antioxidant SMPs displayed large amounts of extractable BHT and Triphen (**Figure 4.4, Table 4.3**). Relative peak heights were substantially greater for these antioxidants, although small peaks are noted for all SMPs. The identities of these peaks were confirmed from fitting the masses at these time points to the starting materials and thermo-oxidative fragments.

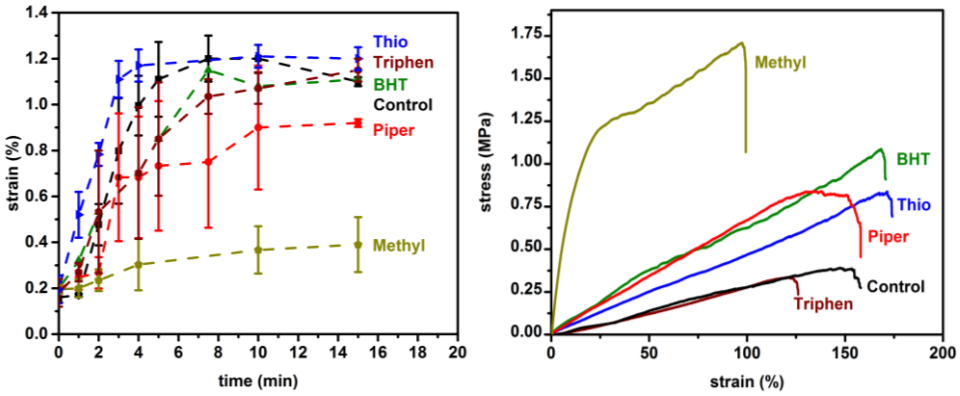

Figure 4.3. Shape memory behavior of porous SMPs (HH40) containing 10% antioxidants (left) and mechanical behavior for HH40 SMPs containing 10% antioxidants.

Table 4.2. Mechanical properties of antioxidant-SMPs.

Foam Composition	Elastic Modulus (MPa)	Strain to Failure (%)	Tensile Strength (MPa)	Toughness ($J*m^3$)
Control	0.25 ± 0.06	165 ± 21	0.41 ± 0.08	333
BHT	0.24 ± 0.06	207 ± 39	0.97 ± 0.14	940
Piper	0.28 ± 0.19	219 ± 27	0.61 ± 0.23	787
Thio	0.24 ± 0.06	283 ± 49	0.81 ± 0.21	722
Triphen	0.11 ± 0.02	170 ± 21	0.35 ± 0.06	204
Methyl	2.32 ± 0.44	128 ± 27	1.77 ± 0.46	1264

The incorporation of the antioxidants into the SMPs resulted in the delay of oxidatively-induced mass loss from H_2O_2 in the Piper SMP only (**Figure 4.5**). Not displayed are mass loss profiles for TMHDI based SMPs, in which BHT was better retained; the mass loss of BHT SMPs was reduced to the same degree as the Piper SMPs. SEM images of the control SMP pores compared with the 10% Piper are displayed in **Figure 4.6**. Pore membranes are rapidly eroded, leading to the eventual collapse of the material in 7 days without antioxidants. By qualitative contrast, the Piper SMP at day 7 corresponds more closely with the control at day 3.

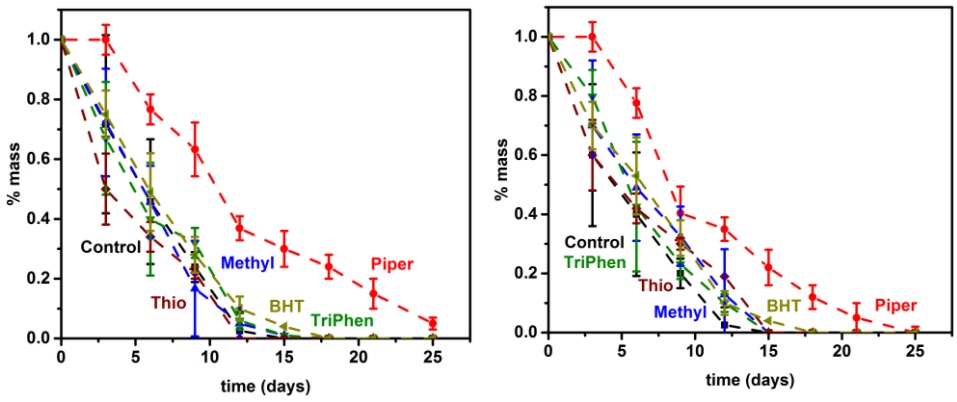

Figure 4.4. 10% antioxidant in HH40 (left) and 5% antioxidant in HH40 (right) degraded in 20% H_2O_2 with 0.1M $CoCl_2$, at 37°C.

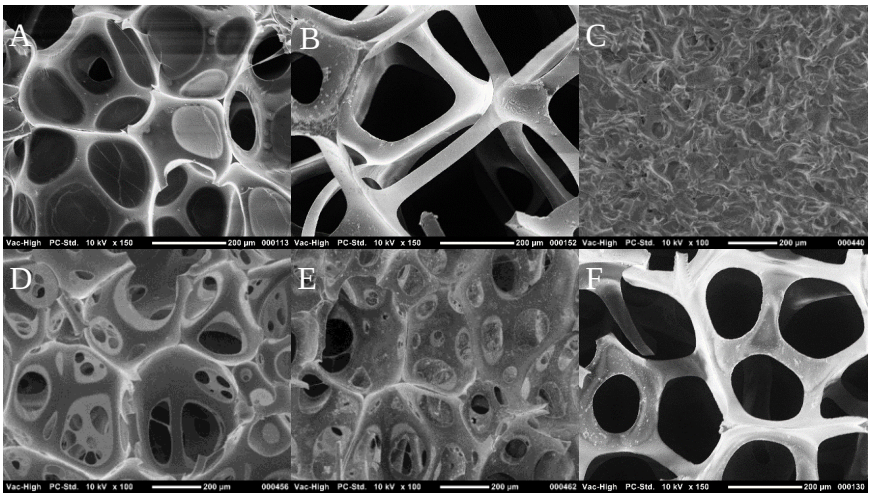

Figure 4.5. Control SEM and 12 Piper at day 0 (A,D), day 3 (B,E), and day 7 (C,F).

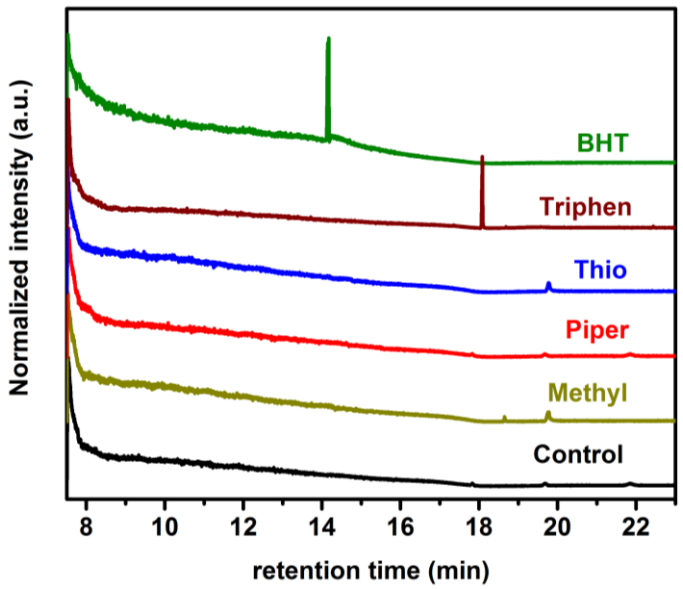

Figure 4.6. GCMS chromatographs for extracted antioxidants from SMPs.

Table 4.3. Mass and concentration of antioxidants added during synthesis and extracted during cleaning, determined using GC/MS.

	Additive Mass (g)	Additive Concentration (mol)	Extract Mass (g)	Extract Concentration (mol)
Piper	2.000	0.012	0.080	0.000
Methyl	2.000	0.006	0.155	0.000
Thio	2.000	0.004	0.149	0.000
Triphen	2.000	0.007	1.928	0.006
BHT	2.000	0.009	1.629	0.007

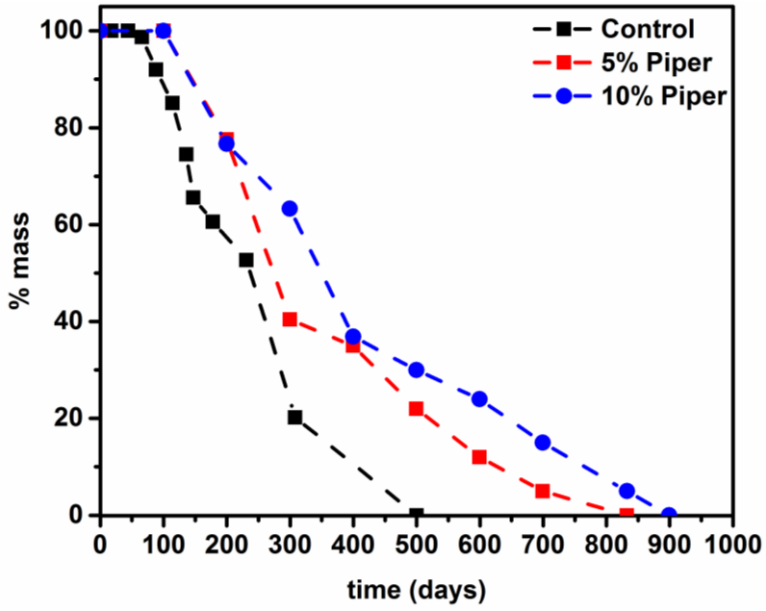

Figure 4.7. Predicted real time oxidative mass loss of antioxidant (Piper) containing HDI-based SMPs. (equivalent of 2% H_2O_2 at 37°C)

BHT, Triphen, Thio, and Methyl were either removed prior to testing during cleaning or were ineffectual for reducing oxidative mass loss with HDI-based SMPs. **Figure 4.7** displays the GCMS curves of the extracted antioxidants. The concentrations of the antioxidants were calculated and compared with the starting concentrations and masses used during synthesis (**Table 4.3**).

4.4 Discussion

From the spectroscopic results, Piper and Methyl was expected to form urethane bonds. BHT does not form these bonds due to the steric hindrance of the hydroxyl group as a result of the surrounding methyl groups. The rotation of the phenol group relative to the second phenol group of the Methyl antioxidant provides a less sterically hindered antioxidant, allowing for more readily reactive hydroxyl groups. These results were determined from both LCMS and NMR. The control group (EtOH reaction with ethyl isocyanate) was used to determine the relative peak shifts for urethane and urea linkages, and these were then compared with obtain spectra for antioxidant model studies.

Subtraction FTIR was used to confirm the presence of antioxidants in the SMPs after synthesis. Triphen displayed a sharp, medium peak at *ca* 2355 cm^{-1}, indicative of phosphines, as well as bands *ca* 1600 cm^{-1} and 906 cm^{-1}, corresponding to the aromatic ring and the phosphite ester, respectively.[218]

The Piper displayed methyl groups at 2800-2900 cm-1 and a urethane bond corresponding to the reaction of the hydroxyl group and the isocyanates. BHT had a sharp peak at *ca* 3600 cm^{-1}, methyl peaks from 2800-3000 cm^{-1}, and peaks at *ca* 1615cm^{-1}, 1550 cm^{-1} and 1480cm^{-1}.[219-220] The Methyl spectra displayed a larger peak at *ca* 3550 cm^{-1} and a smaller peak at *ca* 3625 cm^{-1}, as well as the methyl peaks from 2800-3000cm^{-1}, a peak at *ca* 1480 cm^{-1} and the two peaks at 1200 cm^{-1} and 1240 cm^{-1}.

Methyl-containing SMPs' higher T_gs may be attributed to the formation of crosslinks at the phenol groups, which increases backbone rigidity and therefore the T_g. This may be why the Methyl SMP was found to have reduced shape memory, as a result of the covalent

crosslinks formed, and the BHT, which possesses a slightly raised T_g but does not form covalent crosslinks, does not have altered shape memory.

Mechanically, the Triphen antioxidant may have acted as a plasticizer for the SMP, allowing for increased strain before failure at the expense of the other mechanical properties. Again, the presence of crosslinked Methyl in the SMP backbone would also result in the increased elastic modulus, tensile strength, and toughness, as well as the decreased strain to failure.

For the HDI-based SMPs, it was found the physically added antioxidants were extracted during cleaning, and this may be what prevented the antioxidants from reducing the mass loss, at least for BHT. Methyl SMP would not be able to scavenge radicals due to the formation of covalent crosslinks, leaving only the Piper as an efficient antioxidant.
A lack of solubility could be a reason for the limited efficiency of the other antioxidants. DSC indicated the presence of Thio in the SMP after cleaning (crystallization peak) as did FTIR and GCMS extractions, but model testing was suggested limited solubility and interactions with H_2O_2, even at elevated temperatures. This lack of reactivity could explain the presence of the Thio even while degradation of the SMP was occurring.

Based upon the obtained degradation results, Piper and BHT are the most suitable candidates for controlling oxidatively-induced mass loss for certain medical device applications. A review of literature was performed to determine if either of these antioxidants is known to be cytotoxic.[75-87,217-223] BHT and its derivatives are widely used in cosmetics, foods, and medical devices, providing a means of adsorption and distribution into the body, and these oxidation products are known to occur *in vivo* for these applications.[82-87] Overall

BHT and similar structures are known to be non-genotoxic, non-carcinogenic, and may even reduce the incidences of some related conditions, such as atherosclerosis.[83-86] BHT may be metabolized into the carboxylic acid analog and excreted from the body, as will the oxidation products, indicating its utility in medical applications provided low dosing is ensured.[83-86]

Piper and its derivatives have been proposed for a variety of antibiotic, antimicrobial and similar applications, and similar structures have been found to be non-mutagenic and non-genotoxic.[75-78,224-225] Provided that the Piper is covalently bound to the polymer backbone during synthesis and free Piper does not rapidly diffuse out, this antioxidant may also be appropriate for preventing mass loss in medical devices, although cytotoxicity studies are needed to further confirm this.

Future work would include expanding the range of examined antioxidants to include vitamin E derivative α-tocopherol as a future additive for testing, as well as other polymeric antioxidants, in addition to examining the covalent bonding of the antioxidants to the polymer bulk.[226] These larger antioxidants will not diffuse out as rapidly, but will have to be examined for the impact on thermo-mechanical and shape memory properties.

A synergistic approach may also be beneficial, where the polymeric, physically added antioxidants are selected to be reactive with the free radicals during the initial stages of degradation after the implantation of the material, and a covalently bound antioxidant acting as a long-term radical scavenger to further tune the rates of degradation and degradation product formation.

4.5 Conclusions

We demonstrate the utility of covalently added and physically added small molecule antioxidants in highly porous shape memory polymers. The use of antioxidants in SMPs was intended to control the oxidative degradation and mass loss in these materials, which was accomplished through the use of the covalently added Piper antioxidant. Other antioxidants were shown to be removed through extraction in processes similar to the cleaning of medical materials prior to implantation, but changes in the polymer backbone (increasing hydrophobicity) were found to increase the retention of BHT in the SMPs. The degradation products of the most efficient antioxidants, BHT and Piper, were identified from literature as well as spectroscopic methods, and the proposed structures are presented. The toxicological risk associated with these additives is addressed from a literature review of antioxidant cytotoxicity, proposed uses, and known metabolic outcomes, with the Piper and BHT SMPs showing promise for translation into materials for reduced or tuned degradation in medical, particularly vascular, device applications.

CHAPTER V

POLYURETHANE MICROPARTICLE COMPOSITE SHAPE MEMORY POLYMER POROUS SCAFFOLDS CONTAINING ANTIOXIDANTS FRO ENHANCED OXIDATIVE BIOSTABILITY

5.1 Introduction

The use of amino alcohols in thermoset shape memory polymers (SMPs) has been a source of oxidation, which results in rapid mass loss dependent on the concentration of oxidizing species.[134] For medical devices and materials that incorporate SMPs, the rate of mass loss is directly related with the toxicological risk for the patient, as the rate of mass loss is the inverse of the rate of degradation product formation.[227-229] While these SMPs have been demonstrated to be cyto- and biocompatible, long term risk may be reduced through reduction of mass loss rates, and there are device applications that require long-term presence of implants.[26,227-229] Obtaining the ability to tune the rate of mass loss is a necessary step towards developing a material platform of SMPs for vascular implants. Previous work has demonstrated that common, small molecule antioxidants may be incorporated directly into the SMPs during synthesis as a method of tuning morphological, thermal, shape recovery, and in some cases the degradation-resistant properties.[230] This study found that retention of the antioxidants was dependent on method of incorporation and SMP composition, as many small molecules are removed during the necessary cleaning process required for medical materials intended for implantation.[230] Here the use of poly(urethane urea) microparticles is demonstrated as an alternative method of incorporating the antioxidants into SMP, allowing for enhanced oxidative resistance by utilizing a wider

variety of antioxidants compared with the previously used incorporation of small molecule antioxidants, without the thermo-mechanical and shape memory property changes.

Particle systems have been proposed and tested for a variety of fields, and in medical applications microparticles have been proposed for drug releasing systems, chemical sensors, and visualization.[231-235] A series of antioxidant microparticles, produced from a hydrolytically degradable vanillyl alcohol-containing copolyoxalate, were produced and tested in conjunction with dexamethasone. However, these particles would release *ca* 80% of the drug payload within 12 hours, and had sizes ranging from *ca* 10-15 μm. While the authors did not examine the degradation products, this polymer will also degrade into oxalic acid, which be cytotoxic.[130,236] The same particles were previously studied for their interaction with hydrogen peroxide (H_2O_2) as radical scavengers.[237] Polyketal microparticles were tested for radical scavenging by delivering superoxide dismutase to a model of lung fibrosis, with the ketals displaying no inflammation response compared with the inflammation found using the standard PLGA particles. This method also inhibited lung fibrosis.[238]

Previous work with shape memory polymers (SMP) synthesized from amino alcohols and aliphatic diisocyanates indicates an oxidative degradation mechanism, where the rate of mass loss is directly related with the concentration of H_2O_2, which is used as a model for immune response to the implanted biomaterial.[50,134,230] While the use of small molecule antioxidants has been demonstrated to be useful in delaying the oxidative mass loss of these materials, several of these examined species were found to be unsuitable or to yield less-than-ideal SMP materials due to thermo-mechanical property changes.[230] While

some of these changes occurred as a result of the antioxidants acting as plasticizers, the butylated hydroxy toluene (BHT) was not well retained in the SMP matrix, and BHT derivatives were found to covalently react with the diisocyanates to produce more mechanically rigid SMPs without increasing oxidative biostability.[230] The SMP matrix material has displayed excellent biocompatibility in previous studies and is anticipated to have minimal degradation toxicity.[27,33] A method of incorporating the antioxidants into this matrix without covalent bonding, rather than changing the matrix, may be more suitable for increasing oxidative biostability.[27,33] Previous work with composite SMPs has indicated that metal and metal oxides will result in thermo-mechanical property changes and that loading thresholds are dependent of stability of the porous matrix during synthesis.[37,239] The use of a more compatible particle (polymeric particle) may allow for incorporation of the antioxidants without sacrificing the thermo-mechanical properties of the matrix SMP; poly(urethane urea) chemistries were selected due to the similarities with current synthesis methods, the well understood degradation products that would be produced for such formulations, and for the body of literature surrounding molecule-eluting applications.[134,239-240]

Formation of porous polyurethane microspheres through solution templating using calcium carbonate solution has been attempted, resulting in particles with *ca* 7.5 μm diameters.[241] A solution of dimethyl sulfoxide (DMSO) and water (H_2O) was used to produce porous polyurethane microparticles in a one-pot reaction that included the use of polyvinyl alcohol and isophorone diisocyanate.[243] Castor oil and methylene-di-phenyl diisocyanate were reacted to form thermoplastic polyurethane microparticles, with water

added to produce the polyurea.[244] Acetone/water mixtures have been used with a variety of amines to produce polyurea microspheres and particles with a range of sizes.[245-246]

Here we present a method for producing hollow, shell poly(urethane urea) microparticles with average diameters ranging from 2 to 8 μm, depending on the reaction conditions and starting reagents used. These particles were synthesized with or loaded with antioxidants and incorporated into SMPs as a method of reducing the rate of oxidative mass loss. Characterization of these materials indicates that this method for including antioxidants is superior as there are no thermo-mechanical property changes or shape recovery kinetic differences.

5.2 Experimental

Hexamethylene diisocyanate (98%, HDI, Sigma), isophorone diisocyanate (98%, IPDI, Sigma), triethanolamine (99%, TEA, Sigma), N,N,N',N' tetrakis (hydroxypropyl) ethylenediamine (98%, HPED, Sigma) were used without modification. Butylated hydroxytoluene (BHT), 1,2,2,6,6 tetramethyl piperidinol (piper), and 2,2'-methylenebis(6-tert-butyl-methylphenol (methyl) were chosen as antioxidants and purchased from Sigma Aldrich. Ethanol (97%, EtOH, Sigma Aldrich), acetone (99%, VWR) and isopropyl alcohol (99.5%, Sigma Aldrich) were used as solvents. Cobalt chloride ($CoCl_2$), hydrogen peroxide (H_2O_2, 50%, Sigma Aldrich) were used for degradation solutions. Phloxine B (PhB, Sigma) and Nile blue chloride (Nile, Sigma) were used without modification.

Fourier transform infrared spectroscopy (FTIR) attenuated total reflectance (ATR) was performed using a Bruker ALPHA infrared spectrometer (Bruker, Billerica, MA); 48 scans per spectra for both background and samples were used. Spectra data was collected in

absorption mode with a resolution of 4 cm^{-1}. OPUS software was used to examine spectra, identify peaks, and perform baseline and atmospheric corrections. Examinations were performed in triplicate to confirm results. The obtained spectra were compared to previously reported spectra and a control without antioxidant additives. was used to confirm the formation of urethane and urea linkages. Previous work has confirmed the reactions of antioxidants with isocyanates using NMR. X-ray photoelectron spectroscopy (XPS) (Omicron XPS with Argus detector) using a Mg/Al x-ray source was used to characterize particles and SMPs.

IPDI (5 g, 22.5 mmol) was added to a water/acetone solution (95 g) and mixed for 1 hour at room temperature.[24] Reaction temperature and solvent ratio were varied to optimize synthetic outcomes. TEA (29.97 mmol), DEA, or HPED were dissolved while stirring at 30 rpm in the mixture. 5 g IPDI (22.5 mmol) was added over 10 minutes at a constant rate. The reaction was allowed to proceed overnight, yielding a viscous white solution. The solution was centrifuged for 5 min at 4000 rpm, and the particles were rinsed in H_2O-acetone (30/70 ratio) three times before drying at 70°C overnight. Particles were dried and characterized (Yield 54%).

The thermoplastic core was extracted using IPA/acetone mixtures at 50°C for 12 hours with a one-hour sonication every 4 hours. Particles were then centrifuged and separated from the effluent, and removal of the core was confirmed using differential scanning calorimetry and x-ray diffraction experiments. Loading of the particles was performed by dissolving 20g of antioxidant or fluorescent dye into solution and adding 20 g of particles. The mixture was stirred and heated to 50°C overnight. Particle solutions were

then centrifuged, separated, washed three times using H_2O/acetone, and dried overnight at 50°C.

Synthesis of antioxidant containing particles was repeated with 50% wt of antioxidants added immediately after the alcohol, prior to the additional IPDI. Particles were collected and washed the same way as described previously. Particles produced this way are labeled Synth (i.e. B-Synth).

Porous SMP scaffolds were synthesized using a traditional two-step polyurethane foam synthesis process. An isocyanate premix was first made by adding 42% of the desired alcohols (molar %, with percentage varied to control premix viscosity and thus scaffold pore size) to the entire amount of diisocyanate, with a ratio of NCO:OH of *ca* 2:1. This premix was cured at 50°C for 36 hours. The alcohol premix was then synthesized, consisting of the remaining alcohols, particles (10% wt), surfactants and catalysts. The premix was homogenously mixed, and was then mixed to the isocyanate premix along with microparticles using a high speed shear mixer, followed by the addition of a physical blowing agent. The scaffold was cured at 90°C for 20 minutes, followed by cold curing over night at ambient conditions.

SMP samples were imaged using an Olympus Fluoview 1000 laser scanning confocal microscope (LSCM) (Olympus America Inc, Center Valley, PA), and were excited at 543 nm utilizing <1% maximum intensity.[27] Foam cell structure was determined by cutting axial and transverse samples that were examined using scanning electron microscopy (SEM). Samples were mounted onto a stage and sputter coated with gold using a Cressington Sputter Coater (Ted Pella, Inc., Redding, CA) for 60 seconds at 20 mA. Samples were then

examined using a Joel NeoScope JCM-5000 SEM (Nikon Instruments Inc., Melville, NY) at 11X magnification and 15 kV under high vacuum.

Differential scanning calorimetry (DSC) was also used to measure both wet and dry T_g using a Q-200 DSC (TA Instruments, Inc., New Castle, DE). Samples of *ca* 5.0 mg ± 1.0 mg were sealed in TZero aluminium pans and placed in the heating cell. The sample was cooled to equilibration at -40 °C, heated to 120 °C at 10 °C/min, cooled 10 °C/min to -40 °C and heated to 120 °C at 10 °C/min. The half-height transition of the final heating cycle was the reported T_g. Wet samples were weighed and sealed in the same manner, and were then heated from -40°C to 80°C at 10°C/min.

Shape recovery of cylindrical foam samples (6 mm diameter, 10 mm length, six samples per series) crimped over a wire was examined at 50 °C in RO water to determine the volume recovery behavior (strain recovery). Samples were crimped to a minimal diameter (*ca* 1.0 mm using a SC150-42 Stent Crimper (Machine Solutions, Flagstaff, AZ). To crimp, samples were equilibrated at 100 °C for ten minutes and then radially compressed and cooled to room temperature. Samples relaxed for 12 hours and were tested over the course of 30 minutes. Image J was used for analysis of the change in diameters over time.

Uniaxial tensile testing was performed on ASTM d638 IV samples using an Instron Tensile Tester with 500 N load cell. The extension rate was set to 5 mm/min at room temperature, and seven samples were tested for each species. Elastic modulus, strain to failure, ultimate tensile strength calculated.

Release of antioxidants was studied at 1 hr and 1 wk using 2.0 g SMPs in 50 mL of IPA at 50 °C. Samples were withdrawn and the solution was examined using gas

chromatography mass spectrometry (GCMS). Solution was injected into the column (C18 silica, normal phase) and heated at 20 °C/min to 300 °C.

For analysis of degradation rates, cleaned samples were completely immersed in respective solutions of 20% H_2O_2 with 0.1M $CoCl_2$ at 37 °C. Sample solutions were changed every 3 days to ensure a relatively stable ion concentration, and once per week samples were removed, cleaned in EtOH, and dried in at 50 °C under vacuum (30 in Hg), after which sample mass was recorded and samples returned to fresh solution.

5.3 Results and Discussion

An overview of the synthetic method is displayed in **Figure 5.1**. The three amino alcohols examined for synthesis with IPDI were characterized for size, shown in **Table 5.1**. While the smallest particles are achieved with HPED, the small distribution was achieved with TEA or DEA. HPED resulted in two sizes of particles with a larger standard deviation than with the DEA and TEA monomers. TEA was selected for further examination due to the D_n. **Table 5.2** shows the effect of temperature conditions on the synthesis of TEA-IPDI particles, and **Table 5.3** displays the effect of solvent ratios.

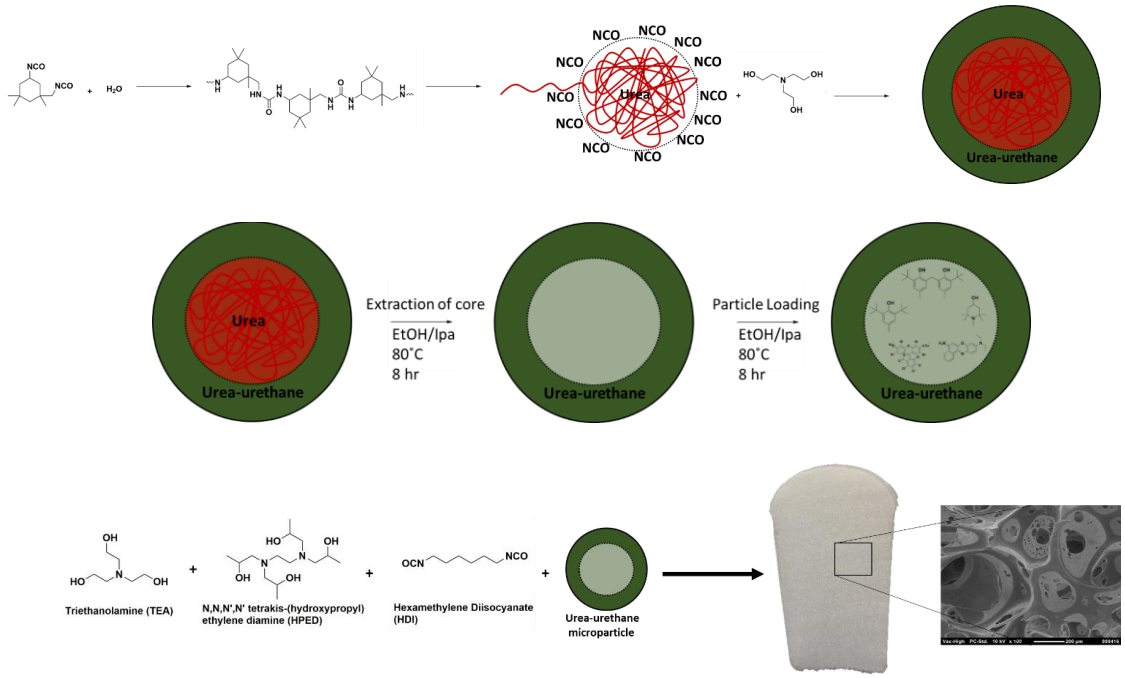

Figure 5.1. Synthesis of polyurethane particles, as first thermoplastic chains that are the core of the crosslinked shell. The particles are then cleaned, the thermoplastic core extracted, and then loaded with antioxidants. The particles are then combined with the displayed monomers to synthesize shape memory polymer foam (SMP).

Once the cores were removed, the particles were loaded with the antioxidants or the fluorescent molecules. Particle loading was analyzed using XPS to determine the composition (**Table 5.4**), which was related to the elemental composition of PhB as a model, using the presence of chlorine as a reference. Loading during synthesis was viable only for BHT and Piper, as Methyl is not soluble in the polymer solution sufficiently. Loading percentages of up to 45% were attempted during synthesis, and did not appear to alter

particle composition or morphology, but removal of BHT was a possibility during particle cleaning and so was not further examined. Loadings of *ca* 45% (wt) were achieved using physical means after synthesis.

Table 5.1. Morphological properties of IPDI microparticles synthesized from three alcohol monomers.

Temperature	Monomer	Diameter (μm)	Number ave Distribution (D_n)	Weight ave Distribution (D_w)	D_w/D_n
50°	TEA	6.15 ± 2.06	6.791	10.690	1.574
50°	DEA	6.85 ± 1.26	7.254	8.742	1.287
50°	HPED	5.61 ± 3.48	9.544	10.484	1.10

Table 5.2. Morphological properties of IPDI-TEA microparticles.

Temperature	Diameter (μm)	Number ave Distribution (D_n)	Weight ave Distribution (D_w)	D_w/D_n
0 °C	6.17 ± 0.78	6.662	9.122	1.369
20 °C	2.43 ± 0.91	2.799	4.176	1.491
50 °C	6.15 ± 2.06	6.791	10.690	1.574
80 °C	5.16 ± 1.93	6.419	9.125	1.421

Table 5.3. Morphological properties of IPDI-TEA microparticles synthesized using varied concentrations of acetone and water.

Temperature	Acetone %	Diameter (μm)	Number ave Distribution (D_n)	Weight ave Distribution (D_w)	D_w/D_n
20°	30	6.26 ± 1.88	6.657	9.723	1.461
20°	50	4.09 ± 1.21	4.526	7.051	1.558
20°	60	5.20 ± 2.13	4.695	8.295	1.767
20°	70	2.43 ± 0.91	2.799	4.176	1.491

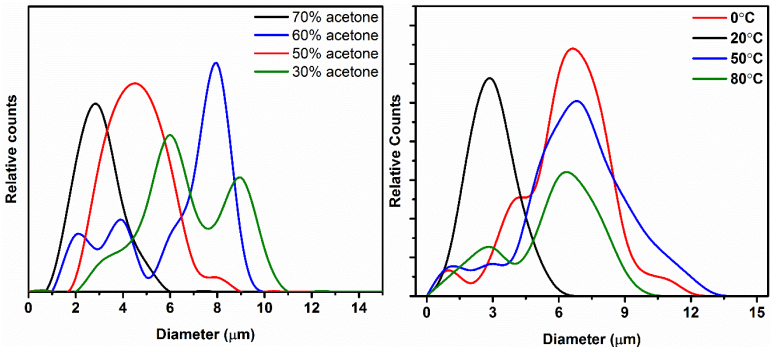

Figure 5.2. Size distribution of IPDI TEA particles synthesized at varied temperatures.

The size distributions of the TEA-IPDI microparticles determined through microscopy are shown for solvent conditions and temperature in **Figure 5.2**, and the morphology of individual particles at 20°C are shown in **Figure 5.3**.

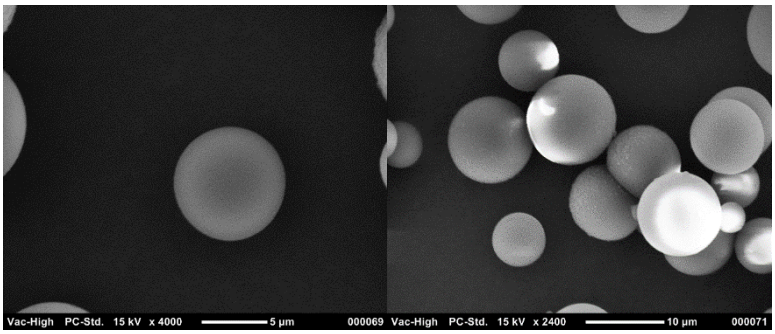

Figure 5.3. Particles synthesized from IPDI and TEA at 20°C.

There particles contain a thermoplastic polyurea core with the poly(urethane urea) crosslinked shell surrounding it. Removal of the core was achieved through sonication in solvent, confirmed using DSC and XRD (**Figure 5.4**).[244]

The formation of urethane and urea linkages was confirmed through the presence of carbonyl peaks at 1689 cm^{-1} and 1640 cm^{-1}, respectively. The lower wavenumbers for the urethane peak are due to the increased hydrogen bonding achieved using aliphatic monomers. XPS confirmed the incorporation of greater amounts of free hydroxyls (286.4 eV) associated with the leftover end groups from the synthesis (**Table 5.4**), as wells are a should peak at 288.7 eV associated with carbonyls.[28] Further analysis of the SMPS confirmed the residual presence of tin, which is used as a catalyst. Silicone is present due to the surfactants used, as well as chlorine in the examined PhB-containing species. The dual binding peak seen for the C1s scan at 286.6 eV may also indicate a greater presence of C-N

bonds as well as hydroxyls, as a result of greater incorporation of the alcohol into the SMP compared with in the microparticle, which possesses a thermoplastic core and linear shell components. The maximum intensities of the PU particle plain and PhB particles N1s peaks were *ca* 37000 counts/sec 31000 counts/sec, while the SMP composite nearly 53000 counts/sec. This is supported by the relative area of the N1s peak displayed for the SMP compared with the particles in the survey scan.[249]

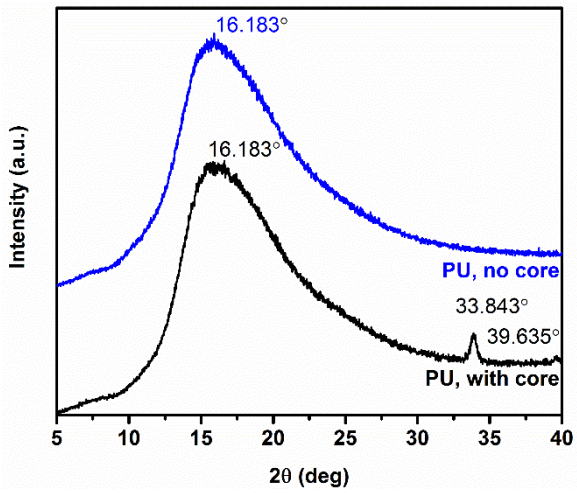

Figure 5.4. A comparison of the areas of the original microspheres (PU with core) and those that have undergone extraction reveals a relative crystallinity of 3.3% for the starting material, which can be attributed to the thermoplastic polyurea core.

Table 5.4. XPS determined elemental composition of selected particles and composite SMPs.

Species	Elemental Composition			
	C%	O%	N%	Additional elements
Pu particle	75.43	11.89	12.69	
BHT	76.6	9.88	13.52	
Methyl	75.49	10.67	13.84	
Piper	77.28	8.58	14.14	
PhB	73.66	13.57	11.54	Cl, Br
SMP Composite	57.40	20.57	2.99	Sn, Cl, Si, Br

Determined from SEM, the average strut diameter is *ca* 20.7 ± 3.6 μm. The average aggregate diameter was 13.4 ± 10.1 μm, as displayed in **Figure 5.4**, determined through optical microscopy of fluorescent-tagged particles. Dry T_g of the examined species was found to be *ca* 65°C, regardless of additive species. Wet T_g was *ca* 28°C.

Shape recovery characterization demonstrates that all composite SMPs examined have similar shape recovery profiles (**Figure 5.5**), a trait that is not reproducible with metal or metal oxide-based additives.[37,239] Previous work with antioxidants added into SMPs as small molecules resulted in changes in the shape recovery behavior, notably in the Methyl and Piper antioxidants due to covalent bond formations.[230] However, the Methyl-loaded particles do not impact shape recovery compared with small molecules, and the Piper-loaded particles have superior shape recovery behavior compared with the small molecules. Piper-loaded composite SMPs are capable of 100% strain recovery over 15 minutes (with full

recovery occurring at *ca* 10 minutes) with similar recovery kinetics to the control material. Piper added as a small molecule results in delayed recovery and a final recoverable strain of *ca* 90%. By 10 minutes only *ca* 75-85% strain is recovered.

Further comparison of the composite SMPs and small-molecule containing SMPs can be made using tensile testing (**Table 5.5**). Previously, the incorporation of covalently bonding antioxidants (Methyl and Piper) resulted in the reduction of strain to failure, increased tensile strength and elastic moduli. In the case of Methyl small molecule antioxidants, the elastic moduli were *ca* 8 times greater and the tensile strength was 4 times greater. Using microparticles, the mechanical properties do not significantly change. The changes that are displayed may be result of this are not statistically significant and may be attributable to the slight change in SMP morphology that is obtained through inclusion of physical additives.[230]

Release of additives from the composite SMP was measured using GCMS (**Table 5.6**). At 1 hr, which would be the equivalent of cleaning the SMP prior to device packaging and sterilization, the particle synthesized with the antioxidants appeared to have released the majority of the release-able payload. BHT-synth released more than 80% of the available antioxidant, by 1 hr. By 1 wk, 91% of the available BHT had been released from the BHT-synth. By comparison, BHT/BHT (containing both microparticles and small molecule antioxidants) released nearly 50% of the available antioxidant, and BHT-load had released *ca* 75%. These release studies were further confirmed using UV-vis experiments.

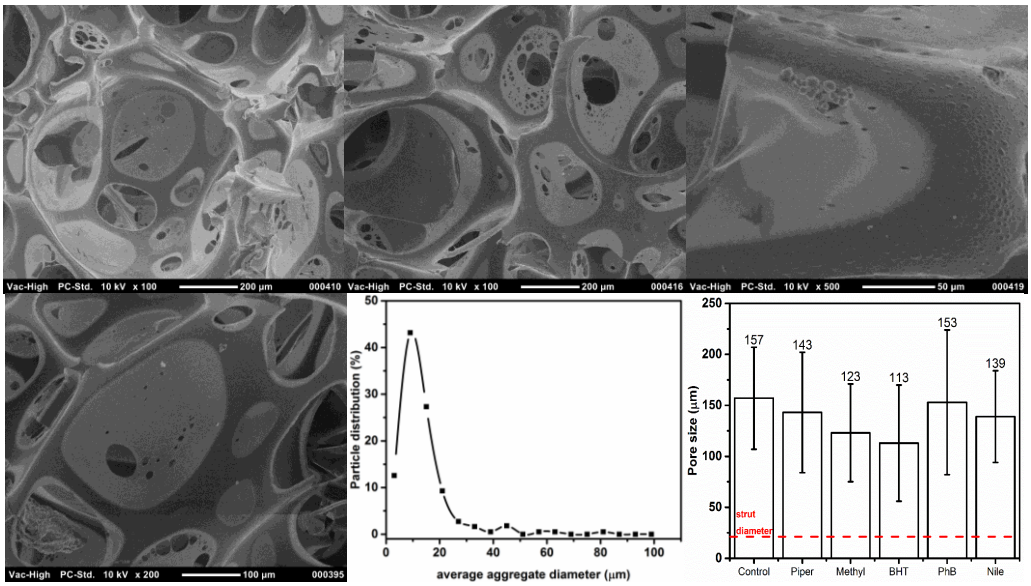

Figure 5.5. SMP foam with TEA-hollow microparticles (A), BHT loaded with BHT-hollow microparticles (B). The agglomeration of microparticles can be seen to occur along the edges of pore membranes (C, D). Aggregate diameters (E) and pore sizes (F) determined using microscopy.

The degradation products of these SMPs have been previously characterized. The amino alcohols are known to oxidize to lower amines and corresponding aldehydes, which may further oxidize to carboxylic acids or are part of the tissue integration process, depending on location and foreign body response.[135] The use of TEA is designed to increase long-term cytocompatibility of the particles and particle degradation products, as TEA will not form oxalic acid as a potential by-product, unlike HPED; particle morphology and size dispersity were other considerations.[135]

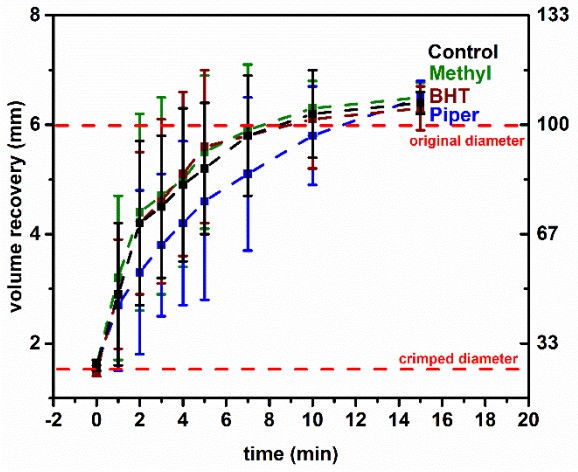

Figure 5.6. Shape recovery characterization over 15 minutes in 37°C RO H_2O displaying the various compositions and their shape recovery behavior.

Table 5.5. Mechanical properties of microparticle composite SMPs.

Species	Elastic Modulus	Strain to Failure	Ultimate Strength
Control (HH60)	1.45 ± 0.19	45.2 ± 11.6 %	0.21 ± 0.1
Piper	1.32 ± 0.26	52.9 ± 8.2 %	0.27 ± 0.1
Methyl	1.19 ± 0.18	61.2 ± 26.1 %	0.26 ± 0.1
BHT	1.52 ± 0.29	51.2 ± 5.8 %	0.27 ± 0.1

From the loading calculations, it appears that these microparticles may be suitable for increasing the oxidative resistance of the matrix SMP, as 10% loading of these particles would provide *ca* 0.85 g of antioxidant (5% wt of the SMP matrix) (**Figure 5.7**). In comparison with the direct addition of these antioxidants to the bulk material, the use of

microparticles may be used to better retain BHT and Methyl antioxidant species for enhancing SMP biostability. Previously, the BHT was not retained in the SMP and the Methyl crosslinked, resulting in increased elastic modulus at the cost of its strain recovery that degraded at the same rate as the control.[215] Utilizing the microparticles, SMPs were developed that had similar thermo-mechanical and shape recovery properties with increased degradation resistance for all examined antioxidants. However, while this method enhances the utility of same antioxidants, for the Piper series it was found to be no more effective than the addition of small molecules into the bulk.

Approximations of real time oxidative mass loss were calculated using the accelerated data. For the control materials, in 2% H_2O_2 the lifespan of the materials is predicted to be *ca* 500 days. For Methyl SMP composites, the lifespan of the material is *ca* 600 days. Piper and BHT had predicted lifespans of *ca* 650 days. From a toxicological risk perspective of the degradation products, increasing the time to total mass loss (decreasing the rate of degradation) achieves a lower production rate of degradation products and a reduced risk.

For the SMP matrix, toxicity assessments have been performed using completely degraded materials, synthesized degradation products, and corresponding literature review of available products. From the cytocompatibility studies, it appears the oxalic acid is the most concerning degradation product. In selecting TEA as the alcohol monomer of the particles, complete particle degradation is not limited by generation of oxalic acid or glyoxal.

Table 5.6. Released concentrations of antioxidants determined from GCMS.

Species	Initial Mass	Initial Concentration (mol)	1 Hr release Mass	1 Hr release Concentration (mol)	1 Wk release Mass	1 Wk release Concentration (mol)
BHT and BHT	2.4000	0.0109	1.1220	0.0051	1.1480	0.0052
BHT Synth	0.8000	0.0036	0.6515	0.0030	0.7312	0.0033
BHT Load	0.8000	0.0036	0.3218	0.0015	0.6008	0.0027
Methyl Synth	0.8000	0.0024	0.0159	0.0001	0.1496	0.0004
Methyl Load	0.8000	0.0024	0.0143	0.0001	0.02117	0.0001
Piper Synth	0.8000	0.0051	0.0243	0.0002	0.0243	0.0002
Piper Load	0.8000	0.0051	0.0143	0.0001	0.0151	0.0001

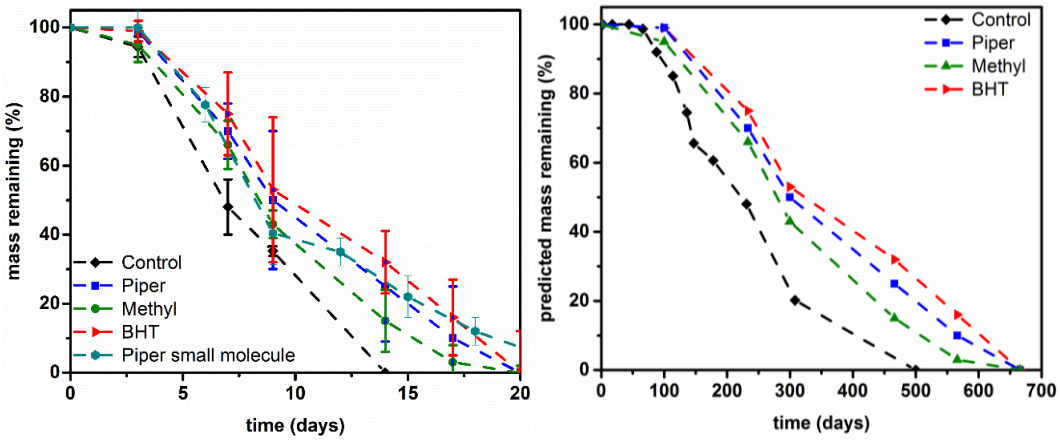

Figure 5.7. Degradation of composite SMPs compared to control and selected small molecule antioxidant containing SMPs over the course of 20 days in accelerated conditions (left, 20% H_2O_2 with 0.1 M $CoCl_2$ at 37°C), and the predicted real time degradation behavior of the SMP composites (right, equivalent of 2% H_2O_2 at 37°C).

5.4 Conclusions

Previous work with inclusion of antioxidants revealed that many species will result in altered thermo-mechanical properties, decrease shape memory, or will be removed from the bulk SMP during cleaning for device preparation. Through the use of microparticles as antioxidant reservoirs, these changes are minimized and oxidative resistance is improved. Microparticles were produced for diisocyanates and amino alcohols, with synthetic conditions and starting reagents examined for particle physical characteristics prior, and antioxidants loaded prior to synthesis of composite SMPs. The materials were characterized and found to exhibit similar mechanical, shape memory, thermal, and morphological properties when compared with control samples, indicating that the particles are compatible

with the SMPs and that the presence of antioxidants will not influence material properties. Oxidative resistance was found to be enhanced with all examined antioxidants.

Comparisons of the Piper small molecule antioxidant and the Piper-containing microparticles indicates similar times to complete mass loss, for real time oxidation. The BHT and Methyl antioxidants, previously incompatible with the HDI-based SMPs, are found to increase oxidative resistance when incorporated into the microparticle-composite SMPs. With this method, the lifespan of the SMP is increased from 500 days to nearly 700 days (**Figure 5.8**). While in some cases the use of the Piper antioxidant may be superior to the microparticles, this method allows for a greater variety of antioxidants and may also increase the functionality of the SMPs, as demonstrated through the brief examination of environmental responsiveness.

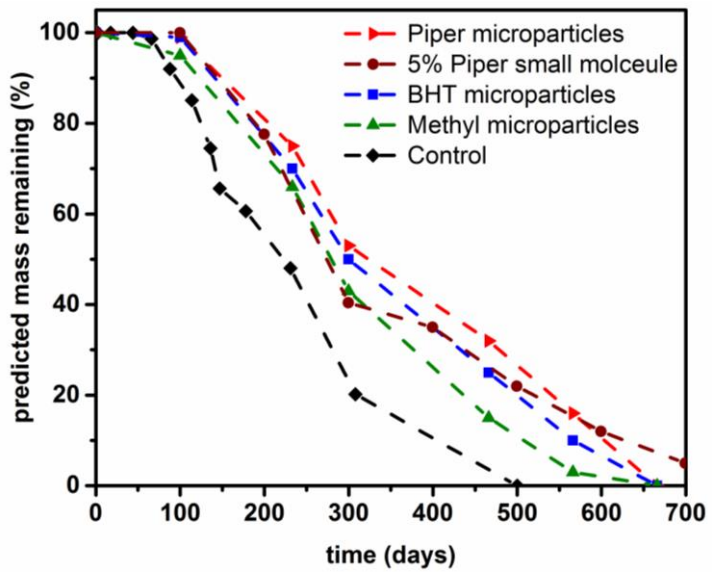

Figure 5.8. Comparison of the predicted mass loss profiles for antioxidant-containing SMPs, with Piper incorporated as both a small molecule antioxidant as well as in the microparticles. The predictions are for 2% H_2O_2, or the equivalent of real time for the HH60 composition being examined.

CHAPTER VI

HIGHLY POROUS THERMOSET SHAPE MEMORY POLYURETHANE TISSUE SCAFFOLD FROM THE RENEWABLE RESOURCE GLYCEROL, AND ITS OXIDATIVE DEGRADATION PATHWAY

6.1 Introduction

Shape memory polymers (SMPs) have been proposed for a variety of medical applications, such as vascular occlusion devices, due their ability to recover their original shapes upon thermal equilibration or the introduction of solvent.[30,32-34,42,180-181] Of these stimuli-responding polymers, polyurethanes (PU) are some of the best candidates for medical devices due to their biocompatibility and wide variety of formulations available, despite the reported cases of PU failures.[1,5-6,18,30,32,42,73] SMP PU compositions may be tuned to allow for shape recovery to take place upon equilibrating with body temperature, or due to the influx of water once the material is placed *in vivo*.[182-184]

Thermoplastic PU have demonstrated a lack of biostability, classically as a result of chain extenders containing hydrolytically labile groups or due to urethane hydrolysis.[18,33,73] However, the developed thermoset SMP PUs based upon aliphatic amino alcohols and diisocyanates, despite possessing improved hydrolytic stability, were still susceptible to degradation.[134] The cause of the oxidative susceptibility was found to be the tertiary amines, which may fragment to form lower amines, aldehydes and acids, and eventually ammonia.[37] The replacement of these amino-alcohols with a less susceptible monomer will result in increased oxidative stability and further reduce patient risk. Glycerol was selected to replace triethanolamine (TEA), the more oxidatively susceptible monomer.[134,185-191] In addition to

the tri-functionality of glycerol, which will theoretically not reduce the crosslink density and strain recovery of the bulk material, it is also renewable and inexpensive. [134,185-191] Degradable polymers have been synthesized utilizing glycerol, but the degradable linkages have been determined to be from the copolymer component, such as dsulfide, ester or ether linkages.[1,5-8,192-194] To our knowledge, no work has been done to characterize what, if any, degradation occurs for "biostable glycerol-based urethanes.

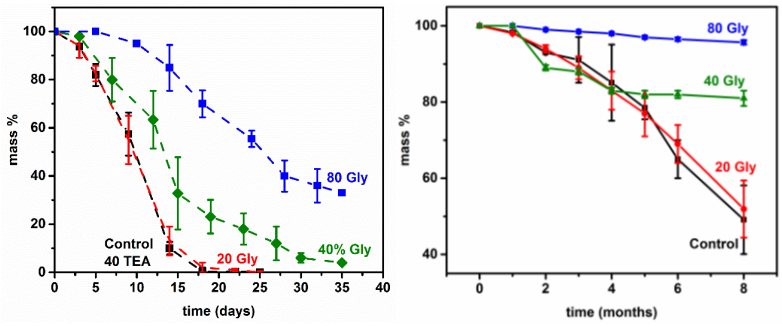

Figure 6.1. Accelerated mass loss (left, 20% H_2O_2 with 0.1 M $CoCl_2$) examined over 35 days, and real time mass loss (right, 2% H_2O_2) examined over the course of real time oxidation out to eight months. All experiments were conducted at 37°C.

Stoichiometric amounts of the amino-alcohol hydroxypropyl ethylene diamine (HPED) and glycerol were varied for characterization of degradation behavior, as well as basic material properties to produce SMPs with 20% glycerol (20 Gly, containing 10% by endgroups glycerol, 40% HPED, and 50% TMHDI), 40% glycerol (40 Gly), and 80% glycerol (80 Gly). The T_gs of the SMPs were found to be *ca* 74°C when dry, although the

plasticized T_g ranges from 42 to 48°C. After real-time oxidative testing, the T_g was found to have decreased by 7° to 20 °C, depending on the extent of degradation. SEM images confirm the gravimetric results, with the control and 20 Gly losing all morphological features by the end of the degradation studies. The 80 Gly was found to have minimal, if any, changes in the pore morphology and membranes.

^{13}C NMR confirms that despite the reactivity differences between primary and secondary alcohols in isocyanate reactions, there will be low concentrations of free secondary alcohols remaining when stoichiometry is balanced. It is expected that with high concentrations of free secondary alcohols that shape recovery may be inhibited, but in all examined cases, strain fixity and strain recovery were found to be greater than 99% when immersed in 50 °C H_2O, with most materials fully recovering within 15 minutes.

Gravimetric analysis of the samples in accelerated oxidative solution (20% H_2O_2 with 0.1 M $CoCl_2$) indicates that the control will undergo complete mass loss by *ca* 18 days, while lower concentrations of glycerol will be extended out to 25 or 35 days (20 and 40 Gly) (**Figure 6.1**). At 35 days, 80 Gly had *ca* 40% of mass remaining, and while the rate of mass loss is similar to 40 Gly, the time to initial mass loss is substantially improved from *ca.* 2 days to 12 days. In real time testing (2% H_2O_2), 80 Gly had *ca.* 96% mass remaining at 8 months, compared to less than 50% remaining for the control samples – an expected result due to the decrease in the tertiary amine concentration. The gel fraction of 80 Gly for real time oxidation conditions reduces from 98% to 88% over the course of testing, but the control and 20% Gly reduce to *ca* 5% and 15%, respectively. With *ca* identical T_gs for control and Gly SMPs, the mass loss from oxidative degradation is dependent on the amines.

While the crosslink density is theoretically the same (excluding reaction kinetic differences between the monomers), the network should be less fragmented at the glycerol units compared with the control TEA units at early time points.

Tensile testing (ASTM Type IV D dogbones, 5 mm/min strain rate) over the course of degradation demonstrated a distinct increase in modulus over time, along with a decrease in strain to failure and tensile strength (**Figure 6.2**). The 20 Gly samples were not robust enough to test after three months; 80 Gly SMPs had elastic moduli 133% of the original at eight months. The strain to failure decreased by *ca* 18%, and tensile strength decreased by 33%. For evaluation of materials in an environment that most closely simulates *in vivo* conditions, the mechanical samples provide the shortest time for performance testing, but without degradation mechanism information.

Liquid chromatography mass spectrometry (LCMS) was used to determine relative abundances and species of 2G (containing 2 urethane linkages and a free secondary alcohol) and 3G (3 urethane linkages) oxidation in 50% H_2O_2 solution (at 37°C over 4 weeks). **Figure 6.3** details the proposed degradation pathway for 2G. The 2G may be consumed to form the ketone (2), then a 1,2 diketone (3), which may undergo further fragmentation to aldehydes (4,7) and carboxylic acids (5,6). The aldehydes may further form carboxylic acids (7 to 5) or an anhydride that will decarboxylate to carbamic acids (4 to 6 to 8). It appears that the majority of the 2G does not undergo fragmentation until *ca.*weeks 2-3, as noted by the increase in ketones prior to increases in carboxylic acids. It appears that by week 4 most of the fragmentation has occurred. The degradation of the 3G molecule indicates minimal

fragmentation will occur under these conditions, as the starting material (15) was found to form ketones (16) and 1,3 diketones (17) over the course of examination (**Figure 6.4**).

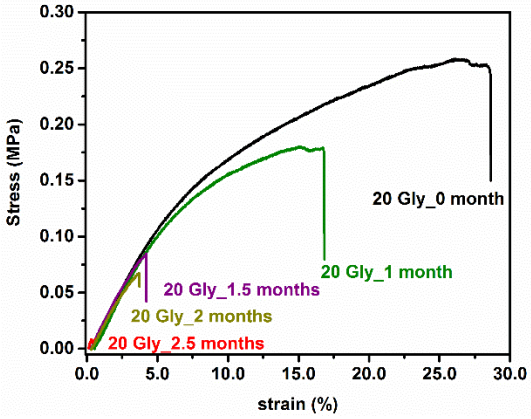

Figure 6.2. Representative stress-strain curve for 20 Gly SMPs at each examined degradation time point in 2% H_2O_2 at 37°C.

As can be determined from the comparison of the model degradation studies, the 3G molecular segments will be much more stable compared with the 2G segments. By 4 weeks, 2G will have formed more than 4 times the number of fragments than the 3G will have, and will be completely consumed in *ca* 2-3 weeks, while 3G starting material is still present (**Figure 6.5**).

The degradation products that were found for the 2G molecule are similar to compounds reported for oxidation of a single glycerol molecule.[185] While mesoxalic acid (ketomalonic acid) is an oxidation product of glycerol, presence of water and peroxide will

shift the equilibrium toward dihydroxymalonic acid.[185] Continued oxidation is also possible, leading to fragmentation. However, spectroscopic analysis of the bulk SMPs revealed a similar carbamate carbonyl peak shift (FTIR) after degradation due to the formation of carboxylic acids, as has been found previously with the degradation of the amino alcohols.[134] This shift was found in the 20 and 40 Gly, but not the 80 Gly, due to the reduced oxidation and lack of COOH formation. Solid state ^{13}C NMR supports these findings. This indicates a lack of 2G linkages in the SMPs, supported by the increase in oxidative stability with sufficiently high concentrations of glycerol, which is expected due to the excess isocyanate used during synthesis (1.05 NCO: 1.0 OH final ratio, 1.05: 0.40 for prepolymer synthesis). Photooxidation experiments of polyglycerol by S Morlat *et al*, where the proposed mechanisms include formation of ester and formate as a result of hydrogen abstraction from the CH2 atom of the glycerol molecule, followed by peroxy radical formation.[195] However, it was suggested that in this case no aldehyde or carboxylic acids would form.[195] This contrasts with oxidation studies of mono-glycerol, which indicates that selective oxidation may result in fragmentation at many points or a fully oxidized molecule, mesoxalic acid.[35,185-191] These are more in agreement with the results that we have presented.

6.2 Conclusions

Overall, we believe that the amines present in the SMP will oxidize preferentially and will be the initial cause of mass loss, as demonstrated with the lower glycerol concentrations in gravimetric studies, such as with the control samples. As the concentration of glycerol increases in the SMP, the fragmentation of amines will have less impact on the initial mass loss, which is demonstrated by the 80 Gly gravimetric results. After the amines

are consumed, which has been demonstrated to occur within the first two weeks of accelerated testing using 50% H_2O_2, then the glycerol will be oxidizing and fragmenting. At this point, the glycerol oxidation will be the primary cause of mass loss from the bulk SMP, albeit at a much slower rate compared with the amines. However, as we demonstrate, unreacted secondary alcohols will be the site of more rapid oxidation and therefore polymer fragmentation. With increasing glycerol concentration in the SMP, there may be more secondary alcohol sites; while optimization of the SMP synthesis process to reduce the secondary alcohol concentration is expected to ultimately yield SMPs with greater oxidative stability compared with their counterparts, spectroscopic analysis presented here does not reveal an abundance of secondary alcohols in the compositions, which may limit the extent to which glycerol may be used to achieve perfect oxidative stability.

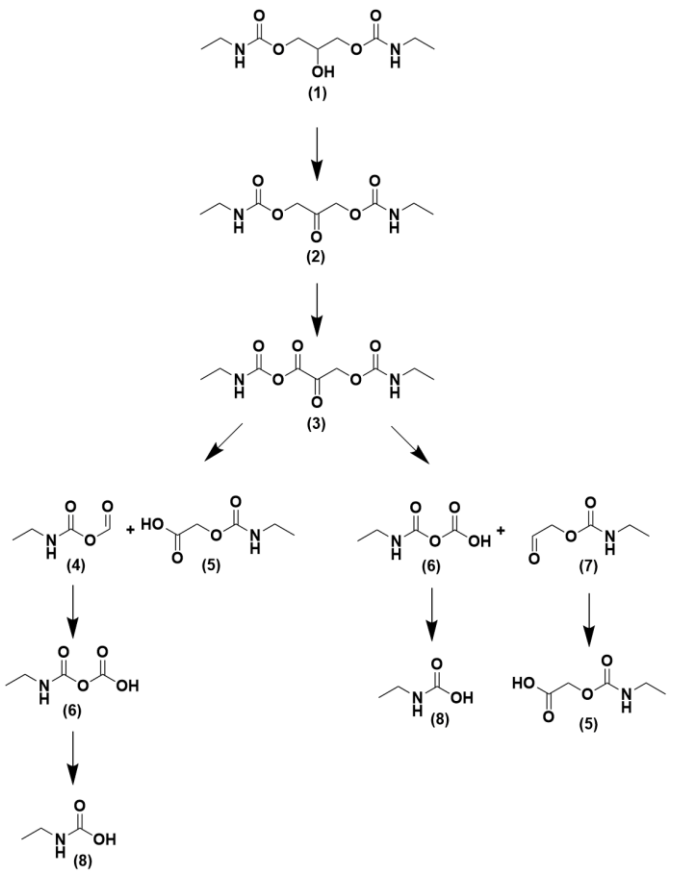

Figure 6.3. Proposed oxidative degradation pathway of the 2G molecule, examined at 37°C in 50% H_2O_2 using LCMS.

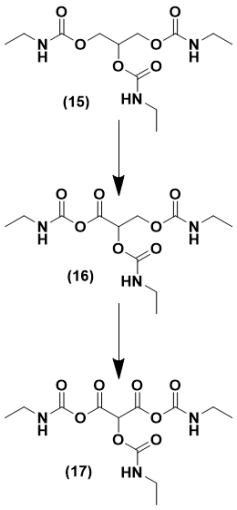

Figure 6.4. Proposed oxidative pathway for the 3G molecular segments.

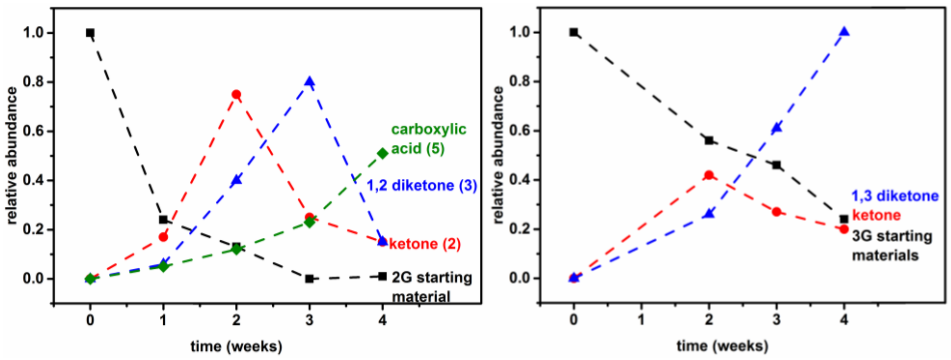

Figure 6.5. Relative rate of product formation from 2G model compounds (top). 3G relative abundances of products are displayed (right). Model compounds were degraded in 50% H_2O_2 at 37°C.

This is further confirmed by the remaining 95.7% mass of the 80 Gly (87.1% gel fraction) in real time oxidative solutions at 8 months, as opposed to the 20 Gly (51.6% mass remaining and 15.3 ± 9.8 % gel fraction) and control (49.1% mass remaining and *ca* 5% gel fraction). For rapidly testing the relative biostabilitly of multiple compositions prior to devoting resources to long-term studies, a model compound study coupled with mechanical testing seems to provide the fastest insight for bulk SMPs. However, based upon the known biocompatibility of glycerol-based polymers, and the presented attributes with regard to degradation, these SMPs do have excellent potential for improving the stability from the current iterations of poly (amino urethane) SMPs. While previous methods of enhancing biostability (antioxidant and antioxidant-containing microparticles) were found to increase the biostability to from *ca* 500 days to *ca* 1350 days (for TMHDI-based SMPs; HDI-based SMPs with antioxidants had lifespans of *ca* 700 days), the use of high concentrations of glycerol was found to produce SMPs with lifespans of *ca* 2250 days (**Figure 6.6**).

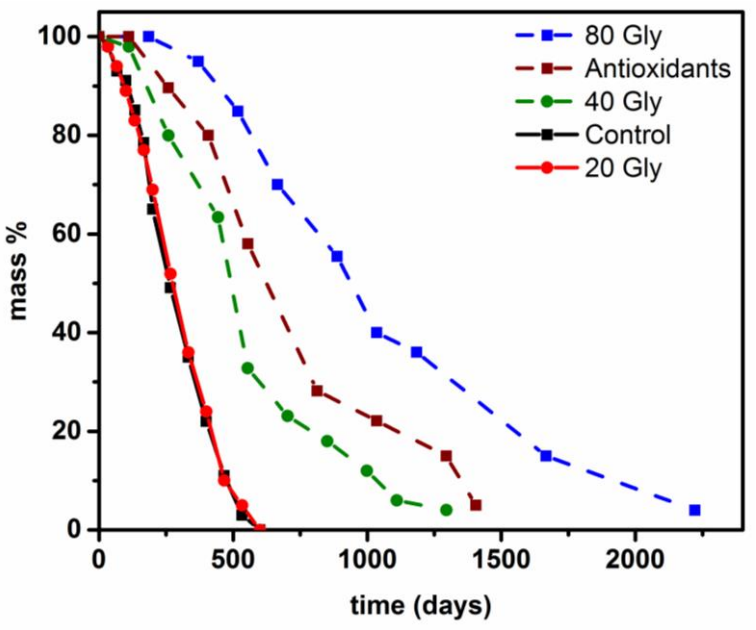

Figure 6.6. Comparison of the predicted real time (2% H_2O_2, 37°C) mass loss profiles for TMHDI-based SMPs, comparing control samples, 5% BHT (antioxidant) SMPs, and various concentrations of glycerol.

CHAPTER VII

ISOCYANURATE TRIOL AS A MORE OXIDATIVELY STABLE STARTING MATERIAL FOR SHAPE MEMORY POLYMERS BASED UPON ALIPHATIC, SYMMETRIC DIISOCYANATES AND AMINO ALCOHOLS

7.1 Introduction

Polyurethane materials have been a gold standard for blood contacting medical devices, particularly for cardiovascular and similar long-term implants.[1,5-7] While there are many studies presented in literature that attempt to develop polyurethanes with tunable rates of degradation, production of more biostable polyurethanes is not widely studied, despite the growing need.[1,5-8] In fact, polyurethane failures, associated with either hydrolytic or oxidative degradation mechanisms, are approximated at resulting in billions of dollars in damages for pacemaker lead coating alone.[13-16] Greater biostability in polyurethanes will result in fewer failures and reduced patient risk due to decreased degradation product exposure, both of which ultimately lead to improved clinical outcomes.[1,9]

Previous work with aliphatic, thermoset polyurethanes possessing shape memory revealed superior hydrolytic stability compared with aromatic polyurethanes.[134] This work indicated that for highly porous systems (densities of 0.01 g/cm^3 or less) in 0.1 M NaOH at 250 days only *ca* 1% of mass has been lost.[134] Unfortunately, these materials were found to have a susceptibility to oxidation due to the presence of tertiary amines, and when exposed to *in vivo* oxidative conditions it is anticipated that complete degradation could occur within one year.[134] While toxic risk from these materials was found to be minimal, further risk reduction could be accomplished through increasing oxidative stability (reducing the rate of

mass loss). To achieve this, several multifunctional alcohol monomers have been examined, notably glycerol as the most successful in increasing biostability.[196] However, these glycerol-based shape memory polymers (SMPs) still were found to degrade oxidatively, indicating that substitution of the amino-alcohols for alternative starting monomers may yield superior biostability.[196] Also, the glycerol monomer was incompatible with HDI without introducing other starting materials limiting its use.[196]

Beginning in the 1980s, it was found that polyurethane materials did not possess sufficient thermal stability.[197-201] Modifications during synthesis could be used to achieve materials with greater thermal stability due to the isocyanate, in the presence of appropriate catalysts, undergoing a cyclization reaction with additional isocyanates to form a six-membered ring structure, an isocynaurate, that has greater thermal stability and imbues the bulk material with more robust mechanical properties.[198-199] While these isocyanurates have been investigated for several applications, including coatings and thermally stable foams, very little work has been pursued in biomedical applications.[200] More recently, these structures have been used as crosslinkers in self-healing, shape memory, and other functional or advanced materials.[201-205]

This cyclic structure is compatible with previously examined starting material, allowing for incorporation into the SMP bulk using established protocols, allowing for production of bulk scale materials for biocompatibility and biostability testing.[27,36-37,43] Here we present the effects of utilizing the isocyanaurate functionality in aliphatic polyurethane SMPs, with the intent of improving biostability, by using tris(2-hydroxyethyl) isocyanurate (Iso) as a starting triol. The SMPs are produced as both porous and non-porous materials,

and thermo-mechanical properties are examined based upon using one of two aliphatic diisocyanates, hexamethylene diisocyanate (HDI) and trimethyl hexamethylene diisocyanate (TMHDI), along with amino alcohols triethanolamine (TEA) and tetrakis (hydroxypropyl) ethylenediamine (HPED) with the Iso (nomenclature is based upon diisocyanate used, amino alcohol used, isocyanurate percentage; i.e HDI TEA Iso 30). It was found that while the more rigid TMHDI reduced toughness, HDI TEA Iso 30 could be used to improve the toughness of both porous and non-porous materials compared with the control SMP (HDI and TEA only). Additionally, the mechanical properties of the non-porous and dry porous SMPs are greater than the controls, but in water the elastic modulus, strain to failure and ultimate tensile strength are similar. Interestingly, while the thermal transitions of the SMP are greatly increased with the addition of the isocyanurate, shape memory is still present at body temperature. Most importantly, the biostability of both porous and non-porous materials is presented using accelerated testing, displaying great improvements over previous compositions, and model compound studies are used to predict the degradation products that will eventually form.

7.2 Methods and Materials

Hexamethylene diisocyanate (98%, HDI, Sigma), isophorone diisocyanate (98%, IPDI, Sigma), triethanolamine (99%, TEA, Sigma), N,N,N',N' tetrakis (hydroxypropyl) ethylenediamine (98%, HPED, Sigma), and tris-(2-hydroxyethyl)-isocyanurate (Sigma) were used without modification. Deuterated dimethyl sulfoxide (d_6-DMSO, 99.99%, Sigma Aldrich), ethanol (97%, Sigma Aldrich), dimethyl formamide (DMF, 99.5%, Sigma), acetone (99.5%, VWR) and isopropyl alcohol (99.5%, Sigma Aldrich) were used as solvents.

Ethyl isocyanate (98%, Sigma Aldrich) was used without purification. Cobalt chloride ($CoCl_2$) and hydrogen peroxide (H_2O_2, 50%, Sigma Aldrich) were used for degradation solutions.

Matrix assisted laser desorption/ionization (MALDI) time of flight mass spectrometry (MS) was used to characterization the prepolymer network.

Fourier transform infrared spectroscopy (FTIR) attenuated total reflectance (ATR) was performed using a Bruker ALPHA infrared spectrometer (Bruker, Billerica, MA); 48 scans per spectra for both background and samples were used. Spectra data was collected in absorption mode with a resolution of 4 cm^{-1}. OPUS software was used to examine spectra, identify peaks, and perform baseline and atmospheric corrections.

Liquid chromatography mass spectrometry (LCMS) was performed using a single quad OrbiTrap (ThermoFisher) with Exactive software and a C_{18} normal phase silica column. The capillary and heater temperatures were set for 50 °C to prevent thermal-induced fragmentation.

Nuclear magnetic resonance (NMR) (^{13}C 125 MHz and ^{1}H 300 MHz) was performed on a Mercury 300 MHz spectrometer operating in the Fourier transform mode with d_6-DMSO as the solvent.

Iso (15.78 g, 0.060 mol) was added at room temperature toin a flask containing DMF (6 mL) and acetone (15 mL). HDI (4.2 g, 0.025 mol) was then added dropwise over the course of 10 minutes while stirring. The flask was then heated with stirring to 180°C over the course of 1 hour and held for another hour before being allowed to cool to room temperature. The clear, viscous polymer product (Iso prepolymer) was then characterized

and used in subsequent syntheses. ^{1}HNMR (d_6-DMSO): 4.38 (2H, d, $NCH_2C\mathbf{H_2}OCO$), 4.05 (2H, d, $NC\mathbf{H_2}CH_2OCO$), 4.04 (2H, d $HOCH_2C\mathbf{H_2}N$), 3.51 (2H, d, $HOC\mathbf{H_2}CH2N$), 3.21 (2H, d, $OCONHC\mathbf{H_2}CH_2CH_2$), 1.66 (2H, d, $OCONHCH_2C\mathbf{H_2}CH_2$) 1.21 (2H, d, $OCONHCH_2CH_2C\mathbf{H_2}$); ^{13}C NMR ($d_6$-DMSO): 157.18, 150.13, 61.38, 58.75, 46.47, 42.98, 37.31, 36.40, 26.27; M_n= 2490 g/mol, PDI (2.05).

Films were produced by reacting stoichiometric amounts of alcohols and isocyanates (105:100 NCO:OH) in solvent. Iso prepolymer (7.649 g, 3.07 mmol, 30% alcohols) and TEA (7.129 g, 47.85 mmol, 70% alcohols) were dissolved in DMF, followed by the addition of HDI (17.22 g, 102.44 mmol, 100% isocyanates). The solution was mixed and cast into films. This protocol was repeated for films containing TMHDI and HPED.

SMP porous scaffolds were synthesized using a traditional two-step process for porous scaffolds. Iso prepolymer (4.208 g, 1.69 mmol) was dissolved in 6 mL DMF, and TEA (3.922 g, 26.32 mmol) was added. HDI (27.07 g, 161.04 mmol) was added over 2 minutes and mixed for 5 minutes until the solution (premix) turned clear. The premix was heated to 50°C and held isothermally under vacuum for 48 hours.

An alcohol premix was then synthesized. The control samples substituted HPED for the Iso prepolymer. Iso prepolymer (2.186 g, 0.88 mmol, 30% Iso), TEA (2.038 g, 13.68 mmol), water (1.081, 59.99 mmol), surfactant DC 5943 (2.8 g), tin catalyst (0.3.g) and amine catalyst (0.75 g) were mixed for 2 minutes and added to the isocyanate premix with a low boiling point blowing agent. The mixture was immediately placed in a 90 °C oven and held for 20 minutes, with the primary foam blowing occurring within the initial 5 minutes. This protocol was followed for varied ratios of TEA and Iso prepolymer (30%, 20%, 10%, and

control compositions were investigated). The SMPs were then cut and washed. The cleaning process consisted of alternating washes in RO H_2O and EtOH, at 50 °C with sonication for 30 minutes, two cycles of each. The SMPs were dried for three days at 50 °C under vacuum (30 in Hg) and stored in a sealed box with dessicant. HDI TEA 30 Iso FTIR: 3321, 2926, 2853, 1688, 1638, 1538, 1457, 1362, 1292, 1182, 1135, 1035 cm^{-1}. The control samples substituted HPED for the Iso.

Gel fraction was determined for selected compositions (n=3). Samples (*ca* 0.10 mg) were immersed in 30 mL of ethanol and heated to 50°C for 2 days. The samples were then removed, blotted dry, and placed in a vacuum oven at 50 °C (30 in Hg) for 2 days to remove any solvent before being weighed. Density was determined from porous SMP cubes (1 cm^3, n=3). Porous SMP samples were removed from vacuum at room temperature, and stored in individual open containers at ambient conditions overnight. Sample mass was taken periodically.

Dynamic mechanical analysis (DMA) of cylindrical samples (6 mm diameter, 5 mm length) was used to conduct thermomechanical analysis using a Q800 TA DMA (TA Instruments, New Castle, DE). Dry temperature sweep samples were equilibrated at 0°C for fifteen minutes and then ramped to 200 °C (films), 90 °C (dry foams), and 70 °C (wet foams) at a rate of 2 °C/min. The storage modulus (E') and the loss modulus (E") were used to determine the peak tan δ (E'/E"), with the maximum value recorded as the T_g.

Differential scanning calorimetry (DSC) was also used to measure both wet and dry T_g using a Q-200 DSC (TA Instruments, Inc., New Castle, DE). Samples of *ca* 5.0 mg ± 1.0 mg were sealed in TZero aluminum pans and placed in the heating cell. The test profile was

as follows: equilibration at -40 °C, heating to 180 °C at 10 °C/min, cooling 10 °C/min to -40 °C and holding for 5 minutes, and a final heating to 180 °C at 10 °C/min. The half-height transition of the final heating cycle was the reported T_g. Wet samples were weighed and sealed in the same manner, and were then heated from -40 °C to 120 °C.

Shape recovery of cylindrical foam samples (6 mm diameter, 10 mm length, six samples per series) crimped over a wire was examined at 37 °C in RO water to determine the volume recovery behavior (strain recovery). Samples were crimped to a minimal diameter (*ca* 1.0 mm using a SC150-42 Stent Crimper (Machine Solutions, Flagstaff, AZ). To crimp, samples were equilibrated at 100 °C for ten minutes and then radially compressed and cooled to room temperature. Samples relaxed for 12 hours in a sealed box with desiccant and were tested over the course of 20 minutes. Image J (NIH, Bethesda, MD) was used for analysis of the change in diameters over time.

Foam cell structure was determined by cutting axial and transverse samples that were examined using scanning electron microscopy (SEM). Samples were mounted onto a stage and sputter coated with gold using a Cressington Sputter Coater (Ted Pella, Inc., Redding, CA) for 60 seconds at 20 mA. Samples were then examined using a Joel NeoScope JCM-5000 SEM (Nikon Instruments Inc., Melville, NY) at 11X magnification and 15 kV under high vacuum.

Mechanical testing of SMP dogbones was performed using tensile testing. An Instron 5965 electromechanical screw driven test frame, equipped with a 500N load cell, was used to test the dogbones at 5 mm/min at room temperature. Both porous and non-porous samples were cut in Type IV D dogbones for testing.

Green fluorescent protein (GFP)-expressing fibroblasts (NIH3T3/GFP, Cell Biolabs Inc., USA) were expanded then seeded onto control (unmodified) and degraded films at a density of 20,000 cells/film in normal growth media, which contained high glucose Dulbecco's Modified Eagle Medium (DMEM, GE Biosciences, USA) with 10% FBS (Atlanta Biologicals, USA), and 1% penicillin/streptomycin (100 U/µg/mL, Invitrogen, USA). For foam studies, foams were soaked overnight in cell-binding media, which contained normal growth media with 1% dissolved gelatin, prior to cell seeding. After initial cell seeding, films and foams were transferred to new well-plates to ensure cell growth was limited to the polymeric biomaterial.

To investigate cell proliferation, an Alamar Blue assay (Thermo Fisher, USA) was utilized per the manufacturer's instructions to calculate percent reduction of resazurin (blue) to resorufin (pink). Proliferation within foam samples was normalized to accessible surface area via considerations of foam volume and percent porosity. At the respective time points (Day 0, Day 1, Day 3, and Day 7), cell morphology was evaluated using fluorescence microscopy with an excitation of 488 nm (Nikon Ti-U Inverted Microscope, USA); at Day 0, cells were allowed to adhere for three hours prior to imaging. Representative images were selected over the course of imaging three replicates for each film or foam.

For analysis of degradation rates, cleaned samples were completely immersed in respective solutions of 3% H_2O_2 (real time oxidation) and 20% H_2O_2 with 0.1 M $CoCl_2$ (accelerated oxidation), both stored at 37 °C. Sample solutions were changed every 3 days to ensure a relatively stable ion concentration, and once per week samples were removed,

cleaned in EtOH, and dried in at 50 °C under vacuum (30 in Hg), after which sample mass was recorded and samples returned to fresh solution.

Model compounds were dissolved in 50% H_2O_2 and placed in a 37°C oven for five weeks, with samples withdrawn for analysis on a weekly basis; peroxide was refreshed at the same time. Hydrolytic samples were added to 2 M NaOH and incubated for the same time. Samples were diluted 100-fold in a 50% methanol (49.95% water, 0.05% formic acid) solution, and injected into the LCMS column. The injection volume was 10 µL, and the flow gradient was varied from 0% acetonitrile to 95% acetonitrile over a 3-minute gradient. Exactive software (ThermoFischer) was used for analysis of the chromatography scan and the peaks.

7.3 Results and Discussion

Films displayed distinctly increased mechanical properties with the incorporation of the Iso compared with the control group consisting on only HDI and TEA monomers. While the T_g of the control was found at *ca* 1.3 °C (**Table 7.1, Figure 7.1**), the addition of the Iso served to increase the T_g by nearly 80 °C. Furthermore, the addition of HPED versus TEA increased the thermo-mechanical properties, as did using the methyl-containing TMHDI rather than the HDI.

Table 7.1. T_g determined by DMA and maximum complex modulus value.

Species	Tan δ (°C)	E*max (MPa)
Control (HDI TEA)	1.3 ± 2.1	9.2
HDI TEA Iso	81.4 ± 3.9	1103.1
HDI HPED Iso	86.8 ± 2.1	1036.2
TM TEA Iso	104.5 ± 0.8	2075.6
TM HPED Iso	125.2 ± 1.0	2786.1

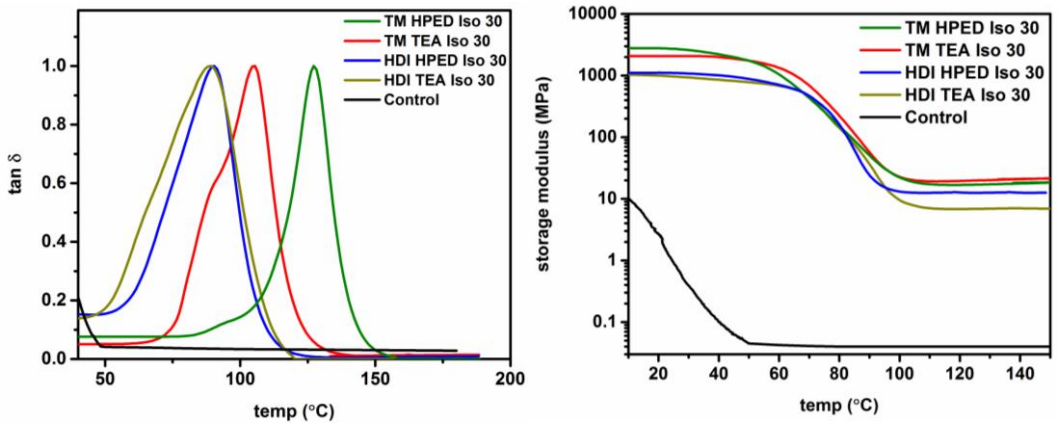

Figure 7.1. **Thermomechanical properties of Iso films, displaying tan δ vs temp (left) and E' (storage moduli) vs temp (right).**

Tensile testing at room temperature further confirmed the mechanical behavior from DMA testing (**Figure 7.2**). The inclusion of the Iso greatly improved the elastic modulus and ultimate strength, but at the cost of the strain to failure and toughness (**Table 7.2**). The exception to this is for the HDI TEA Iso composition. This also indicates that further increasing the Iso concentration in the SMP may reduce mechanical properties even more.

Results of the cellular compatibility study confirm that the TEA-containing films is a more compatible surface compared with the HPED-containing films, and that the presence of the Iso does not alter biocompatibility (**Figure 7.3**).

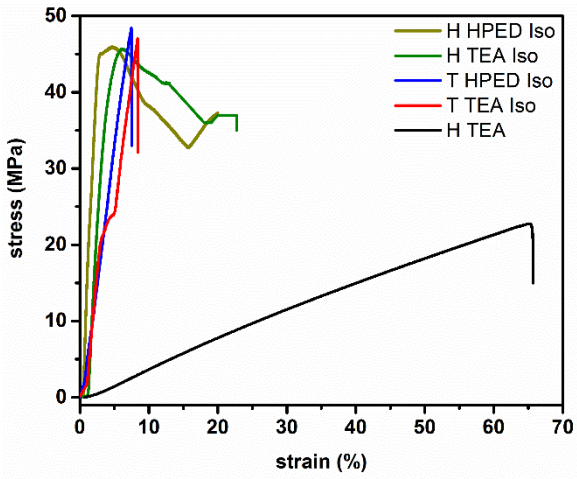

Figure 7.2. Stress-strain behavior of non-porous SMPs, comparing the role of diisocyanate, amino alcohol monomers, and isocyanurate triol on mechanical properties under ambient conditions.

Table 7.2. Mechanical properties of SMP films at ambient conditions, incorporating isocyanurates and varied diisocyanate and amino alcohol monomer units.

Species	Elastic Modulus (MPa)	Strain to Failure (%)	Ultimate Strength (MPa)	Toughness (J/m^3)
Control (HDI TEA)	8.99 ± 1.10	65.7 ± 25.1%	4.54 ± 1.22	792.18
HDI TEA Iso	502.48 ± 22.7	22.7 ± 1.4 %	45.67 ± 0.74	815.35
HDI HPED Iso	671.30 ± 2.38	20.7 ± 4.2 %	45.97 ± 3.61	724.04
TM TEA Iso	826.24 ± 153.8	16.4 ± 4.9 %	47.02 ± 0.78	191.42
TM HPED Iso	889.92 ± 92.2	7.5 ± 1.9 %	48.44 ± 6.67	178.33

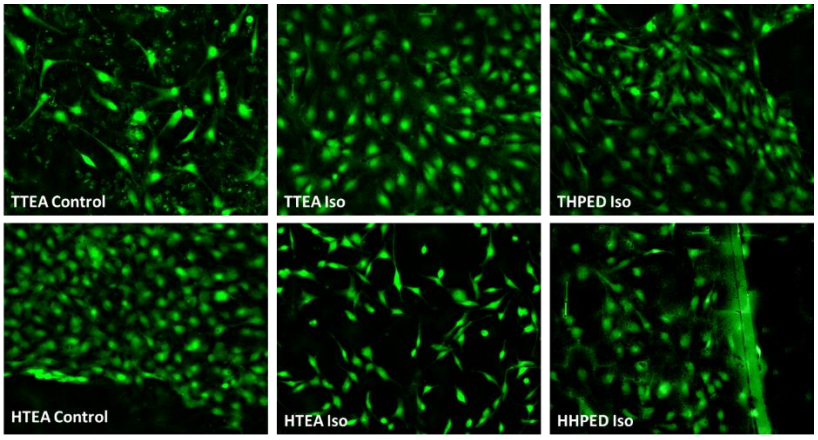

Figure 7.3. Fluorescent 3T3 fibroblasts seeded on films at 7 days incubation.

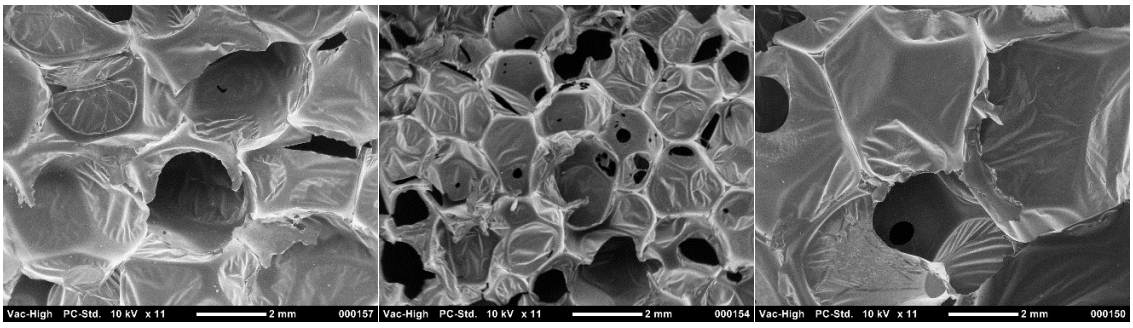

Figure 7.4. SEM images of 10% (left), 20% (middle) and 30% (right) Iso SMPs.

While the use of solvent for foam blowing of porous scaffolds is not common, the presented SMPs obviously are not morphologically hindered by this method (**Figure 7.4**). Pore sizes are shown to vary, with an average diameter of 1.1 mm ± 0.4 mm. The variation in pore sizes do not appear to be due to composition, but rather with premix viscosity and the mixing during synthesis.

As expected from previous work with porous SMPs, these crosslinked polymers may be produced with ultra-low density and a high gel fraction. With sufficient presence of the isocyanurate, the T_g is also high enough to be clinically relevant when dry (greater than room temperature), but will easily plasticize and undergo shape recovery in water (**Table 7.3**). HDI TEA Iso 30 porous samples examined using tensile testing compared with the control SMPs in both ambient and wet, 37 °C conditions. While there were significant mechanical differences when the samples were dry, upon exposure to moisture both series

of SMPs possessed similar elastic moduli (0.05 MPa), strain to failure (*ca* 60%), and ultimate strength (0.02 MPa). The Iso series displayed slightly improved toughness as well (**Table 7.4**).

Table 7.3. Physical and thermal properties of porous Iso SMPs (HDI TEA Iso).

Composition	Gel fraction (%)	Density (g/cc)	Wet DSC (°C)	Dry DSC (°C)
Control	98.1 ±0.02	0.022 ± 0.001	-5.0	55.3
10% Iso	98.0 ±0.04	0.032 ± 0.002	-1.2	34.6
20% Iso	96.4 ±0.01	0.025 ± 0.003	-2.1	37.2
30% Iso	97.5 ±0.04	0.032 ± 0.004	-1.1	57.6

Table 7.4. Mechanical properties of control and HDI TEA Iso 30 porous SMPs at ambient conditions and submerged in 37°C water.

Species	Elastic Modulus (MPa)	Strain to Failure (%)	Ultimate Strength (MPa)	Toughness (J/m^3)
Control Dry	0.04 ± 0.01	130.0 ± 13.1	0.05 ± 0.01	32.5
Iso 30	1.12 ± 0.25	39.4 ± 11.4	0.19 ± 0.06	41.2
Control Wet	0.05 ± 0.01	64.7 ± 12.4	0.02 ± 0.01	5.0
Iso 30	0.05 ± 0.04	57.6 ± 19.4	0.02 ± 0.00	5.2

Despite the changes in dry mechanical properties, the Iso-SMPs possessed full strain recovery and strain fixity (**Figure 7.5**). However, the presence of the isocyanurate also

causes distinct uptake in water, determined both through a change in mass and a brief examination of mechanical properties using samples that were allowed to equilibrate with the room's conditions over the course of hours. The SMPs displayed increased masses by *ca* 3% over the course of hours, and mechanical properties qualitatively changed within 2 hours (less than a full standard deviation tested over the course of this experiment) (**Figure 7.6**).

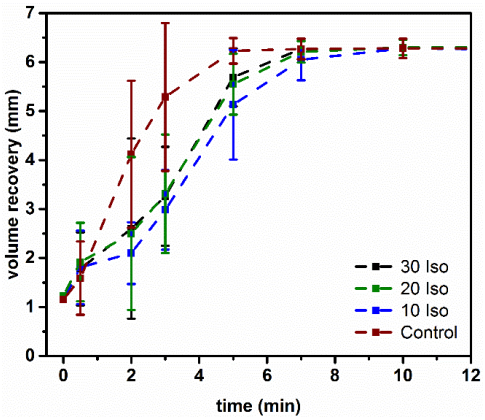

Figure 7.5. Shape recovery behavior of porous SMPs.

Degradation testing using gravimetric analysis indicates that while the control SMPs will undergo rapid oxidative mass loss, depending on the porosity of the SMP, within days or weeks. With the addition of the isocyanurate, oxidative stability is greatly increased in both films and porous SMPs (**Figure 7.7**). At day 110, films possessed *ca* 70% of the original

mass (HDI TEA Iso 30) or up to 90% (TM HPED Iso 30). For the porous SMPs (HDI TEA Iso composition), while the control samples had undergone total mass loss by 15 days, the Iso series retained greater than 90% mass loss at this point. Only after did any significant mass loss begin to occur.

Model compound studies were used to propose the mechanisms of degradation, and to predict if any toxic by- products would be produced. Hydrolytic degradation studies using model compounds indicates that the most likely route to polymer fragmentation is due to the urethane (carbamate) hydrolysis rather than a ring opening of the isocyanurate, determined by MS (**Figure 7.8**). While some ring opening product was obtained, the primary route of degradation will be cleavage of the urethane to produce a primary amine and an alcohol.

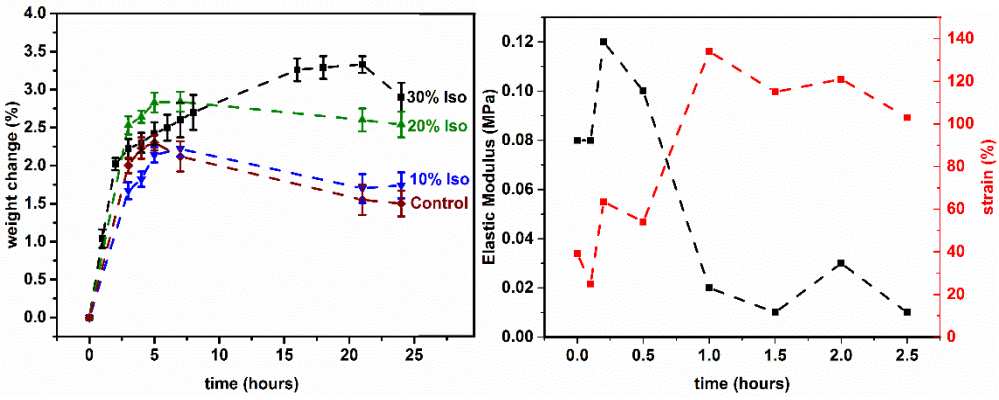

Figure 7.6. (Left) Water uptake studies is gravimetric analysis and (right) plots of elastic modulus and strain to failure for 30 Iso SMPs allowed to equilibrate with the room over the course of 2.5 hrs (n=2 at each time point for tensile testing).

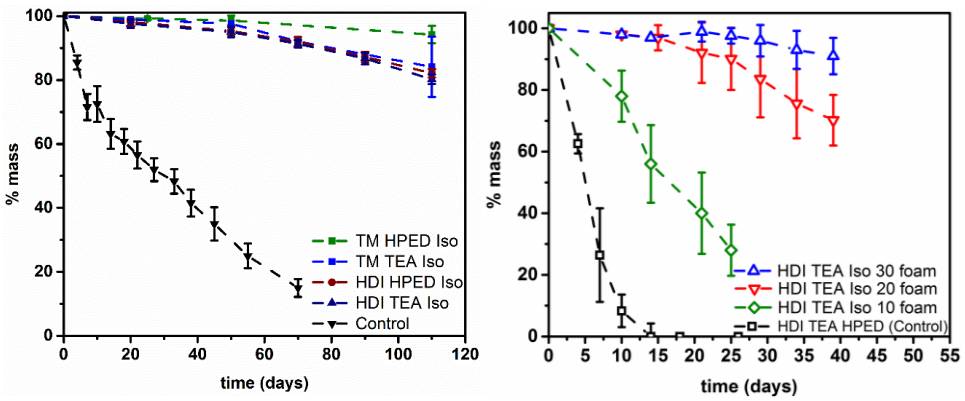

Figure 7.7. Oxidative degradation of non-porous SMP containing isocyanurate (left) and of porous SMPs (HDI TEA Iso) containing (right). Samples were degraded in 20% H_2O_2 catalyzed by 0.1 M $CoCl_2$ at 37°C.

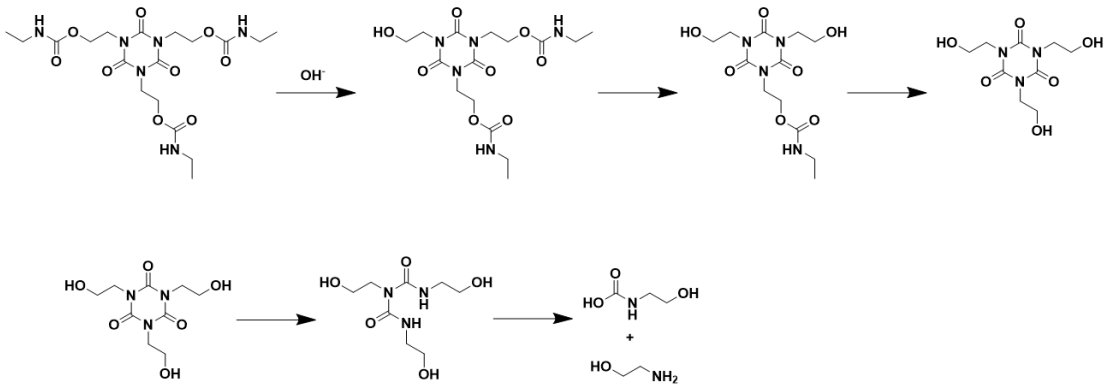

Figure 7.8. Proposed main hydrolysis steps for isocyanurate-urethane linkages as determined using model compound studies and MS, determined from model compounds in 2M NaOH at 37°C.

Oxidatively, the SMPs are stable compared with previous compositions, but degradation may occur in the bulk SMP due to the continued presence of the tertiary amine crosslinkers. The isocyanurate model compound may undergo fragmentation to produce disubstituted isocyanurates as a result of oxidative degradation (**Figure 7.10**).

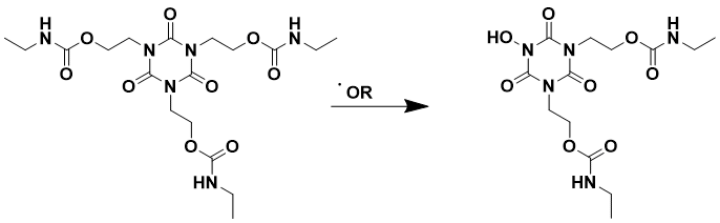

Figure 7.9. Proposed main oxidative step for isocyanurate-urethane linkages as determined using model compound studies and MS over 5 weeks in 50% H_2O_2 at 37°C.

The hydrolysis of isocyanurates has been reported for disubstituted structures resulting in the formation of linear biuret structures.[206-207] The model compound study shows degradation occurring over the course of weeks, in conditions that extremely accelerated compared with physiological environments, as demonstrated by the bulk degradation studies. Previous work with the degradation of polyurethane foams in non-physiological conditions was the source of regulatory discussion, substantial research, and the recalling of many implanted devices; these studies inaccurately claimed that carcinogenic byproducts would form from the polyurethane degradation *in vivo*.[1,5-8,16-17] In this case, the model studies

are not meant to demonstrate the rates of formation of toxic products, but rather to examine possible hydrolysis pathways. For the Iso-containing SMPs, the pathway to degradation is still likely oxidative, as the primary hydrolysis degradation pathway is through carbamate hydrolysis. Previous studies of aliphatic carbamates have indicated that there is hydrolytic stability in 0.1 M NaOH out to at least 250 days (1% mass loss of the bulk material in this time); the presented experiment utilized 2 M NaOH, with carbamate hydrolysis still appearing to be the favored degradation pathway.[135] The oxidative pathway for these SMPs is again due to the amino alcohols used as starting materials.

In the control films, total mass loss in accelerated oxidative solution occurs by *ca* 40 days. In the TM HPED Iso 30 (30% isocyanurate and 70% HPED), *ca* 95% of the original mass is retained at this point. At 110 days in accelerated oxidative solution, TM HPED Iso 30 has lost only 5.8% of the original mass. HDI TEA Iso 30, 82.1% of the original non-porous films' mass is retained at 110 days. In porous SMPs, the controls are completely degraded within approximate 25 days; HDI TEA Iso 30 97.7% of the original mass at the same time point. It appears that tuning the rate of oxidation can be achieved through incorporation of varying concentrations of the Iso prepolymer to achieve higher oxidative stability compared with the control SMPs. This is useful for ultimately allowing native tissue to replace the SMP, but the longer degradation times ensure less toxic risk associated with the released degradation products.

Oxidatively, the degradation that is demonstrated for these materials is due to the amino alcohol TEA used in synthesis. It is apparent that the presence of the Iso group increases oxidative stability. The end groups that will preferentially form are most likely

primary amines, aldehydes and carboxylic acids as a result of fragmentation of the tertiary amine to a secondary amine and corresponding aldehyde, followed by further fragmentation to a primary amine. The oxidation of the Iso structure is unlikely, but if it occurs may yield a disubstituted isocyanurate. This ring structure may undergo hydrolysis in the presence of hydroxyl ions due to the possible resonance structures between the surrounding carbonyls and the amine (equilibrium results in the partially charged species and water), possibly resulting in a 1,6 ring opening to form disubstituted biurets.[206]

Both degradation schemes, as well as accelerated degradation studies, indicate that the isocyanurate ring is not likely to undergo fragmentation in the *in vivo* environment. In studies of similar molecules, in this case small molecule isocyanurates with substituted end groups, clearance occurred via the renal system without change to the ring structure in similar concentrations for what may be produced from oxidative degradation of the SMPs.[208-210] Reports of toxic effects are associated with end groups rather than the cyclic structure (epoxides from triglycidyl isocyanurate, for example).[209-210]

Based upon the degradation profiles of the control SMPs, it appears that *ca* 100% mass loss will occur within 1.5 years; 30 Iso will have lost *ca* 2.5%. For decreasing the degradation cytotoxicity risk associated with the degradation, the 30 Iso is 26 times less (0.0001 %/day) than the control (0.23 %/day). While these SMPs are not as biostable as non-porous polyurethanes used in alternative applications, the use of the isocyanurate does provide a means to improve biostability for these porous materials.

7.4 Conclusions

While the oxidative degradation of porous SMPs is rapid in oxidative environments, reduction in the mass loss may be achieved through the incorporation of isocyanurate triols into the SMP. With some SMP systems, this will increase mechanical toughness and other properties without sacrificing shape memory and biocompatibility, both of which are necessary for translating a material system out of the lab and into the clinic. It found that these new SMPs do possess reduced rates of oxidative degradation, and it is predicted that they will possess high hydrolytic stability, as well, due to the main path of hydrolytic degradation being hydrolysis of the urethane bonds. Overall, this seems like a valid method for pursuing more biostable SMPs for vascular devices.

Predictions of real-time degradation indicate that inclusion of the Iso prepolymer results in greater overall biostability compared with the previously examined methods, including antioxidants and glycerol. The HDI TEA Iso 30 (**Figure 7.10**) is predicted to be completely degraded after *ca* 7520 days, or 20 years. While it is not possible to achieve true biostability with polyurethanes, the inclusion of isocyanurates does allow for significant reduction in the rate of oxidative mass loss, and is useful for producing SMPs with greater biostability compared with previous iterations, including those containing glycerol and antioxidants.

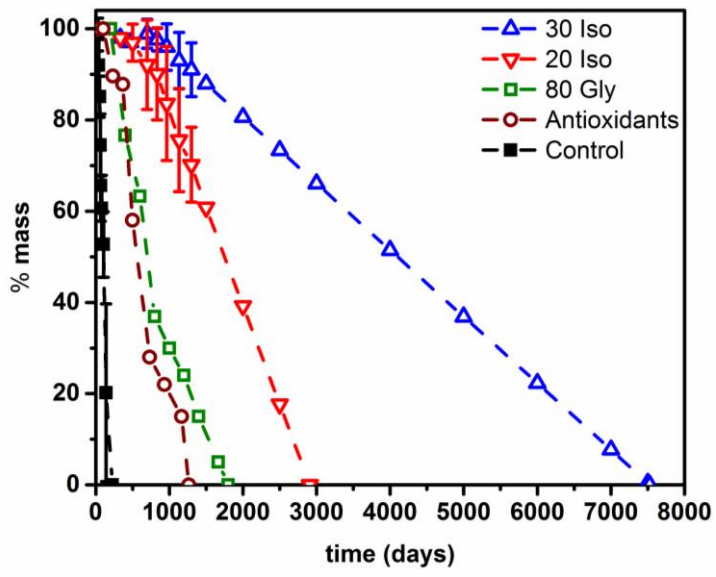

Figure 7.10. **Mass loss profiles of SMPs in real time oxidative solution (2% H_2O_2), predicted from real time data and accelerated testing (20% H_2O_2 in 0.1 M $CoCl_2$).**

CHAPTER VIII

CONCLUSIONS

8.1 Summary

Shape memory polymers (SMPs) synthesized from aliphatic, symmetric amino alcohols and diisocyanate monomers were characterized for their degradation behavior. The SMPs and the starting materials were tested through examination of the bulk and model compounds, in order to determine that the mechanism of degradation was a result of tertiary amine oxidation. The degraded SMPs and the degradation mechanism was then used to examine the cytocompatibility over the course of implantation. Degradation products were synthesized and tested simultaneously to the degraded bulk SMPs examine the toxic risk to patients over the lifespan of the SMP. Results indicated that these SMPs may pose minimal risk to patients, and that translation of this technology into clinical devices is possible.

Antioxidants were examined as alternative methods for controlling oxidation. Results varied due to reactions with the isocyanates during synthesis or poor compatibility with the SMP bulk that resulted in removal of the antioxidants during polymer cleaning. Thermo-mechanical properties were found to be widely variable based upon this, as well as shape memory properties. When the antioxidants were loaded into synthesized polyurethane microparticles and added to the SMPs, the thermo-mechanical property changes found when using small molecule antioxidants were minimized; mechanical properties and shape recovery kinetics were improved for the examined antioxidants. While SMPs containing Piper as a small molecule were not improved upon through the use of microparticles, the use of BHT and Methyl antioxidants did improve oxidative stability. These methods are

predicted to expand the life-span of these SMP compositions from 500 days out to nearly 900 days (*ca* 1.5 years to *ca* 2.5 years), and may also be useful for expanding the functionalities of the SMPs.

Glycerol and isocyanurate triol were examined to improve oxidative stability, with both monomers decreasing the rate of oxidative mass loss without sacrificing shape memory or thermal properties. While the glycerol was used primarily with the more hydrophobic SMPs based upon trimethyl hexamethylene diisocyanate (TMHDI), isocyanurate triol was found to be compatible with the hexamethylene diisocyante (HDI)-based SMPs and demonstrated greater oxidative stability than the glycerol SMPs, despite their greater T_gs. Glycerol is predicted to further extend the SMP life-span to *ca* 5 years, while sufficient concentration of isocyanurate may yield SMPs that degrade in 20 years.

The amino-alcohol based SMPs are promising candidates for translation into the clinic. While the cytocompatibility of HDI-based SMPs has been confirmed, studies examining the use of alternative diisocyanates, such as TMHDI, are required for the translation of other SMP compositions into medical devices. These studies would also have bearing on the alterative compositions that were proposed here, including the use of glycerol, isocyanurate triol, antioxidants, and microparticles.

For further tuning oxidative stability, alternative antioxidants, such as larger molecules or molecules that degrade into antioxidant products, could be examined. For increasing the degradation rates, the use of HPED-based esters, as well as other renewable monomers, could be examined to further tune the increased oxidation rates for degradable SMPs. Developing various starting monomer and macromers for these applications will

require gaining an understanding of the limitations of the foaming process, as well as how to improve the compatibility of some starting materials with the currently utilized reagents.

REFERENCES

1. DK Dempsey, C Carranza, CP Chawla, P Gray, JH Eoh, S Cereceres, EM Cosgriff-Hernandez. Comparative analysis of in vitro oxidative degradation of poly(carbonate urethanes) for biostability screening. *J Biomed Mater Res A*, **2014**, 102A; 3649-3665. DOI:10.1002/jbm.a.35037
2. RS Smith, Z Zhang, M Bouchard, J Li, HS Lapp, GR Brotske, DL Lucchino, D Weaver, LA Roth, A Coury, L Biggerstaff, S Sukavaneshvar, R Langer, C Loose. Vascular catheters with a nonleaching polysulfobetaine surface modification reduce thrombus formation and microbial attachment. *Sci Trans Med*, **2012**, 153 (4), DOI: 10.1126/scitranslmed.3004120.
3. D Grafahrend, K Heffels, MV Beer, P Gasteier, M Moller, G Boehm, PD Dalton, J Groll. Degradable polyester scaffolds with controlled surface chemistry combining minimal protein adsorption with specific bioactivation, *Nat Mater*, **2011**, 10, 67-73. DOI: 10.1038/nmat2904.
4. JR Martin, MK Gupta, JM Page, F Yu, JR Davidson, SA Guelcher, CL Duvall. A porous tissue engineering scaffold selectively degraded by cell-generated reactive oxygen species. *Biomaterials*, **2014**, 35(12), 3766-3776. DOI:10.1016/j.biomaterials.2014.01.026
5. EM Christenson, JM Anderson, A Hiltner. Biodegradation mechanisms of polyurethane elastomers. *Corr Eng Sci Tech*, **2007**, 42 (4), 312-323. DOI: 10.1179/174327807X238909.

6. JP Santerre, K Woodhouse, G Laroche, RS Labow. Understanding the biodegradation of polyurethanes: from classical implants to tissue engineering materials. *Biomaterials*, **2005**, 26(35), 7457-7470. DOI: 10.1016/j.biomaterials.2005.05.079.
7. EM Christenson, JM Anderson, A Hiltner. Antioxidant inhibition of poly(carbonate urethane) in vivo biodegradation. *J Biomed Mater Res A*, **2006**, 76A, 480-490. DOI:10.1002/jbm.a.30506.
8. D Sarkar, ST Lopina. Oxidative and enzymatic degradations of L-tyrosine based polyurethanes. *Polym Degrad Stab*, **2007**, 92(11), 1994-2004. DOI: 10.1016/j.polymdegradstab.2007.08.003
9. A Padsalgikar, E Cosgriff-Hernandez, G Gallagher, T Touchet, C Iacob, L Mellin, A Norlin0Weissenrieder, J Runt. Limitations of predicting *in vivo* biostability of multiphase polyurethane elastomers using temperature-accelerated degradation testing. *J Biomed Mater Res B Appl Biomater*, **2015**, 103 (1), 159-168. DOI: 10.1002/jbm.b.33161.
10. KA Chaffin, X Chen, L McNamara, FS Bates, MA Hillmyer. Polyether urethane hydrolytic stability after exposure to deoxygenated water. *Macromol*, **2014**, 47 (15), 5220-5226. DOI: 10.1021/ma500904d.
11. KA Chaffin, AJ Buckalew, JL Schley, X Chen, M Jolly, JA Alkatou, JP Miller, DJ Untereker, MA Hillmyer, FS Bates. Influence of water on the structure and properties of PDMS-containing multiblock polyurethanes. *Macromol*, **2012**, 45 (22), 9110-9120. DOI: 10.1021/ma301965y.

12. C Scarpa, GF Borso, V Vindigni, F Bassetto. Polyurethane foam-covered breast-implants: a justified choice? *Euro Rev Med Pharm Sci*, **2015**, 19, 1600-1606.
13. United States General Accounting Office. Medical Technology, For somc cardiac pacemaker leads, the public health risks are still high. (September 23, 1992). http://www.gao.gov/assets/220/216942.pdf
14. CI Nichols, JG Vose, S Mittal. Incidence and costs related to lead damage occurring within the first year after a cardiac implantable electronic device replacement procedure. *J Am Heart Assoc.* **2016**, 5, DOI: 10.1161/JAHA.115.002813.
15. RG Hauser, RH Abdelhadi, DM McGriff, LK Retel. Failure of a novel silicone-polyurethane copolymer (Optim^{TM}) to prevent implantable cardioverter-defibrillator lead insulation abrasions. *Europace*, **2013**, 15, 278-283. DOI: 10.1093/europace.eus245.
16. L X Liu, L Zhou, F Pan, Y Gao, X Yuan, D Fan. Comparison of the postoperative incidence rate of capsular contracture among different breast implants: a cumulative meta-analysis. *PLOS One*, **2015**. DOI:10.1371/journal.pone.0116071
17. N Castel, Polyurethane-coated breast implants revisited: a 30 year follow up, Arch Plast Surg, **2015**, 42(2), 186-193. DOI: 10.5999/aps2015.42.2.186.
18. C Batich, J Williams, R King. Toxic hydrolysis product from a biodegradable foam implant. *J Biomed Mater Res A*, **1989**, 23 (S14), 311-319. DOI: 10.1002/jbm.820231406.
19. KG Brand. Foam-covered mammary implants. *Clinc Plast Surg*, **1984**, 73, 498.

20. JA De la Pena-Salcedo, MA Soto-Mirada, JF Lopez Salero. Back to the future: a 15-year experience with polyurethane foam-covered breast implants using the partial-subfascial technique. *Aesth Plast Surg*, **2012**, 36, 331-338.
21. SY Pan, E Lavigne, EJ Holowaty, PJ Villeneuve, L Xie, H Morrison, J Brisson. Canadian incidence in a cohort: extended follow-up of cancer incidence. *Int J Cancer*, **2012**, 131, E1148-1157.
22. A Lattuati-Derieux, S Thao-Heu, B Lavedrine. Assessment of the degradation of polyurethane foams after artificial and natural ageing by using pyrolysis-gas chromatography/mass spectrometry and headspace-solid phase microextraction-gas chromatography/mass spectrometry. *J Chromatog A*, **2011**, 1218, 4498-4508. DOI: 10.1016/j.chroma.2011.05.013
23. A Gledhill, A Wake, P Hext, E Leibold, R Shiotsuka. Absorption, distribution, metabolism and excretion of an inhalation dose of ^{14}C 4,4'-methylenediphenyl diisocyanate in the male rat. *Xenobio*, **2008**, 35 (3), 273-292. DOI: 10.1080/00498250500057591.
24. DOI:10.339/jfb3040706
25. MA Hughes, M Carson, MA Collins, AT Jolly, DM Molenaar, W Steffens, GMH Swaen. Does diisocyanate exposure result in neurotoxicity? *Clin Toxicol*, **2014**, 52 (4), 242-257. DOI: 10.3109/15563650.2014.898769.
26. M Cabanlit, D Maitland, T Wilson, S Simons, T Wun, ME Gershwin, J Van der Water. Polyurethane shape-memory polymers demonstrate functional

biocompatibility in vitro. *Macromol Biosci,* **2007**, 7(1), 48-55. DOI:10.1002/mabi.200600177

27. P Singhal, JN Rodriguez, W Small, S Eagleston, J Van der Water, DJ Maitland, TS Wilson. Ultra low density and highly crosslinked biocompatible shape memory polyurethane foams. *J Polym Sci B Polym Phys*, **2012**, 50(10), 724-737. DOI:10.1002/polb.23056.
28. A Lendlein, S Kelch. Shape memory polymers, *Angew Chem Int Ed*, **2002**, 41, 2035-2057.
29. A Lendlein, S Kelch. Shape-memory polymers. *Ange Chemie*, **2002**, 41 (12), 2034-2057. DOI: 10.1002/1521-3773(20020617)41.
30. W Sokolowski, A Metcalfe, S Hayashi, L Yahia, J Raymond. Medical applications of shape memory polymers. *Biomed Mater,* **2007**, 2 (1), 23-27. DOI: 10.1088/1748-6041/2/1/S04.
31. D Zhang, OJ George, KM Petersen, AC Jimenez-Vergara, MS Hahn, MA Grunlan. A bioactive "self-fitting" shape memory polymer scaffold with potential to treat cranio-maxillo facial bone defects. *Acta Biomater*, **2014**, 10 (11), 4597-4605. DOI: 10.1016/j.actbio.2014.07.020.
32. A Metcalfe, AC Desfaits, I Salazkin, L Yahia, WM Sokolowski, J Raymond. Cold hibernated elastic memory foams for endovascular interventions. *Biomater*, **2003**, 24 (3), 491-497. DOI: 10.1016/S0142-9612(02)00362-9.
33. JN Rodriguez, FJ Clubb, TS Wilson, MW Miller, TW Fossum, J Hartman, E Tuzun, P Singhal, DJ Maitland. In vivo response to an implanted shape memory

polyurethane foam in a porcine aneurysm model. *J Biomed Mater Res A*, **2014**, 102 (5), 1231-1242. DOI: 10.1002/jbm.a.34782.

34. J Horn, H Hwang, SL Jessen, BK Keller, MW Miller, E Tuzun, J Hartman, FJ Clubb, DJ Maitland. Comparison of shape memory polymer foam versus bare metal coil treatments in an in vivo porcine sidewall aneurysm model. *J Biomed Mater Res B Appl Biomater*, **2016**, DOI: 10.1002/jbm.b.33725.
35. AC Weems, KT Wacker, JK Carrow, AJ Boyle, DJ Maitland. Shape Memory Polyurethanes with Oxidation-induced Degradation: In vivo and In vitro Correlations for Endovascular Material Applications. *Acta Biomaterialia*, submitted.
36. TS Wilson, JP Bearinger, JL Herberg, JE Marion III, WJ Wright, CL Evans, DJ Maitland. Shape memory polymers based on uniform aliphatic urethane networks. *J Appl Polym Sci*, **2007**, 106(1), 540-551. DOI:10.1002/app.26593.
37. AC Weems, JE Raymond, KT Wacker, TP Gustafson, B Keller, KL Wooley, DJ Maitland. Examination of radio-opacity enhancing additives in shape memory polyurethane foams. *J Appl Polym Sci*, **2015**, 132(23). DOI:10.1002/app.42054.
38. Q Zhao, W Zou, Y Luo, T Xia. Shape memory polymer network with thermally distinct elasticicty and plasticity. *Sci Adv*, **2016**, 2 (1), DOI: 10.1126/sciadv.1501297.
39. AJ Boyle, TL Landsman, MA Wierzbicki, LD Nash, W Hwang, MW Miller, E Tuzun, SM Hasan, DJ Maitland. In vitro and in vivo evaluation of a shape memory polymer foam-over-wire embolization device delivered in saccular aneurysm

models. *J Biomed Mater Res B Appl Biomater*, **2016**, 104 (7), 1407-1415. DOI: 10.1002/jbm.b.33489.

40. AJ Boyle, AC Weems, SM Hasan, LD Nash, MBB Monroe, DJ Maitland. Solvent stimulated actuation of polyurethane-based shape memory polymer foams using dimethyl sulfoxide and ethanol. *Smart Mater Struct*, **2016**, 25 (7), DOI: 10.1088/0964-1726/25/7/04514.
41. A Lendlein, AM Schmidt, R Langer. AB-polymer networks based on oligo(ε-caprolactone) segments showing shape-memory properties. *PNAS*, **2001**, 98 (3), 842-847. DOI: 10.1073/pnas.98.3.842.
42. M Behl, A Lendlein. Shape-memory polymers. *MaterToday*, **2007**, 10(4), 20-28. DOI: 10.1016/S1369-7021(07)70047-0.
43. P Singhal, A Boyle, ML Brooks, S Infanger, S Letts, W Small, DJ Maitland, TS Wilson. Controlling the actuation rate of low-density shape-memory polymer foams in water. *Macromol Chem Phys*, **2012**, 214 (11), 1204-1214. DOI: 10.1002/macp.201200342.
44. K Hearon, MA Wierzbicki, LD Nash, TL Landsman, C Laramy, AT Lonnecker, MC Gibbons, S Ur, KO Cardinal, TS Wilson, KL Wooley, DJ Maitland. A processible shape memory polymer system for biomedical applications. *Adv Health Mater*, **2015**, 4, 1386-1398. DOI: 10.1002/adhm.201500156.
45. P Singhal, W Small, E Cosgriff-Hernandez, DJ Maitland, TS Wilson. Low density biodegradable shape memory polyurethane foams for embolic biomedical

applications. *Acta Biomater*, **2014**, 10 (1), 67-76. DOI: 10.1016/j.actbio.2013.09.027.

46. SJ Tey, WM Huang, WM Sokolowski. Influence of long-term storage in cold hibernation on strain recovery and recovery stress of polyurethane shape memory polymer foam. *Smart Mater Struct*, **2001**, 10, 321-325. DOI: 10.1018/0964-1726/10/2/318.
47. PT Knight, KM Lee, T Chung, PT Mather. PLGA-POSS end-linked networks with tailored degradation and shape memory behavior. *Macromol*, **2009**, 42, 6596-6605. DOI: 10.1021/ma901237h
48. W Guo, H Kang, Y Chen, B Guo, L Zhang. Stronger and faster degradable biobased poly(propylene sebacate) as shape memory polymer by incorporating boehmite nanoplatelets. *ACS Appl Mater Inter*, **2012**, 4, 4006-4014. DOI: 10.1021/am300828u.
49. ED Rodriguez, X Luo, PT Mather. Linear/network poly(ε-caprolactone) blends exhibiting shape memory assisted self-healing (SMASH). *ACS Appl Mater Inter*, **2011**, 3, 152-161. DOI: 10.1021/am101012c.
50. ISO 10993:13. Biological evaluation of medical devices, Pt 13. Identification and quantification of degradation products from polymeric medical devices. **2003**.
51. M Ding, J Li, X Fu, J Zhou, H Tan, Q Gu, Q Fu. Synthesis, degradation, and cytotoxicity of multiblock poly(ε-caprolactone urethane)s containing gemini quaternary ammonium cationic groups. *Biomacromol*, **2009**, 10, 2857-2865. DOI: 10.1021/bm9006826.

52. H Fu, Y Hong, SR Little, WR Wagner. Collagenase-labile polyurethane urea synthesis and processing into hollow fiber membranes. *Biomacromol*, **2014**, 15, 2924-2932. DOI: 10.1021/bm500552f.

53. J Fang, S Ye, J Wang, T Zhao, X Mo, WR Wagner. Thiol click modification of cyclic disulfide containing biodegradable polyurethane urea elastomers. *Biomacromol*, **2015**, 16, 1622-1633. DOI: 10.1021/acs.biomac.5b00192.

54. C Englert, M Hartlieb, P Bellstedt, K Kempe, C Yang, SK Chu, X Ke, JM Garcia, RJ Ono, M Fevre, RJ Wojtecki, US Schubert, YY Yang, JL Hedrick. Enhancing the biocompatibility and biodegradadbility of linear poly(ethylene imine) through controlled oxidation. *Macromol*, **2015**, 48, 7420-7427. DOI: 10.1021/acs.macromol.5b017940.

55. AE Pegg, Toxicity of polyamines and their metabolic products, *Chem Res Tox*, **2013**, 26, 1782-1800. DOI: 10.1021/tx400316s.

56. HN Chia, BM Wu. Recent advances in 3D printing of biomaterials. *J Biolog Eng*, 2005, 9 (4), DOI: 10.1186/s13036-015-0001-4.

57. WT Scott, JM Waechter, DL Rick, AL Mendrala. Adsorption, distribution, metabolism and excretion of intravenously and dermally administered triethanolamine in mice. *Food Chem Toxico,* 2000, 38 (11), 1043-1051. DOI:10.1016/S0278-6915(00)00095-8

58. SS Hermann, L Duedahl-Olesen, T Christensen, PT Olensen, K Granby. Dietary exposure to volatile and non-volatile N-nitrosamines from processed meat products

in Denmark. *Food Chem Toxico,* 2015, 80, 137-143. DOI:10.1016/0165-1218(82)90123-9

59. MN Akhtar, WTA Harrison, M Shahid, *et* al. Synthesis, crystal structure and biological activity of a cobalt (II) complex of N,N,N',N'-tetrakis(2-hydroxypropyl)ethylenediamine. *Trans Metal Chem*, **2016,** 41 (3), 325-330. *DOI*:10.1007/s11243-016-0025-8
60. AM Kirillov, MV Kirillova, LS Shl'pina, PJ Figiel, KR Gruenwald, MFCG da Silva, M Haukka, AJL Pombeiro, GB Shul'pin. Mild oxidative functionalization of alkanes and alcohols catalyzed by new mono- and dicopper (II) aminopolyalcoholates. *J Mol Cata A Chem,* **2011,** 350. DOI: 10.1016/j.molcata.2011.08.028
61. S Lee, SC Yu, YS Lee. Degradable polyurethanes containing poly(butylene succinate) and poly(ethylene glycol). *Poly Degrade Stabl*, **2001,** 72 (1), 81-87.
62. S Li, J Yu, MB Wade, GM Policastro, ML Becker. Radiopaque, iodine functionalized, phenylalanine-based poly(ester urea)s. *Biomacromolecules*, **2015**, 16 (2), 615-624.
63. J Zhou, AP Defante, F Lin, Y Xu, J Yu, Y Gao, E Childers, A Dhinojwala, ML Becker. Adhesion properties of catechol-based biodegradable amino acid-based poly(ester urea) copolymers inspired from mussel proteins. *Biomacromolecules*, **2015**, 16 (1), 266-274.
64. GM Policastro, F Lin, LAS Callahan, A Esterle, M Graham, KS Stakleff, ML Becker. OGP functionalized phenylalanine-based poly(ester urea) for enhancing

osteoinductive potential of human mesenchymal stem cells. *Biomacromolecules*, **2015**, 16 (4), 1358-1371.

65. J Yu, F Lin, ML Becker. Branched amino acid poly(ester ureas) with tunable thermal and water uptake properties. *Macromolecules*, **2015**, 48 (9), 2916-2924.
66. KS Stakleff, F Lin, LAS Callahan, MB Wade, A Esterle, J Miller, M Graham, ML Becker. Resorbable amino acid-based poly(ester ureas) crosslinked with osteogenic growth peptide with enhanced mechanical properties and bioactivity. *Acta Biomaterialia*, **2013**, 9 (2), 5132-5142.
67. A Alteheld, Y Feng, S Kelch, A Lendlein. Biodegradable amorphous copolyester-urethane networks having shape-memory properties. *Angewandte Chemie*, **2005**, 44 (8), 1188-1192.
68. H Matsumoto, Shape memory porperties of electrospun non-woven fabrics prepared from degradable polyesterurethanes containing poly(w-pentadecalactone) hard segments
69. S Lee, SC Yu, YS Lee. Degradable polyurethanes containing poly(butylene succinate) and poly(ethylene glycol). *Poly Degrade Stabl*, **2001,** 72 (1), 81-87.
70. S Hu, C Wan, Y Li. Production and characterization of biopolyols and polyurethane foams from crude glycerol based liquefaction of soybean straw. *Bioresource Technology*, **2012**, 103 (1), 227-233.
71. J Yu, F Lin, P Lin, Y Gao, ML Becker. Phenylalanine-based poly(ester urea): synthesis, characterization, and in vitro degradation. *Macromol*, **2014**, 47 (1), 121-129. DOI: 10.1021/ma401752b

72. EM Christenson, JM Anderson, A Hiltner. Oxidative mechanisms of poly(carbonate urethane) and poly(ether urethane) biodegradation: in vivo and in vitro correlations. *J Biomed Mater Res A*, **2004**, 70 (2), 245-255. DOI: 10.1002/jbm.a.30067

73. A Bistolfi, A Bellare. The relative effects of radiation crosslinking and type of counterface on the wear resistance of ultrahigh-molecular weight polyethylene. *Acta Biomater*, **2011**, 7 (9), 3398-3403. DOI: 10.1016/j.actbio.2011.05.018.

74. P Gijsman, J Hennekens, D Tummers. The mechanim of action of hindered amine light stabilizers. *Polym Degrad Stabl*, **1993**, 29, 225-233. DOI:

75. DR Bauer, JL Gerlock, DJ Mielewski. Photo-degradation and photo-stabilization in organic coatings containing a hindered amine light stabilizer: part VI-esr measurements of nitroxide kinetics and mechanism of stabilization.*Polym Degrad Stabl*, **1990**, 28 (2), 115-129. DOI: 10.1016/0141-3910(90)90001-N.

76. H Yamashita, Y Ohkatsu. A new antagonism between hindered amine light stabilizers and acidic compounds including phenolic antioxidant. *Polym Degrad Stabl*, **2003**, 80 (3), 421-4262. DOI: 10.1016/S0141-3910(02)00373-7.

77. P Gijsman, HJ Smelt, D Schumann. Hindered amine light stabilizers: an alternative for radiation crosslinked UHMwPE implants. *Biomater*, **2010**, 31(26), 6685-6691. DOI: 10.1016/j.biomaterials.2010.05.053.

78. JE Weaver, CL Stabler. Antioxidant cerium oxide nanoparticle hydrogels for cellular encapsulation. *Acta Biomater*, **2014**, 16 (1), 136-144. DOI: 10.1016/j.actbio.2015.01.017.

79. S Beibmann, M Reisinger, K Grabmayer, G Wallner, D Nitsche, W Buchberger. Analytical evaluation of the performance of stabilization systems for polyolefinic materials. Pt 1: interactions between hindered amine light stabilizers and phenolic antioxidants. *Polym Degrad Stabl*. **2014**, 110, 498-508. DOI: 10.1016/j.polymdegradstab.2014.09.020.
80. V Taresco, F Crisante, I Fancolini, A Martinelli, L D'Ilario, L Ricci-Vitiani, M Buccarelli, L Pietrelli, A Piozzi. Antimicrobial and antioxidant amphiphilic random copolymers to address medical device-centered infections. *Acta Biomater*, **2015**, 22, 131-140. DOI: 10.1016/j.actbio.2015.04.023.
81. I Bauer, WD Habicher, S Korner, S Al-Malaika. Antioxidant interaction between organic phosphites and hindered amine light stabilizers: effects during photoxidation of polypropylene-II. *Polym Degrad Stabl*, **1997**, 55 (2), 217-224.
82. H Yamashita, Y Ohkatsu. A new antagonism between hindered amine light stabilizers and acidic compounds including phenolic antioxidant. *Polym Degrad Stabl*, **2003**, 80 (3), 421-426. DOI: 10.1016/S0141-3910(02)00373-7.
83. HG Wahl, A Hoffmann, H Haring, HM Liebich. Identification of plasticizers in medical products by a combined direct thermodesorption-cooled injection system and gas chromatography-mass spectrometry. *J Chrom A*, **1999**, 847 (1-2), 1-7. DOI: 10.1016/S0021-9673(99)00138-7.
84. RS Lanigan, TA Yamarik. Final report on the safety assessment of BHT. *Intern J Tox*, **2002**, 21, 19-94. DOI: 10.1080/109158102990096513.

85. I Bjorkhem, A Henriksson-Freyschuss, P Breuer, U Diczfalusy, L Berglund, P Henriksson. The antioxidant butylated hydroxytoluene protects against atherosclerosis. *Arteriosclerosis, Thrmobosis, and Vascular Biology*, **1991**, 11, 15-22. DOI: 10.1161/01.ATV.11.1.15.

86. AL Branen. Toxicology and biochemistry of butylated hydroxyanisol and butylated hydroxytoluene. *J Amer Oil Chem Soc*, **1979**, 52, 59-65. DOI: 10.1007/BF02901825.

87. S Hsu, C Tang, H Tseng. Biostability and biocompatibility of poly(ester urethane) gold nanocomposites. *Acta Biomater*, **2008**, 4(6), 1797-1808. DOI: 10.1016/j/actbio.2008.06.015.

88. PP Wattamwar, Y Mo, R Wan, R Palli, Q Zhang, TD Dziubla. Antioxidant activity of degradable polymer poly(trolox ester) to suppress oxidative stress injury in the cells. *Adv Func Mater*, **2010**, 20 (1), 147-154. DOI: 10.1002/adfm.200900839.

89. PP Wattamwar, D Biswal, DB Cochran, AC Lyvers, RE Eitel, KW Anderson, JZ Hilt, TD Dziubla. Synthesis and characterization of poly(antioxidant B-amino esters) for controlled release of polyphenolic antioxidants. *Acta Biomater*, **2012**, 8(7), 2529-2537. DOI: 10.1016/j.actbio.2012.03.022.

90. UG Spizzirri, F Iemma, F Puoci, G Cirillo, M Curcio, OI Parisi, N Picci. Synthesis of antioxidant polymers by grafting of gallic acid and catechin on gelatin. *Biomacro*, **2009**, 10(7), 1923-1930. DOI: 10.1021/bm900325t.

91. F Iemma, F Puoci, M Curcio, OI Parisi, G Cirillo, UG SPizzirri, N Picci. Ferulic acid as a comonomer in the synthesis of a novel polymeric chain with biological properties. *J Appl Polym Sci*, **2010**, 115 (2), 784-789. DOI: 10.1002/app.31067.

92. MA Ouimet, J Griffin, AL Carbone-Howell, WH Wu, ND Stebbins, R Di, KE Uhrich. Biodegradable ferulic acid-containing poly(anhydride-ester): degradation products with controlled release and sustained antioxidant activity. *Biomacro*, **2013**, 14 (3), 854-861. DOI: 10.1021/bm3018998.

93. J Yang, R van Lith, K Baler, RA Hoshi, GA Ameer. A thermoresponsive biodegradable polymer with intrinsic antioxidant properties. *Biomacro*, **2014**, 15 (11), 3942-3952. DOI: 10.1021/bm5010004.

94. DWL Huskins, A Mahomed, SN Kukureka. Accelerated aging for testing polymeric biomaterials and medical devices. *Med Eng Phys*, **2008**, 30 (10), 1270-1274.

95. A Mahomed, DWL Hukins, SN Kukureka, DET Shepard. Effect of accelerated aging on the viscoelastic properties of Elast-Eon^{TM}: a polyurethane with soft poly(dimethylsiloxane) and poly(hexamethylene oxide) segments. *Mater Sci Eng C*, **2010**, 30(8), 1298-1303. DOI: 10.1016/j.msec.2010.07.014.

96. P Davies, G Evrard. Accelerated ageing of polyurethanes for marine applications. *Polym Degrad Stabl*, **2007**, 92, 1455-1464.

97. M Sonnenschein, BL Wendt, AK Schrock, JM Sonney, AJ Ryan. The relationship between polyurethane foam microstructure and foam aging. *Polym*, **2008**, 49, 934-942.

98. A Boubakri, N Guermazi, K Elleuch, HF Ayedi. Study 0f UV-aging of thermoplastic polyurethane material. *Mater Sci Eng A*, **2010**, 527, 1649-1654.

99. H Tobushi, R Matsui, S Hayashi, D Shimada. The influence of shape-holding conditions on shape recovery of polyurethane-shape memory polymer foams. *Smart Mater Struct*, **2004**, 13, 881-887.

100. M Ahmad, D Singh, YQ Fu, M Miraftab, JK Lo. Stability and deterioration of a shape memory polymer fabric composite under thermomechanical stress, *Polym Degrad Stab*, **2011**, 96, 1470-1477. DOI: 10.1016/j.polymdegradstab.2011.05.009.

101. C G'Sell, GB McKenna. Influence of physical ageing on the yield response of model DGEBA/poly(propylene oxide) epoxy glasses. *Polym*, **1992**, 33, 2103-2113.

102. J Choi, AM Ortega, R Xiao, CM Yakacki, TD Nguyen. Effect of physical aging on the shape-memory behavior of amorphous network. *Polym*, **2012**, 53 (12), 2453-2464.

103. KJ Hemmerick, General aging theory and simplified protocol for accelerated aging of medical devices, *Med Dev Diagnos Ind Qual Assur*, **1998**, http://www.mddionline.com/article/general-aging-theory-and-simplified-protocol-accelerated-aging-medical-devices

104. KT Gillen, RL Clough. Time-temperature-dose rate superposition: a methodology for extrapolating accelerated radiation aging data to low dose rate conditions. *Polym Degrad Stabl*, **1989**, 24, 137-168.

105. R Reich. Accelerated aging of packaging: considerations, suggestions, and use in expiration date verification. *Med Dev Diag Ind*, **1988**, 10(3), 34.

106. SS Das, LW Schroeder. Estimation of shelf life of natural rubber latex exam-gloves based on creep behavior. *J Biomed Mater Res Pt B Appl Biomater*, **2008**, 85B, 398-408. DOI: 10.1002/jbm.b.30958.

107. J Donohue, Predicting post-rad shelf life from accelerated aging data. Society of Plastics Engineers, Conference proceedings, 1983.

108. BJ Lambert, FW Tang. Rationale for practical medical device accelerated aging programs in AAMI TIR 17. *Rad Phys Chem*, **2000**, 57(3-6), 349-353. DOI: 10.1016?S0969-806X(99)00403-X

109. K Hemmerich. General Aging Theory and Simplified Protocol for Accelerated Aging of Medical Devices. Medical Plastics and Biomaterials (1998) 16-23.

110. CM Yakacki, AM Ortega, CP Frick, N Lakhera, R Xiao, TD Nguyen. Unique recovery behavior in amorphous shape-memory polymer networks. *Macromol Mater Eng*, **2012**, 297, 1160-1166. DOI: 10.1002/mame.201200275.

111. H Tobushi, R Matsui, S Hayashi, D Shimada. The influence of shape-holding conditions on shape recovery of polyurethane-shape memory polymer foams. *Smart Mater* Struct, **2004**, 13 (4), 881-887. DOI: 10.1088/0964-1726/13/4/026

112. H Tobushi, D Shimada, S Hayashi, M Endo. Shape fixity and shape recovery of polyurethane shape-memory polymer foams. *J Mater Design Appl*, 2003, 217 (2), 135-143. DOI: 10.1177/146442070321700205.

113. JD Byrne, MNR Jajja, AT O'Neill, LR Bickford, AW Keeler, N Hyder, K Wagner, A Deal, RE Little, RA Moffitt, C Stack, M Nelson, CR Brooks, W Lee, JC Luft, ME Napier, D Darr, CK Anders, R Stack, JE Tepper, AZ Wang, WC Zamboni, JJ Yeh,

JM deSimone. Local iontophoretic administration of cytotoxic therapies to solid tumors. *Sci Trans Med*, **2015**, 273 (7), DOI: 10.1126/scitranslmed.3009951.

114. WE Katzin, Pathology of lymph nodes from patients with breast implants, Am J Surg Pathol, **2005**

115. J Zhou, J Liu, CJ Cheng, TR Patel, CE Weller, JM Piepmier, Z Jiang, WM Saltzman. Biodegradable poly(amine-co-ester) terpolymers for targeted gene delivery. *Nat Mater*, **2012**, 11, 82-90. DOI: 10.1038/nmat3187.

116. M Colladon, A Scarso, G Strukul. Mild catalytic oxidation of secondary and tertiary amines to nitrones and N-oxides with H2O2 mediated by Pt (II) catalysts. *Green Chem*, **2008**, 10, 793. DOI:10.1039/B8050404E.

117. C Gella, E Ferrer, R Alibes, F Busque, P de March, M Figueredo, J Font. A metal-free general procedure for oxidation of secondary amines to nitrones. *J Org Chem*, **2009**, 74 (16), 6365-6367. DOI: 10.1021/jo901108u.

118. K Suzuki, T Watanabe, S Murahashi. Oxidation of primary amines to oximes with molecular oxygen using 1,1-diphenyl-2-picrylhydrazyl and WO_3/Al_2O_2 as catalysts. *J Org Chem*, **2013**, 78, 230-2310. DOI:10.1021/jo302262a.

119. K Bergstad, JE Backvall. Mild and efficient Flavin-catalyzed H_2O_2 oxidation of tertiary amines to amine N-oxides. *J Org Chem*, **1998**, 63, 6650-6655. DOI: 10.1021/jo980926d.

120. SC Ghosh, JXY Ngiam, AM Seayad, DT Tuan, CLL Chai, A Chen. Copper-catalyzed oxidative amidation of aldehydes with amine salts: synthesis of primary,

secondary, and tertiary amines. *J Orgo Chem*, **2012**, 77, 8007-8015. DOI: 10.1021/jo301252c.

121. JD Fields, PJ Kropp. Surface-mediated reactions. 9. Selective oxidation of primary and secondary amines to hydroxylamines. *J Org Chem*, **2000**, 65, 5937-5941. DOI: 10.1021/jo0002083.

122. AM Fracoli, H Furukawa, M Suzuki, M Dodd, S Okajima, F Gandara, JA Reimer, OM Yaghi. Metal-organic frameworks with precisely designed interior for carbon dioxide capture in the presence of water. *J Am Chem Soc*, **2014**, 136, 8863-8866. DOI:10.1021/ja503296c.

123. C Englert, M Hartlieb, P Bellstedt, K Kempe, C Yang, SK Chu, X Ke, JM Garcia, RJ Ono, M Fevre, RJ Wojtecki, US Schubert, YY Yang, JL Hedrick. Enhancing the biocompatibility and biodegradability of linear poly(ethylene imine) through controlled oxidation. *Macromol*, **2015**, 48(20), 7420-7427. DOI:10.1021/acs.macromol.5b01940.

124. M Kagan, M Chleno, S Melnikov, A Greenfield, J Gross, RC Bernostas. Optimization of normal-phase chromatographic separation of compounds with primary, secondary, and tertiary amino groups. *J Chromatog A*, **2008**, 1194, 80-89. DOI:10.1016/j.chroma.2008.04.052.

125. GT Rochelle. Amine scrubbing for CO_2 capture. *Science*, **2009**, 5948 (325), DOI: 10.1126/science.1176731.

126. Z Zhang, R Guidoin, MW King, TV How, Y Marois, G Laroche. Removing fresh tissue from explanted polyurethane prostheses: which approach facilitates physico-

chemical analysis? *Biomaterials*, **1995**, 16(5), 369-380. DOI:10.1016/0142-9612(95)93854-7.

127. BD Ratner. Reducing capsular thickness and enhancing angiogenesis around implant drug release systems. *J Control Release*, **2002**, 78, 211-218. DOI: 10.1016/So168-3659(01)00502-8

128. EM Sussman, MC Halpin, J Muster, RT Moon, BD Ratner. Porous implants modulate healing and induce shifts in local macrophage polarization in the foreign body reaction. *Ann Biomed Engin*, **2014**, 42(7), 1508-1516. DOI: 10.1007/s10439-013-0933-0.

129. JM Anderson, A Rodriguez, DT Chang, Foreign body reaction to biomaterials. *Sem Immunol*, **2008**, 20 (2), 86-100. DOI: 10.1016/j.smim.2007.11.004.

130. Health Council of the Netherlands: Committeee on Updating of Occupational Exposure Limits. Oxalic acid; Health-based reassessment of administrative occupational exposure limits. The Hague: Health Council of the Netherlands, **2004**, 2000/15OSH/106.

131. M Tsujihata. Mechanism of calcium oxalate renal stone formation and renal tubular cell injury. *Int J Urolo*, **2007**, 15 (2), 115-120. DOI: 10.1111/j.1442-2042.2007.01953.x

132. N Olivia, M Carcole, M Beckerman, S Seliktar, A Hayward, J Stanley, NMA Parry, ER Edelman, N Artzi. Regulation of dendrimer/dextran material performance by altered tissue microenvironment in inflammation and neoplasia. *Sci Trans Med*, **2015**, 272 (7), DOI: 10.1126/scitranslmed.aaa1616.

133. BD Ratner. Healing with medical implants: the body battles back. *Sci Trans Med*, **2015**, 272 (7), DOI: 10.1126/scitranslmed.aaa5371.

134. AC Weems, KT Wacker, JK Carrow, AJ Boyle, DJ Maitland. Characterization of the degradation behavior of shape memory poly(amino urethane ureas) intended for vascular occlusion applications. In prep.

135. CG Collins, JM Baumes, BD Smith. Thermally-activated chemiluminescent squaranine rotaxane endoperoxide with green emission. *Chem Comm*, **2011**, 47, 12352-12354. DOI: 10.1039/C1CC15550D.

136. C Spyropoulos, CG Kokotos. One-pot synthesis of ureas from boc-protected amines. *J Orgo Chem*, **2014**, 79, 4477-4483. DOI: 10.1021/jo500492x.

137. A Lapolla, Rapid Commun Mass Spec, 2003, DOI: 10.1002/rcm.992

138. Health Council of the Netherlands: Committeee on Updating of Occupational Exposure Limits. Oxalic acid; Health-based reassessment of administrative occupational exposure limits. The Hague: Health Council of the Netherlands, **2004**, 2000/15OSH/106.

139. M Tsujihata. Mechanism of calcium oxalate renal stone formation and renal tubular cell injury. *Int J Urolo*, **2007**, 15 (2), 115-120. DOI: 10.1111/j.1442-2042.2007.01953.x

140. J Gharavi, P Marks, K Moran, B Kingsborough, R Verma, Y Chen, R Deng, M Levine. Chiral cationic polyamines for chiral microcapsules and siRNA delivery. *Bioorg Med Chem Lett*, **2013**, DOI: 10.1016/j.bmcl.2013.08.083.

141. G Pietig, T Mehrens, JR Hirsch, I Cetinkaya, H Piechota, E Schlatter. Properties and regulation of organic cation transport in freshly isolated human proximal tubules. *J Biolog Chem*, **2001**, 276 (36), 33741-33746.

142. CMS Schophuizen, MJ Wilmer, J Jansen, L Gustavsson, C Hilgendorf, JGJ Hoenderop, LP van den Heuvel, R Masereeuw. Catioinic uremic toxins affect human renal proximal tubule cell functioning through interaction with the organic cation transporter. *Eur J Physiol*, **2013**, 465, 1701-1714. DOI: 10.1007/s00424-013-1307z.

143. GL Glorieux, AW Dhondt, P Jacobs, JV Langeraert, NH Lameire, PP de Deyn, RC Vanholder. In vitro study of the potential role of guanidines in leukocyte functions related to atherogenesis and infection. *Kid Intern*, **2004**, 65, 2184-2192.

144. Polymer Synthesis: Theory and Practice, Fundamentals, Methods, Experiments, 5th Edition. Editors: D Bruan, H Cherdon, M Rehahn, H Ritter, B Voit.

145. AC Weems, JE Raymond, M Wierzbicki, T Gustavson, DJ Maitland. Synthesis of multifunctional fluorescent shape memory polyurethanes. *RSC Adv*. **2016**, in prep.

146. AC Weems, AD Easley, JM Szafron, J Smolen, DJ Maitland. Synthesis and characterization of magnetic resonance visible shape memory polymer foams. *Biomater*, **2016**, *submitted.*

147. AC Weems, AJ Boyle, DJ Maitland. Two-year performance study of porous, thermoset, shape memory polyurethanes intended for vascular medical devices. *Smart Mater Struct*, **2016**, *in review.*

148. AJ Boyle, MA Wierzbicki, SM Herting, **AC Weems**, A Nathan, W Hwang, DJ Maitland. In vitro performance of a shape memory polymer foam-coated coil embolization device. *Med Engin Phys*, **2016**, in prep
149. BD Ahn, J Appl Polym Sci, 2001, DOI: 10.1002/app.2135
150. BAJ Noordover, Biomacromolecules, 2006, DOI: 10.1021/bm060713v.
151. JR Lindsay Smith, ROC Norman, AG Rowley. Amine oxidation. Pt VIII. Evidence for intramolecular hydrogen-atom transfer in amine radical cations. *J Chem Soc Perkin Trans I*, **1973**, 565-571. DOI: 10.1039/P19730000566.
152. SS Rawalay, H Shechter. Oxidation of primary, secondary, and tertiary amines with neutral permanganate. Simple method for degrading amines to aldehydes and ketones. *J Org. Chem*. **1967**, 32 (10), 3129. DOI: 10.1021/jo01285a042.
153. H Shechter, SS Rawalay. Oxidation of primary, secondary, and tertiary amines with neutral potassium permanganate. II. *J Am Chem Soc*, **1964**, 86 (9), 1706-1709. DOI: 10.1021/ja01063a013.
154. A Gopferich, Mechanisms of polymer degradation and erosion. *Biomater*, **1996**, 17 (2), 103-114. DOI: 10.1016/0142-9612(96)85755-3;
155. BD Ratner, KW Gladhill, TA Horbett. Analysis of in vitro enzymatic and oxidative degradation of polyurethanes. *J Biomed Mater Res*, **1988**, 22 (6), 509-527. DOI: 10.1002/jbm.820220607;
156. JR Frautschi, JA Chinn, RE Phillips, QH Zhao, JM Anderson, R Joshi, RJ Levy. Degradation of polyurethanes in vitro and in vivo: comparison of different models. *Coll Surf B Biointer*, **1993**, 305-313. DOI: 10.1016/0927-7765(93)80005-J;

157. H Seyednejad, AH Ghassemi, CF van Nostrum, T Vermonden, WE Hennink. Functional aliphatic polyesters for biomedical and pharmaceutical applications. *J Control Releas*, **2011**, 152 (1), 168-176. DOI: 10.1016/j.conrel.2010.12.016.

158. M Hakkarainen, A Hoglund, K Odelius, A Albertsson. Tuning the release rate of acidic degradation products through macromolecular design of caprolactone-based copolymers. *J Am Chem Soc*, **2007**, 129, 6308-6312. DOI: 10.1021/ja0702871.

159. H Li, J Chang. In vitro degradation of porous degradable and bioactive PHBV/wollastonite composite scaffolds. *Polym Degrad Stab*, **2005**, 87 (2), 301-307. DOI: 10.1016/j.polymdegradstab.2004.09.001.

160. H Liu, EB Slamovich, TJ Webster. Less harmful acidic degradation of poly(lactic-co-glycolic acid) bone tissue engineering scaffolds through titania nanoparticle addition. *Int J Nanomed*, **2006**, 1 (4), 541-545.

161. K Cheng, G Wang, J Zeng, J Zhang. Improved succinate production by metabolic engineering. *Biomed Res Inter*, **2013**, 538790. DOI: 10.1155/2013/538790.

162. M de castro Fonseca, CJ Agular, JA Da Rocha Franco, RN Gingold, MF Leite. GPR91: expanding the frontiers of Krebs cycle intermediates. *Cell Comm Sign*, **2016**, 14 (3). DOI: 10.1186/s12964-016-0126-1;

163. C Varela, DR Kutyna, RM Solomon, CA Black, A Borneman, PA Henschke, IS Pretorius, PJ Chambers. Evaluation of gene modification strategies for the development of low-alcohol-wine yeasts. *Appl Environ Microbiol*, **2012**, 78 (17), DOI: 10.1128/AEM.01279-12.

164. E Jager, RK Donato, M Perchacz, A Jager, F Surman, A Hocherl, R Konefal, KZ Donato, CG Venturini, VZ Bergamo, HS Schrekker, AM Fuentegria, MG Raucci, L Ambrosio, P Stepanek. Biocompatible succinic acid-based polyesters for potential biomedical applications: fungal biofilm inhibition and mesenchymal stem cell growth. *RSC Adv*, **2015**, 5, 85756-85766. DOI: 10.1039/C5RA15858C.

165. JB Knaak, Toxicology of mono-, di-, and triethanolamine, 1997, Reviews of environmental contamination and toxicology, vol 149

166. AL Mendrala et al (The pharmacokinetics of diethanolamine in Sprague-Dawley rats foolwing intravenous administration, 2001

167. National research Council (US) Committee on Toxicology. Emergency and continuous exposure limits for selected airborne contaminants: vol 2. Washington (DC): National Academies Press (US); 1984. Ethanolamine.

168. BH Rumack. POISINDEX(R) Information System Micromedex, Inc. Englewood, CO, 2016. CCIS vol 169, 2016.

169. AD Woolf, Intentional infantile ethylene glycol poisoning presenting as an inherited metabolic disorder, *J Pediatrics*, **1992**, 120 (3), 421-424. DOI: 10.1016/S0022-3476(05)80910-2;

170. T Hlozek, Fast determination of ethylene glycol, 1,2-propylene glycol and glycolic acid in blood serum and urine for emergency and clinical toxicology by GC-FID, *Talanta*, **2014**, 130 (1), 470-474. DOI: 10.1016/j.talanta.2014.07.020;

171. BS Carter, S Sheth, E Chang, M Sethl, CS Ogilvy. Epidemiology of the size distribution of intracranial bifurcation aneruysms: smaller size of distal aneurysms

and increasing size of unruptured aneurysms with age. *Neurosurg*, **2006**, 58 (2), 217-223. DOI: 10.1227/01.NEU.0000194639.37803.F8;

172. BAJ Noordover, R Duchateau, RATM van Benthem, W Ming, CE Koning. Enhancing the functionality of biobased polyester coating resins through modification with citric acid. *Biomacromol*, **2007**, 8, 3860-3870. DOI: 10.1021/bm70775e;

173. S Ma, DC Webster, F Jabeen. Hard and flexible, degradable thermosets from renewable bioresources with the assistance of water and ethanol. *Macromol*, **2016**, 49, 3780-3788. DOI: 10.1021/acs.macromol.6b00594.;

174. RT Duan, QX He, X Dong, DF Li, XL Wang, YZ Wang. Renewable sugar-based diols with different rigid structure: comparable investigation on improving poly(butylene succinate) performance. *ACS Sustainable Chem Eng*, **2016,** 4, 350-362. DOI: 10.1021/acssuschemeng.5b01335.;

175. J Yang, AR Webb, GA Ameer. Novel citric acid-based biodegradable elastomers for tissue engineering. *Adv Mater*, **2004**, 16 (6), 511-516. DOI: 10.1002/adma.200306264.;

176. H Qiu, J Ynag, P Kodali, J Koh, GA Ameer. A citric acid-based hydroxyapatite composite for orthopedic implants. *Biomater*, **2006**, 27, 34, 5845-5854. DOI: 10.1016/j.biomaterials.2006.07.042.;

177. D Gyawali, P Nair, Y Zhang, RT Tran, C Zhang, M Samchukov, M Makarov, HKW Kim, J Yang. Citric acid-derived in situ crosslinkable biodegradable polymers

for cell delivery. *Biomater*, **2010**, 31 (34), 9092-9105. DOI: 10.1016/j.biomaterials.2010.08.022.;

178. JM Halpern, R Urbanski, AK Weinstock, DF Iwig, RT Mathers, H von Recum. A biodegradable thermoset polymer made by esterification of citric acid and glycerol. *J Biomed Mater Res A*, **2014**, 102 (5), 1467-1477. DOI: 10.1002/jbm.a.34821.)

179. JM Robertson, HB Nejad, PT Mather. Dual-spun shape memory elastomeric composites. *ACS Macro Lett*, **2015**, 4, 436-440. DOI: 10.1021/acsmacrolett.5b00106.

180. MI Lawton, KR Tillman, HS Mohammed, W Kuang, DA Shipp, PT Mather. Anhydride-based reconfigurable shape memory elastomers. *ACS Macro Lett*, **2016**, 5, 203-207. DOI: 10.1021/acsmarcolett.5b00854.

181. J Mendez, PK Annamalai, SJ Eichhorn, R Rusli, SJ Rowan, EJ Foster, C Weder. Bioinspired mechanically adaptive polymer nanocomposites with water-activated shape-memory effect. *Macromol*, **2011**, 44 (17), 6827-6835. DOI: 10.1021/ma201502k.

182. T Wu, M Frydrych, K O'Kelly, B Chen. Poly(glycerol sebacate urethane)-cellulose nanocomposites with water-active shape-memory effects. *Biomacromol*, **2014**, 15 (7), 2663-2671. DOI: 10.1021/bm500507z.

183. A Biswas, VK Aswal, PU Sastry, D Rana, P Maiti. Reversible bidirectional shape memory effect in polyurethanes through molecular flipping. *Macromol*, **2016**, 49 (13), 4889-4897. DOI: 10.1021/acs.macromol.6b00536.

184. C Zhou, JN Beltramini, Y Fan, GQ Lu. Chemoselective catalytic conversion of glycerol as a biorenewable source to valuable commodity chemicals. *Chem Soc Rev*, **2008**, 37, 527-549. DOI: 10.1039/B707343G

185. P McMorn, G Roberts, GJ Hutchings. Oxidation of glycerol with hydrogen peroxide using silicalite and aluminophosphate catalyst. *Catal Lett*, **1999**, 63 (3), 193-197. DOI: 10.1023/A:1019073122592

186. IA Shkrob, TW Marin, SD Chemerisov, MD Sevilla. Mechanistic aspects of photooxidation of polyhydroxylated molecules on metal oxides. *J Phys Chem C*, **2011**, 115, 4642-4648. DOI: 10.1021/jp110612s

187. LS Sharninghausen, J Campos, MG Manas, RH Crabtree. Efficient selective and atom economic catalytic conversion of glycerol to lactic acid. *Nat Comm*, **2014**, 5, 5084, DOI: 10.1038/ncomms6084

188. T Laino, C Tuma, A Curioni, E Jochnowitz, S Stolz. A revisited picture of the mechanism of glycerol dehydration. *J Phys Chem A*, **2011**, 115, 3592-3595. DOI: 10.1021/jp201078e

189. MR Nimlos, SJ Blanksby, X Qian, ME Himmel, DK Johnson. Mechanisms of glycerol dehydration. *J Phys Chem A*, **2006**, 110, 6145-6156. DOI: 10.1021/jp060597q

190. AA Vitale, EA Bernatene, MG Vitale, AB Pomilio. New insights of the Fenton reaction using glycerol as the experimental model. Effect of O2, inhibition by Mg2+, and oxidation state of Fe. *J Phys Chem A*, **2016**, 120, 5435-5445. DOI: 10.1021/acs.jpca.6b03805

191. S Son, E Shin, B Kim. Redox-degradable biocompatible hyperbranched polyglycerols: synthesis, copolymerization kinetics, degradation, and biocompatibility. *Macromol*, **2015**, 48 (3), 600-609, DOI: 10.1021/ma502242v
192. S Son, H Park, E Shin, Y Shibasaki, B Kim. Architecture-controlled synthesis of redox-degradable hyperbranched polyglycerol block copolymers and the structural implications of their degradation. *J Polym Sci A Poly Chem*, **2016**, 54 (12), 1752-1761. DOI: 10.1002/pola.28031
193. D Wilms, S Stiriba, H Frey. Hyperbranched polyglycerols: from the controlled synthesis of biocompatible polyether polyols to multipurpose applications. *Acc Chem Res*, **2010**, 43 (1), 129-141. DOI: 10.1021/ar900158p.
194. S Morlat, N Cezard, B Loubinoux, J Philippart, J Gardette. Mechanisms of photooxidation of polyglycerol. *Polym Degrad Stab*, **2001**, 199-208.
195. AC Weems, KT Wacker, DJ Maitland. The use of glycerol to produce more oxidatively biostable shape memory polyurethane biomaterials. *Macromol*, **2016**¸ in prep.
196. H Ulrich, A Odinak, B Tucker, AAR Sayigh. Recycling of polyurethane and polyisocyanurate foam. *Polym Engin Sci*, **1978**, 18 (11), 844-848.
197. H Ulrich. Recent advances in isocyanaurate technology. *J Cell Plas*, **1981**, 31-34
198. HE Reymore, PS Carleton, RA Kolakowski, AAR Sayigh. Isocyanurate foams: chemistry, properties, and processing. *J Cell Plas*, **1975**, 328-345
199. DK Hoffman, Model system for a urethane-modified isocyanurate foam. *J Cell Plast*, **1984**, 129-137

200. Y Qiu, L Qian, W Xi. Flame-retardant effect of a novel phosphaphenanthrene/triazine-trione bi-group compound on an epoxy thermoset and its pyrolysis behavior. *RSC Adv*, **2016**, 6, 56018-56027. DOI: 10.1039/C6RA10752D;

201. LT Nguyen, TT Truong, HT Nguyen, L Le, VQ Nguyen, TV Le, AT Luu. Healable shape memory (thio)urethane thermosets. *Polym Chem*, **2015**, 6, 3143-3154. DOI: 10.1039/C5PY00126A;

202. SK Ghosh, S Bureekaew, S Kitagawa. A dynamic, isocyanurate-functionalized porous coordination polymer. *Angew Chem*, **2008**, 120 (18), 3451-5454. DOI: 10.1002/ange.200705986.;

203. C Peng, K Chang, C Weng, M Lai, C Hsu, S Hsu, S Li, Y Wei, J Yeh. UV-curable nanocasting technique to prepare bio-mimetic super-hydrophobic non-fluorinated polymeric surfaces for advanced anticorrosive coatings. *Polym Chem*, **2013**, 4, 926-932. DOI: 10.1039/C2PY20613G.;

204. E Preis, N Schindler, S Adrian, U Scherf. Microporous polymer networks made by cyclotrimerization of commercial, aromatic diisocyanates. *ACS Macro Lett*, **2015**, 4, 1268-1272. DOI: 10.1021/acsmarcolett.5b00726.

205. PA Argabright, BL Philips. On the basic hydrolysis of disubstituted isocyanurates. *J Hetero Cycl Chem* **1970**, 999-1000.

206. ER Garret, JT Bojarski, GJ Yakatan. Kinetics of hydrolysis of barbituric acid derivatives, *J Pharm Sci*, **1971**, 60 (8), 1145- 1155.;

207. BG Hammond, SJ Barbee, T Inoue, N Ishida, GJ Levinskas, MW Stevens, AG Wheeler, T Cascieri. A review of the toxicology studies on cynaurate and its chlorinated derivative. *Environ Health Perspec*, **1986**, 69, 287-292.

208. JL Dorne, DR Doerge, M Vandenbroeck, J Fink-Gremmels, W Mennes, HK Knutsen, F Vernazza, L Castle, L Edler, D Benford. Recent advances in the risk assessment of melamine and cyanuric acid in animal feed. *Toxico Appl* Pharm, **2013**, 270 (3), 218-229. DOI: 10.1016/j.taap.2012.01.012.

209. G Johanson, V Kristjansson, K Savolainen, V Skaug. The Nordic expert group for criteria documentation of health risks from chemicals. 128: triglycidyl isocyanaurate, National Institute for Working Life, **2001**, 18.